

**SENSITIVITY ANALYSIS OF MATERIAL PARAMETERS
ON THE MICRO-SCALE STRESS DISTRIBUTION IN
FIBER REINFORCED COMPOSITES**

**FİBER TAKVİYELİ KOMPOZİTLERİN MİKRO-
ÖLÇEKLİ GERİLME DAĞILIMINDA MALZEME
PARAMETRELERİNİN DUYARLILIK ANALİZİ**

BERKAY BEKTAŞ

ASSOC. PROF. DR BARIŞ SABUNCUOĞLU

Supervisor

Submitted to

Graduate School of Science and Engineering of Hacettepe University

as a Partial Fulfillment to the Requirements

for the Award of the Degree of Master of Science

in Mechanical Engineering

2023

Aileme...

ABSTRACT

SENSITIVITY ANALYSIS OF MATERIAL PARAMETERS ON THE MICRO-SCALE STRESS DISTRIBUTION IN FIBER REINFORCED COMPOSITES

Berkay BEKTAŞ

Master of Science, Department of Mechanical Engineering

Supervisor: Assoc. Prof. Dr. Barış SABUNCUOĞLU

January 23, 78 pages

Knowing the mechanical behavior of fiber-reinforced composites are important since unidirectional (UD) composite materials have been widely used in many industries. Different methods in macro-scale and micro-scale have been used to determine the properties of the composite. While macro-scale methods fail to predict properties under transverse loading, many studies were done in micro-scale methods where the fiber and matrix are modeled separately. Finite element method is the most widely used method for micro-scale analysis.

It is known that matrix properties dominate the failure behavior of the UD composites. Since these distributions are affected by the composite material properties, it is important to see the relation between them. The stress distribution is highly dependent on the distribution of the fiber. Therefore, random packing methods were developed to capture the real composite structure. With each run, fiber locations changes. Understanding the stresses and concentrations due to selected material properties is possible with a sensitivity analysis.

In this thesis, the effect of material parameters on micro-scale stress distribution in fiber reinforced composites in transverse loading was analyzed. Different micro-scale models were generated due to generated fibers in the matrix being different than the actual structure. The models were prepared and solved by a commercial finite element software, ABAQUS. Material parameters that can be selected by the designer or engineer were analyzed within a preliminary analysis and were defined to the models. Their results were compared to see their importance in the sensitivity analysis. It was seen that fiber Poisson's ratio does not have any meaningful effect on stress concentration within the ranges given in the study. Chosen material parameters and their values taken from the literature were defined to the models. To calculate the relation between the stress concentration results gathered and the material parameters, a commonly known statistical analysis method called parametric correlation was used and correlation coefficients were interpreted. It was seen that composites Young's modulus ratio has lower relation with stress concentration than fiber's volume ratio. A parameter called overstressed volume percentage was introduced in the thesis. The correlation coefficient of this parameter with the input parameters was also calculated and interpreted.

Keywords: Composite materials, finite element method, sensitivity analysis, monte carlo simulation, parametric correlation, micro-scale modelling.

ÖZET

FİBER TAKVİYELİ KOMPOZİTLERİN MİKRO-ÖLÇEKLİ GERİLME DAĞILIMINDA MALZEME PARAMETRELERİNİN DUYARLILIK ANALİZİ

Berkay BEKTAŞ

Yüksek Lisans, Makine Mühendisliği Bölümü

Tez Danışmanı: Doç. Dr. Barış SABUNCUOĞLU

Ocak 2023, 78 sayfa

Tek yönlü (UD) kompozit malzemeler birçok endüstride yaygın olarak kullanıldığından, fiber takviyeli kompozitlerin mekanik davranışlarını bilmek önemlidir. Kompozitin özelliklerini belirlemek için makro ölçekte ve mikro ölçekte farklı yöntemler kullanılmıştır. Makro ölçekli yöntemler, enine yükleme altındaki özellikleri tahmin etmekte başarısız olurken, fiber ve matrisin ayrı ayrı modellendiği mikro ölçekli yöntemlerde birçok çalışma yapılmıştır. Sonlu elemanlar yöntemi, mikro ölçekli analizler için en yaygın kullanılan yöntemdir.

Matris özelliklerinin UD kompozitlerin kırılma davranışına hakim olduğu bilinmektedir. Bu dağılımlar kompozit malzeme özelliklerinden etkilendiği için aralarındaki ilişkinin bilinmesi önemlidir. Gerilme dağılımı büyük ölçüde fiberin dağılımına bağlıdır. Bu nedenle, gerçek kompozit yapıyı yakalamak için rastgele paketleme yöntemleri geliştirilmiştir. Her çalışmada, fiber konumları değişir. Hassasiyet analizi ile seçilen malzeme özelliklerinden kaynaklanan gerilmeleri ve konsantrasyonları anlamak mümkündür.

Bu tezde, malzeme parametrelerinin enine yüklemde fiber takviyeli kompozitlerde mikro ölçekli gerilme dağılımı üzerindeki etkisi analiz edilmiştir. Matriste oluşturulan fiberlerin gerçek yapıdan farklı olması nedeniyle, çeşitli mikro ölçekli modeller oluşturulmuştur. Modeller, ticari bir sonlu elemanlar yazılımı olan ABAQUS ile hazırlanmış ve çözülmüştür. Tasarımcı veya mühendis tarafından seçilebilen malzeme parametreleri bir ön analiz ile analiz edilerek modellere tanımlanmıştır. Duyarlılık analizindeki önemlerini görmek için sonuçları karşılaştırılmıştır. Çalışmada verilen aralıklarda fiberin Poisson oranının stres konsantrasyonu üzerinde önemli bir etkisinin olmadığı görülmüştür. Seçilen malzeme parametreleri ve literatürden alınan değerleri modellere tanımlanmıştır. Toplanan gerilim konsantrasyonu sonuçları ile malzeme parametreleri arasındaki ilişkiyi hesaplamak için yaygın olarak bilinen parametrik korelasyon adı verilen istatistiksel analiz yöntemi kullanılmış ve korelasyon katsayıları yorumlanmıştır. Kompozitlerin Young modül oranının, fiberin hacim oranına göre gerilme konsantrasyonu ile ilişkisinin daha düşük olduğu görülmüştür. Tezde aşırı gerilmiş hacim yüzdesi adı verilen bir parametre tanıtılmıştır. Bu parametrenin giriş parametreleri ile korelasyon katsayısı da hesaplanmış ve yorumlanmıştır.

Anahtar Kelimeler: Kompozit malzemeler, sonlu elemanlar yöntemi, monte carlo simülasyonu, parametrik korelasyon, micro-ölçekli modelleme

ACKNOWLEDGEMENTS

Firstly, I would like to thank and express my regards to my supervisor, Assoc. Dr. Barış SABUNCUOĞLU for his support and guidance. Special thanks to Assoc. Dr. Abdullah SANDIKKAYA for his help and contributions to this thesis. Their support and assistance encouraged me greatly to finish my study.

I also would like to thank my parents, Sadegül UÇAK and Haydar BEKTAŞ.

I would like to thank my chief in MEGETEKNIK, Berk YERALTI, for his patience and kind attitude during my study.

CONTENTS

ABSTRACT	i
ÖZET	iii
ACKNOWLEDGEMENTS	v
CONTENTS	vi
TABLES	viii
FIGURES	ix
SYMBOLS	xii
ABBREVIATIONS	xii
1. INTRODUCTION	1
1.1. Aim of the Study	1
1.2. Research Methodology	2
1.3. Outline of the Study	2
2. NUMERICAL AND STATISTICAL ANALYSIS OF COMPOSITES	4
2.1. Introduction to Composite Materials	4
2.2. Finite Element Method	7
2.3. Macro-Scale and Micro-Scale Analysis	8
2.4. Statistical Analysis of Composite Materials	15
3. MONTE-CARLO AND PARAMETRIC CORRELATION METHODS	22
3.1. Pearson Correlation	24
3.2. Spearman Correlation	25
4. MICROMECHANICAL MODELS USED IN THE STUDY	28
4.1. RVE Used in the Analysis	28
4.2. Application of Periodic Boundary Conditions	35
4.3. Loading and Boundary Conditions	36
4.4. Stress Concentration Calculation	37
5. SELECTION OF MATERIAL PARAMETERS	39
6. SENSITIVITY ANALYSIS METHOD	46
6.1. Monte-Carlo Method	46

6.2. Fibers Young's Modulus Variance	48
7. RESULTS	50
7.1. Fibers Young's Modulus Variance Results	50
7.2. Monte-Carlo and Sensitivity Analysis Results	53
8. CONCLUSION	71
8.1. Summary of the Study	71
8.2. Outcomes of the Study	71
8.3. Further Studies	72
9. REFERENCES.....	73
APPENDIX	77
CURRICULUM VITAE.....	78

TABLES

Table 2.1. Typical mechanical properties of fibers	6
Table 2.2. Typical mechanical properties of matrices	6
Table 3.1. General Rule of Thumb for r values.....	25
Table 4.1. RVE models used in the sensitivity analysis.....	28
Table 4.2. RVE model properties used in the sensitivity analysis.....	33
Table 5.1. Preliminary Analysis Material Parameters	39
Table 6.1. Glass fiber properties used in the fiber variance analysis.....	49
Table 7.1. Maximum stress concentration results for the fiber Young's modulus variance analysis.	50

FIGURES

Figure 2.1. Landing gear brake discs constructed of carbon composite material for aircraft [2].....	4
Figure 2.2. Ivan-30 (Catamaran yacht) made from carbon-epoxy composite [3].....	5
Figure 2.3. Finite element method schematic.....	7
Figure 2.4. Crack-tip and crack-wake debonding schematic representation [14].....	10
Figure 2.5. Nano-reinforced interphase around fibers having (a) hexagonal; (b) circular cross-sections [16].....	10
Figure 2.6. Unit cell quadrants of square and hexagonal array for finite element analysis [18].....	11
Figure 2.7. (a) Square RVE, (b) Hexagonal RVE [25].....	12
Figure 2.8. RVE models graphical illustration [26].....	12
Figure 2.9. Generated RVEs and mesh structure [23].....	13
Figure 2.10. Fiber distribution examples for different volume fractions [27].	14
Figure 2.11. Mesh structure for a circular cross-section model [17].....	14
Figure 2.12. Mesh structure of the hexagonal model [16].....	15
Figure 2.13. Linear correlation results for constituent's basic properties [29].....	16
Figure 2.14. Square-packed array unit cell [29].....	17
Figure 2.15. Finite element model of discontinuous fiber-reinforced composite [30].....	18
Figure 2.16. PDF of Von Mises stress on mechanical loading. [30].....	18
Figure 2.17. Unit Cell models used [32].	19
Figure 2.18. Stiffness properties comparison for hexagonal unit cell (HEX), square unit cell (SQR), Simple Rule of Mixture (SRM), Modified Rule of Mixture (MROM) and test data [32].....	20
Figure 2.19. Spearman Rank Order correlation coefficient matrix [32].....	21
Figure 3.1. Monte Carlo simulation example [33].	22
Figure 3.2. (a) +1 correlation coefficient example, (b)-1 correlation coefficient example.....	23
Figure 3.3. Normal (Gaussian) distribution [36].....	24
Figure 3.4. Input 1 - Output Graph for only 1 RVE and matrix Young's moduli of 1 GPa.....	26
Figure 3.5. Input 1 - Output Graph for one of the RVE and all matrix Young's modulus values.....	27
Figure 3.6. Input 2 - Output Graph for one of the RVE and all matrix Young's modulus values.	27
Figure 4.1. Example RVE model with $V_f = 0.45$	33
Figure 4.2. Example mesh structure used for the RVE model.....	34
Figure 4.3. Graphical representation of PBC [38].....	35
Figure 4.4. Boundary conditions of the RVE model.	37
Figure 4.5. Maximum principle stress result for a RVE used in the sensitivity analysis, $V_f \cong 0.60$	38
Figure 5.1. (a) E_f distribution, (b) E_m distribution.....	40
Figure 5.2. E_f distribuion OVP histograms.....	41
Figure 5.3. E_m distribution OVP histograms.....	42
Figure 5.4. v_f distribution defined to the RVE models.....	43
Figure 5.5. K_{max} distribution of $V_f \approx$ (a) 0.30, (b) 0.45, (c) 0.60 for Poisson's ratio distribution.	44

Figure 5.6. Ef distribution used in the sensitivity analysis.....	45
Figure 6.1. Structure of the Sensitivity Analysis for a single Em	47
Figure 6.2. Normalized Volume – Stress Concentration histogram of $V_f = 0.40675$ RVE model. Ef = 70.9 GPa.....	47
Figure 6.3. Ef distributed RVE model. Each color represents a different Young’s Modulus value.....	48
Figure 6.4. Ef distributions defined to the RVE models. (a) G1, (b) G2, (c) G3 and (d) G4.....	49
Figure 7.1. Maximum stress concentration differences in fibers distributed RVE models for (a) $V_f \cong 0.30$, (b) $V_f \cong 0.45$, (c) $V_f \cong 0.6$. (DXX.X represents the fiber diameter used while creating the RVE).....	52
Figure 7.2. $V_f = 0.30258$, S1max result for Em = 1 GPa.....	53
Figure 7.3. $V_f = 0.30258$, S1max result for Em = 2 GPa.....	54
Figure 7.4. $V_f = 0.30258$, S1max result for Em = 3 GPa.....	54
Figure 7.5. $V_f = 0.30258$, S1max result for Em = 4 GPa.....	55
Figure 7.6. $V_f = 0.30258$, S1max result for Em = 5 GPa.....	55
Figure 7.7. $V_f = 0.45368$, S1max result for Em = 1 GPa.....	56
Figure 7.8. $V_f = 0.45368$, S1max result for Em = 2 GPa.....	56
Figure 7.9. $V_f = 0.45368$, S1max result for Em = 3 GPa.....	57
Figure 7.10. $V_f = 0.45368$, S1max result for Em = 4 GPa.....	57
Figure 7.11. $V_f = 0.45368$, S1max result for Em = 5 GPa.....	58
Figure 7.12. $V_f = 0.60410$, S1max result for Em = 1 GPa.....	58
Figure 7.13. $V_f = 0.60410$, S1max result for Em = 2 GPa.....	59
Figure 7.14. $V_f = 0.60410$, S1max result for Em = 3 GPa.....	59
Figure 7.15. $V_f = 0.60410$, S1max result for Em = 4 GPa.....	60
Figure 7.16. $V_f = 0.60410$, S1max result for Em = 5 GPa.....	60
Figure 7.17. Normalized Volume/K histogram of $V_f = 0.30258$	61
Figure 7.18. Normalized Volume/K histogram of $V_f = 0.30279$	61
Figure 7.19. Normalized Volume/K histogram of $V_f = 0.30423$	62
Figure 7.20. Normalized Volume/K histogram of $V_f = 0.45368$	62
Figure 7.21. Normalized Volume/K histogram of $V_f = 0.45437$	63
Figure 7.22. Normalized Volume/K histogram of $V_f = 0.45689$	63
Figure 7.23. Normalized Volume/K histogram of $V_f = 0.58884$	64
Figure 7.24. Normalized Volume/K histogram of $V_f = 0.60410$	64
Figure 7.25. Normalized Volume/K histogram of $V_f = 0.61829$	65
Figure 7.26. Probability Histogram for all K results.....	66
Figure 7.27. OVP histogram of the sensitivity analysis.....	66
Figure 7.28. Parametric correlation matrix. (a) Graphic representation and (b) Spearman’s correlation values for 450 simulations.	67
Figure 7.29. Parametric correlation matrix. (a) Graphic representation and (b) Spearman’s correlation values for 900 simulations.	67

Figure 7.30. Parametric correlation matrix. (a) Graphic representation and (b) Spearman's correlation values for 1350 simulations.....	68
Figure 7.31. Parametric correlation matrix. (a) Graphic representation and (b) Spearman's correlation values for 1800 simulations.....	69
Figure 7.32. Parametric correlation matrix. (a) Color Graph and (b) Spearman's correlation values for 2250 simulations.....	69

SYMBOLS

E_c	Young's moduli of composite
E_f	Young's moduli of fiber
E_m	Young's moduli of matrix
V_f	Volume fraction of fiber
V_m	Volume fraction of matrix
r	Pearson correlation coefficient
r_s	Spearman's rank correlation coefficient
ε_0	Strain
$S1_{\max}$	Maximum principle stress
$S(i, j)$	Principle stress of respected element
K	Stress concentration
K_{\max}	Maximum stress concentration
ν_f	Poisson's ratio of fiber
ν_m	Poisson's ratio of matrix

ABBREVIATIONS

UD	Unidirectional
FEM	Finite Element Method
S-C	Self-consistent Model
RVE	Representative Volume Element
PBC	Periodic Boundary Condition
PDF	Probability Density Function
RMG	Random Microstructure generation
std	Standard Deviation
OVP	Overstressed Volume Percentage
GFRC	Glass Fiber Reinforced Composite
SROM	Simple Rule of Mixture
MROM	Modified Rule of Mixture

1. INTRODUCTION

1.1. Aim of the Study

For engineers, it is vital to know the mechanical behavior of fiber-reinforced composites since unidirectional (UD) composite materials have been widely used in the automotive and defense industry due to their ability to provide high stiffness with relatively low weight. Their properties can be tailored according to the needs of the designer. Various methods in macro-scale have been used to determine the properties of the composite. Although these methods can predict composite material properties in the fiber direction under transverse loading, prediction of these are challenging. In transverse loading, matrix properties dominate the failure behavior of the UD composites. These behaviors cannot be accurately predicted by homogenized properties. Therefore, many studies have been performed in which the fiber and surrounding matrix are modeled separately. Such a modelling type is called micro-scale as the dimensions of fibers generally vary between 3-15 microns. Finite element method is the most widely used method for micro-scale analysis.

Since the matrix properties dominate the failure behavior of the UD composites, the distribution of the stresses in the matrix are important. These distributions are significantly affected by the composite material properties. The effects of these parameters and their evaluation are significant for the designers and engineers. The distribution of the fiber in the matrix significantly affects the stress distribution. Regular packing methods are used in various studies, but these methods cannot properly reflect the distribution of the fiber in matrix. Because of this, different techniques and algorithms were developed to generate randomly distributed fibers in the matrix. With these algorithms, generated fibers in the matrix will be different than the actual structure, and with each run, their location will be changed. Therefore, statistical analysis is needed to understand the stresses and concentrations due to selected material properties.

The aim of this study is to analyze the effect of material parameters on micro-scale stress distribution in fiber reinforced composites in transverse loading. Due to generated fibers in the matrix being different than the actual structure, different micro-scale models were generated. The models are prepared and solved by a commercial finite element software, ABAQUS. Material parameters that can be selected by the designer or engineer are

analyzed within a preliminary analysis and are defined to the models. Their results are compared to see their importance in the sensitivity analysis. Chosen material parameters and their values taken from the literature are defined to the models. To calculate the relation between the stress concentration results gathered and the material parameters, a commonly known statistical analysis method called parametric correlation was used and correlation coefficients were interpreted.

1.2. Research Methodology

This study starts with a brief introduction to composite materials and methods to determine their properties. Then, the finite element analysis of composite materials, examples, and applications are investigated. Statistical analysis performed on the composite materials in order to understand the mechanical behavior is investigated. Parametric correlation and its methods are explained in detail. After these, the micromechanical model used in this study is described. Chosen materials parameters for the sensitivity analysis are presented. In section 6, the sensitivity analysis method used in the study is described in detail. Gathered results are proposed and discussed. At last, conclusions upon this study are given.

1.3. Outline of the Study

There are 8 chapters in this thesis. A short explanation of all chapters can be found below:

Chapter 1: Introduction

A brief introduction about the thesis study is given.

Chapter 2: Numerical and Statistical Analysis of Composites

Information about composite materials and their analysis methods are given. Macro-scale analysis methods and micro-scale analysis methods are explained. Statistical analysis done in composite materials in literature are given and described in detail. The literature review about the study is also given in this chapter.

Chapter 3: Monte-Carlo and Parametric Correlation Methods

Monte-Carlo method, parametric correlation, and its methods are explained. The parametric correlation method used in this study is also explained in this chapter.

Chapter 4: Micromechanical Models Used in The Study

Generated micromechanical model is given and explained in detail. Key properties of the model are given.

Chapter 5: Selection of Material Parameters

Material parameters and why they are chosen are explained in detail. Preliminary analyses are given in this chapter.

Chapter 6: Sensitivity Analysis Method

The sensitivity analysis method that is used for this thesis study is presented in detail.

Chapter 7: Results

Obtained results from the sensitivity analysis are presented and discussed in this chapter.

Chapter 8: Conclusion

A summary of the analysis and conclusions are given in this chapter.

Appendix

TBD

2. NUMERICAL AND STATISTICAL ANALYSIS OF COMPOSITES

2.1. Introduction to Composite Materials

Composite materials are made by combining two or more components to produce a material with superior qualities to those materials used alone. The two components are normally a matrix and a fiber. Glass and carbon are the most widely used fibers, which can be continuous or discontinuous. Polymers, epoxy, or ceramics are widely used matrices [1]. Mechanical properties of some fibers and matrices are given in (Table 2.1) and (Table 2.2), respectively. The reinforcement material lies in the matrix, increasing the overall material stiffness and other mechanical properties. Unidirectional composite materials have been widely used in automotive, defense, and other industries (Figure 2.1, Figure 2.2).

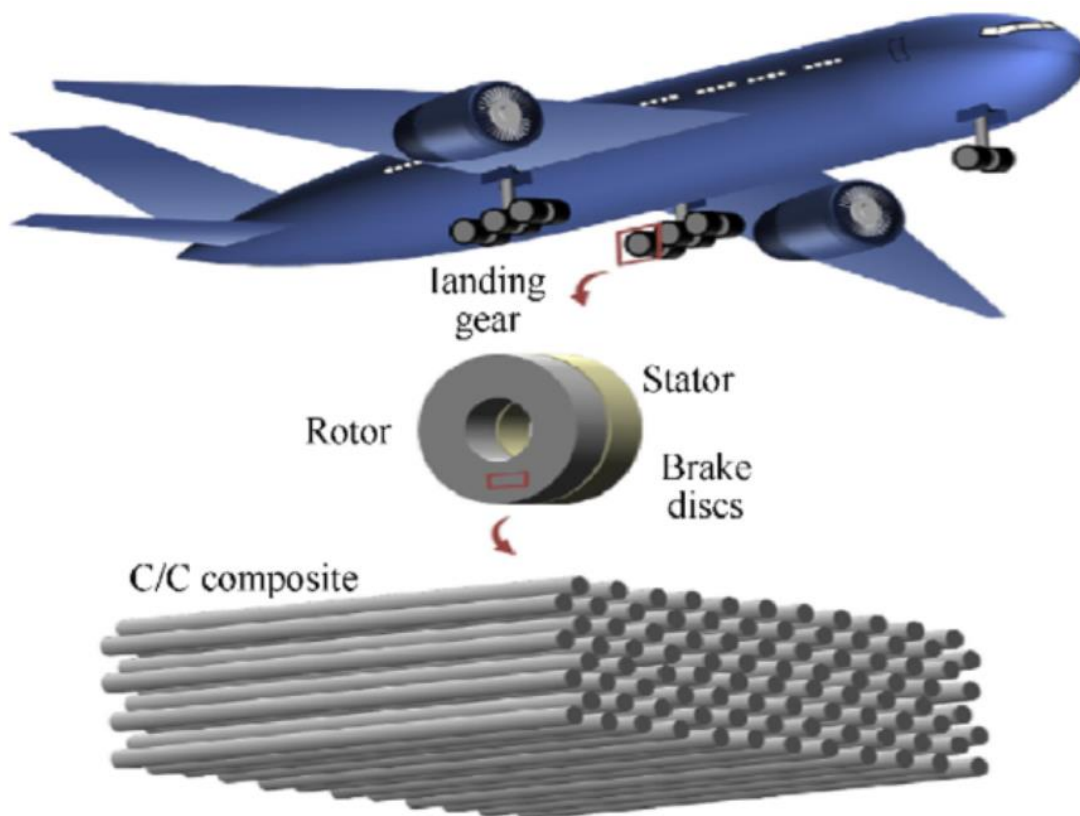


Figure 2.1. Landing gear brake discs constructed of carbon composite material for aircraft [2].



Figure 2.2. Ivan-30 (Catamaran yacht) made from carbon-epoxy composite [3].

Composite materials exhibit complex mechanical behaviors, and this manufacturing can be expensive due to the need for complex production tools. Thus, it is crucial to know the mechanical behavior of these materials. Therefore, analysis of the composite materials is critical.

Table 2.1. Typical mechanical properties of fibers

Fiber	Mechanical Properties		Reference
	Tensile Strength	Elastic Modulus	
	(GPa)	(GPa)	
E-glass	3.8	75	[4]
S-glass	4.5	85	[4]
P-25 Carbon	1.38	159	[5]
P-120 Carbon	2.41	827	[5]
XN-50A Carbon	3.83	520	[5]
Flax	0.457	41.6	[6]

Table 2.2. Typical mechanical properties of matrices

Matrix	Mechanical Properties		Reference
	Tensile Strength	Elastic Modulus	
	(MPa)	(GPa)	
Epoxy	6.2 - 103	2.8 - 3.4	[7]
Polyimide	55 - 110	3.2	[3]
Polyester	21 - 69	3.4 - 5.6	[7]
Polysulfone	69	2.8	[7]
PEEK	90-100	3.1 - 3.8	[3]
Al 1024	414	72	[7]

2.2. Finite Element Method

Examining the mechanical behavior of materials using analytical methods can be practically impossible due to having to solve complex partial differential equations. Therefore, numerical methods are developed. Finite element method (FEM) is a numerical method aiming to approximate the analytically challenging distribution of field variables in the application. FEM divides the problem domain into numerous elements and performs a solution to each element [8]. Solving a problem by using FEM is illustrated in (Figure 2.3).

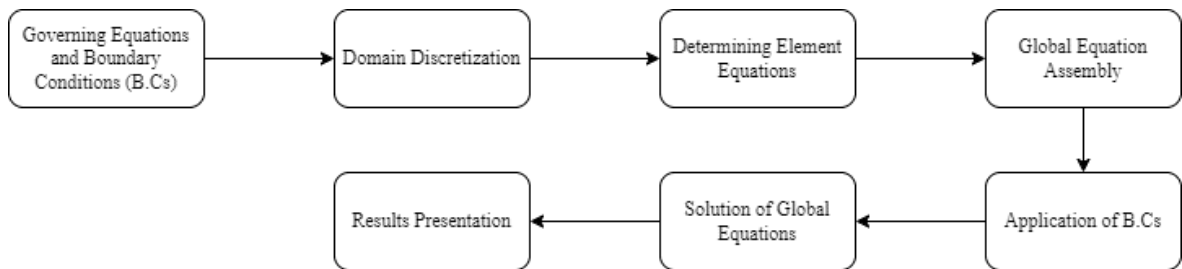


Figure 2.3. Finite element method schematic

Governing Equations and Boundary Conditions

The differential equations that govern the behavior and the related boundary condition must be determined in order to achieve an approximate solution for the problem. The behavior of the problem can be explained via mathematical modeling. Afterward, the approximate finite element formulation can be used.

Domain Discretization

The entire solution domain of the problem is divided into small elements in this step. It is called meshing. Care must be taken to use sufficient elements to obtain the behavior of the solution. Although a larger number of elements in smaller sizes provides better convergence to the result, it increases computation time to solve the problem. Therefore, attention should be paid to the balance between for the solution domain.

Determining Element Equations

The algebraic equations that must be solved for each element are created after the meshing is complete. The form of these equations are all the same for every element.

Global Equation Assembly

Combining the created element equations creates a system of equations for the solution domain. Interelement continuity conditions are identified between primary variables by associating element nodes with global nodes. Between secondary variables, the equilibrium conditions are identified. Then, elements are assembled.

Application of Boundary Conditions

Constraints necessary to solve the boundary value problem are defined.

Solution of Global Equations

The system of equations is solved. Depending on the problem type, numerous differential equations are approximated.

Results Presentation

In this step, the results are represented in tabular and/or graphical form.

2.3. Macro-Scale and Micro-Scale Analysis

Analysis of composite materials has been studied in the literature for many years. At first, macro-scale methods in which the fiber and matrix properties are combined using analytical methods. Various methods have been used in the literature to analyze UD composite materials in macro-scale. Although in the fiber direction, due to fibers having very high stiffness and strength values, their properties can be predicted with these theories; under transverse loading, prediction of these behaviors are challenging. The properties of the matrix material dictate the failure mode of these UD composites under transverse loading. Rule of mixtures, one of the most used theory in homogenization methods, given in equation (2.1), is a weighted mean of a material property according to the material volume fractions.

$$E_c = fE_f + (1 - f)E_m \quad (2.1)$$

$$f = \frac{V_f}{V_m + V_f} \quad (2.2)$$

Where E_c , E_f and E_m are Young's moduli of the composite, fiber and matrix, respectively for transverse loading. f is the volume fraction (2.2), where V_f and V_m are the volume fraction of fiber and matrix, respectively.

Halpin-Tsai model [9] is commonly used to predict the effective stiffness for fiber reinforced composites. Although the model predicts stiffnesses very well at low-volume fractions, it cannot sufficiently predict some stiffnesses at high-volume fractions. Common form is given in equation (2.3)

$$\frac{P}{P_m} = \frac{1 + \xi\zeta V_f}{1 - \eta V_f}, \eta = \frac{(P_f/P_m) - 1}{(P_f/P_m) + \zeta} \quad (2.3)$$

Where ζ is the measure of the reinforcement geometry, ξ is the reinforcement parameter, P , P_f and P_m are the properties of the composite, fiber and matrix, respectively.

Chamis model [10] gives formulation for all five independent elastic properties, longitudinal and transversal Young's moduli E_{11} and E_{22} , major Poisson's ratio ν_{12} , longitudinal and transversal shear moduli G_{12} and G_{23} . In this model square root of the fiber volume fraction is used to calculate shear and transverse elastic properties.

Mori-Tanaka [11] developed a model which is widely used for modeling different kinds of composite materials. In this model, inclusions are buried in a homogeneous medium to simulate fibers. Hill [12] and Budianski [13] proposed an iterative model called the self-consistent model (S-C) to predict the elastic properties of composite materials reinforced by isotropic spherical fibers.

Composite materials have weak properties under transverse loading. Hence prediction of these properties, especially failure behavior, is complex and challenging. It is known that the properties of matrix material dominate the failure mode of the UD composites. These failure modes are generally fiber-debonding and matrix cracking (**Figure 2.4**). Prediction of these cannot be made accurately with homogenized properties.

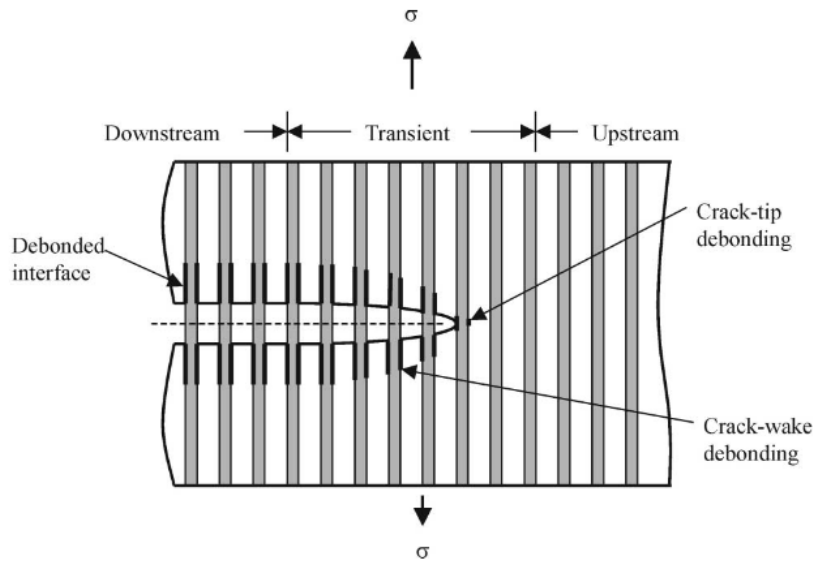


Figure 2.4. Crack-tip and crack-wake debonding schematic representation [14].

For composites, if the fiber and matrix properties are modeled separately, it is called micro-scale as the fibers have dimensions in microns. In particular, the finite element approach has become the predominant method for micro-scale analysis (**Figure 2.5**, **Figure 2.6**) [15-18].

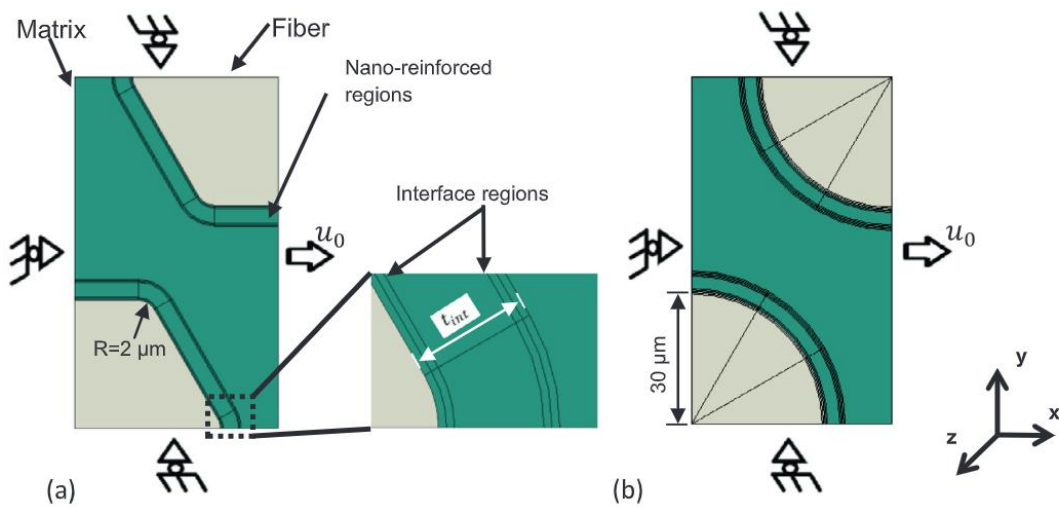


Figure 2.5. Nano-reinforced interphase around fibers having (a) hexagonal; (b) circular cross-sections [16].

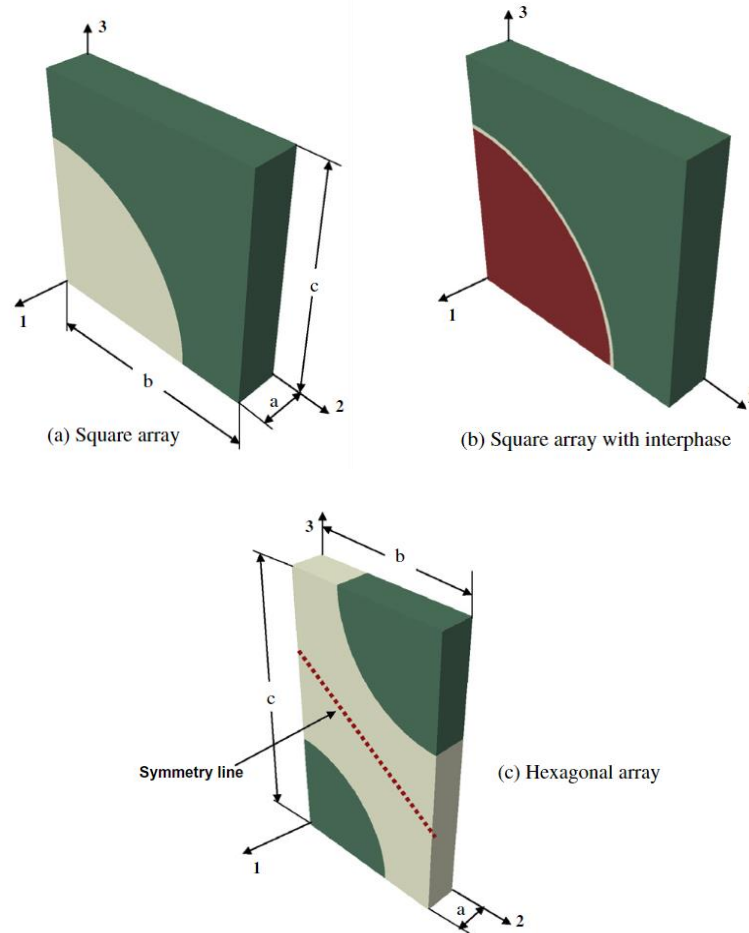


Figure 2.6. Unit cell quadrants of square and hexagonal array for finite element analysis [18].

Many studies to predict the stresses and failures have been done in micro-scale in the literature. While modeling composites, the distribution of these fibers significantly affects the distribution of stresses in the matrix. Regular packings such as square or hexagonal packing (**Figure 2.7**) [19-21] cannot reflect composite distributions properly. Therefore, different algorithms and techniques were developed to generate randomly distributed fibers in the matrix [22]. Randomly distributed fibers with the periodic structure are generated with material input parameters, such as fiber diameter, representative volume element (RVE) size, and fiber volume fraction (**Figure 2.8**). Melro et al. [23] presented a new constitutive damage model for an epoxy matrix on micro-mechanical analyses of polymer composite materials. The algorithm developed by Melro et al. [22] was used for random microstructure generation. Periodic boundary conditions (PBCs) were applied to

the RVEs [24]. Different fiber distributions with different fiber volume fractions were analyzed throughout the study (Figure 2.9).

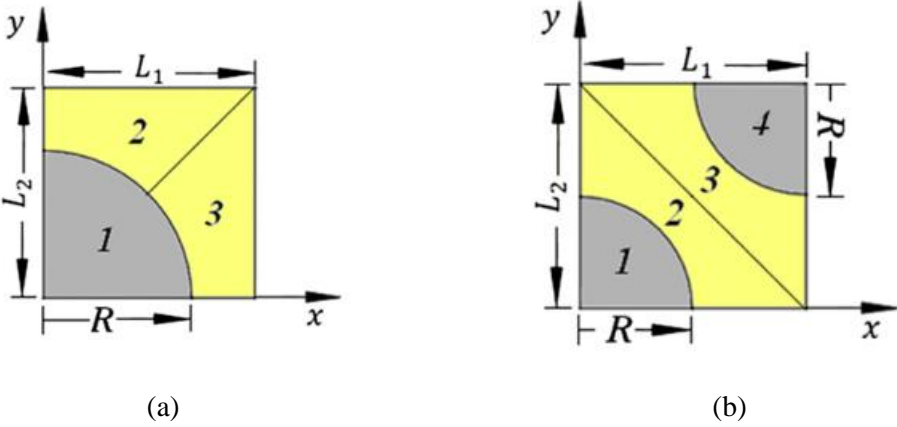


Figure 2.7. (a) Square RVE, (b) Hexagonal RVE [25].

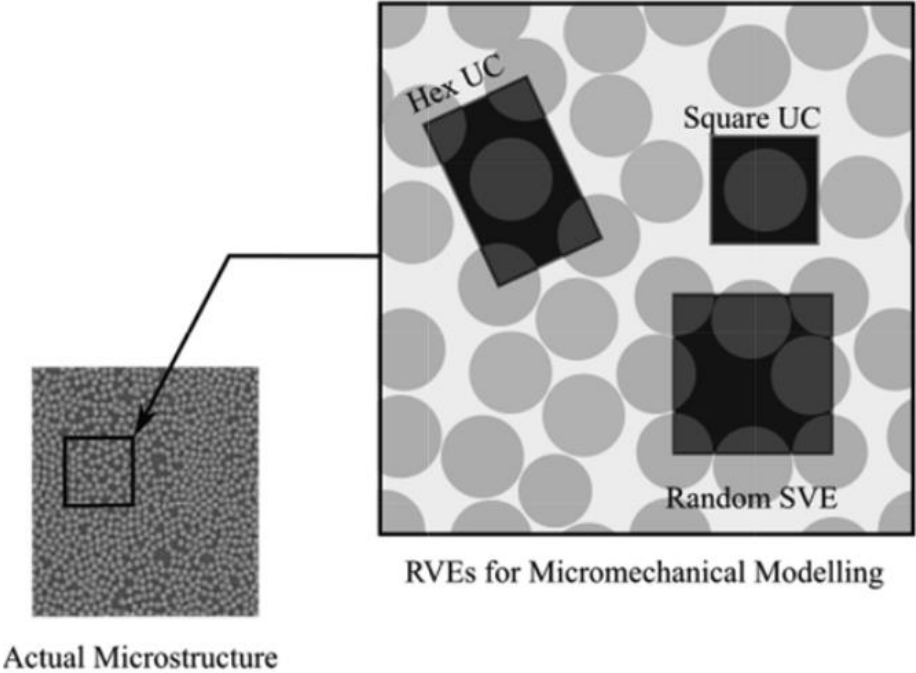


Figure 2.8. RVE models graphical illustration [26].

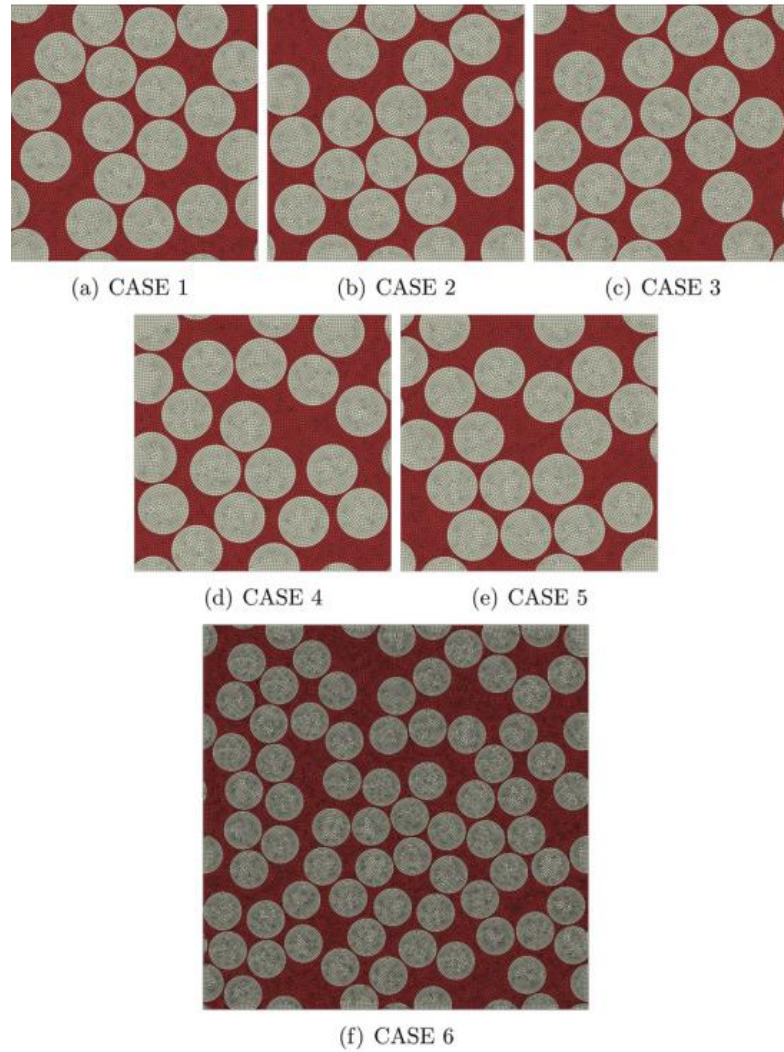


Figure 2.9. Generated RVEs and mesh structure [23].

Danzi et al. [27] performed a finite element micromechanical study of carbon/epoxy material (**Figure 2.10**). Because of the small thickness of the inter-phase with respect to fiber and matrix dimensions, they proposed 3-D cohesive elements governed with a traction separation constitute behavior to this critical zone in the model.

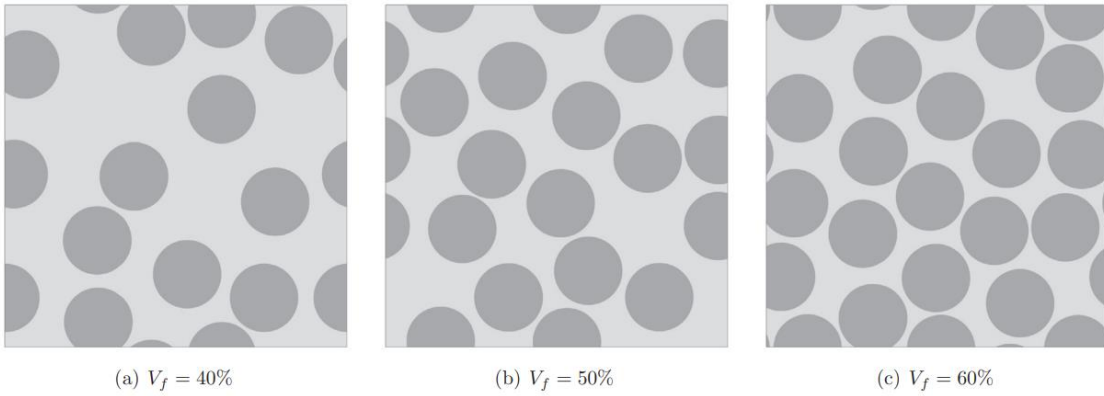


Figure 2.10. Fiber distribution examples for different volume fractions [27].

To effectively simulate the interaction between constituents, there should be continuity between discretized elements. Providing continuity does not become an issue when simple-shaped materials are used. An example of mesh structure with a circular cross-section is given in **Figure 2.11**.

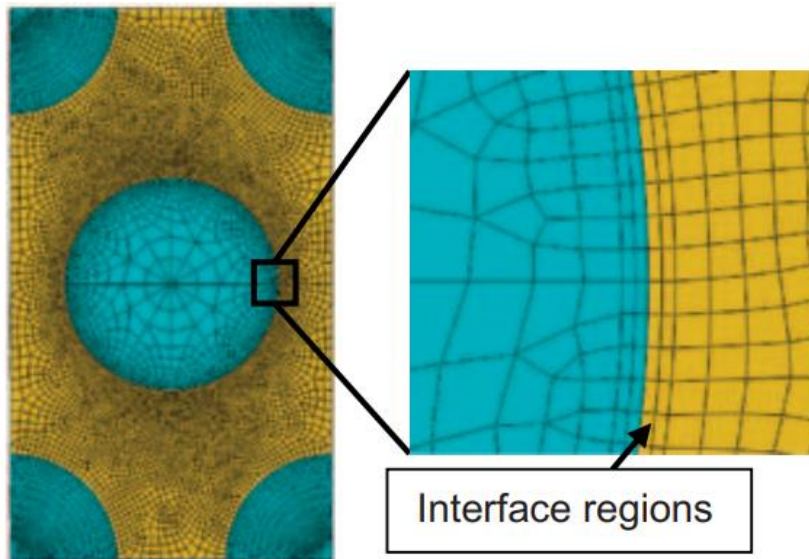


Figure 2.11. Mesh structure for a circular cross-section model [17].

Sabuncuoglu et al. [16] evaluated the effect of nano-reinforced interphase on the stress concentration. Study was carried out using FEM, in micro-scale. Intermediate homogenization step was used to obtain elastic properties of the nano-reinforced interphase.

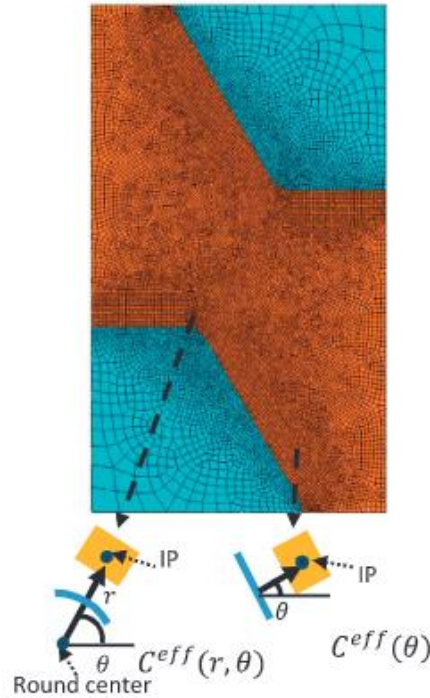


Figure 2.12. Mesh structure of the hexagonal model [16].

Under quasi-static tensile loading, De Greef et al. [28] investigated at how carbon nanotubes affected the initiation and progression of damage in woven carbon fiber/epoxy composites.

2.4. Statistical Analysis of Composite Materials

The previous section states that fibers are randomly distributed with an algorithm through the matrix while modeling the composite. Therefore, with each run, they are generated in different locations. Statistical analysis is required to understand the stresses and concentrations caused by the chosen material attributes.

In order to understand the mechanical behavior of composites, various types of statistical analysis were performed. Seung-Pyo Lee et al. [29] used the homogenization method and Monte-Carlo simulation to probabilistically estimate the equivalent properties of glass fiber-reinforced composite materials. The Monte-Carlo methods are an algorithm that depends on repeated random sampling to obtain numerical results. The core is to use randomness to find deterministic solutions to the problem. In this study, the mechanical properties of composite materials are treated as probabilistic instead of deterministic. Firstly, a randomly distributed set of basic properties of fiber and matrix is generated. Then, calculations based on the homogenization method using the generated properties

are done. Lastly, the probability is determined from a large number of repetitions. A linear correlation analysis was done between the constituent's basic properties (**Figure 2.13**). However, in the study, a micromechanical model with periodic fiber arrangement was used (**Figure 2.14**).

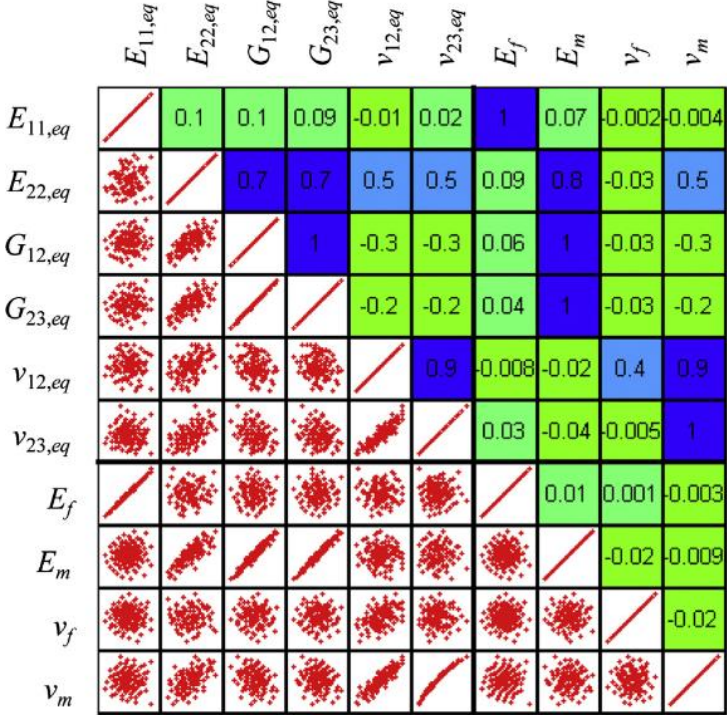


Figure 2.13. Linear correlation results for constituent's basic properties [29].

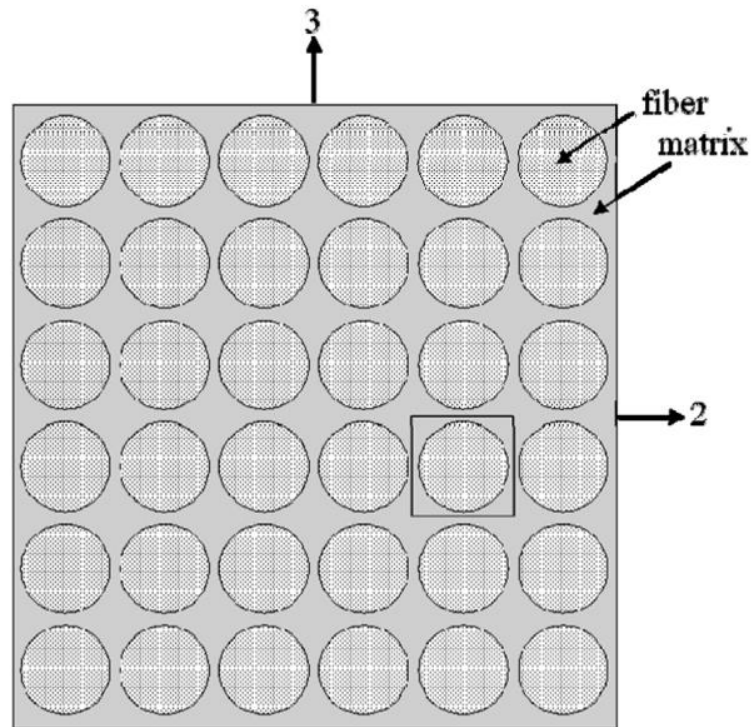


Figure 2.14. Square-packed array unit cell [29].

Wu et al. [30] studied discontinuous fiber-reinforced composite under thermal and mechanical loads. RVE was created with respect to the 3D X-ray CT image of the composite (**Figure 2.15**). Therefore, the effect of the randomness of the fiber distribution is excluded from the analysis. The probability density functions (PDF) of Von Mises stress (**Figure 2.16**) were compared. They showed that Von Mises stress on the fiber increases with Young's modulus of the resin where the fibers have a much higher Young's modulus than the resins. PDF represents a continuous random variable's density between a particular range of values.

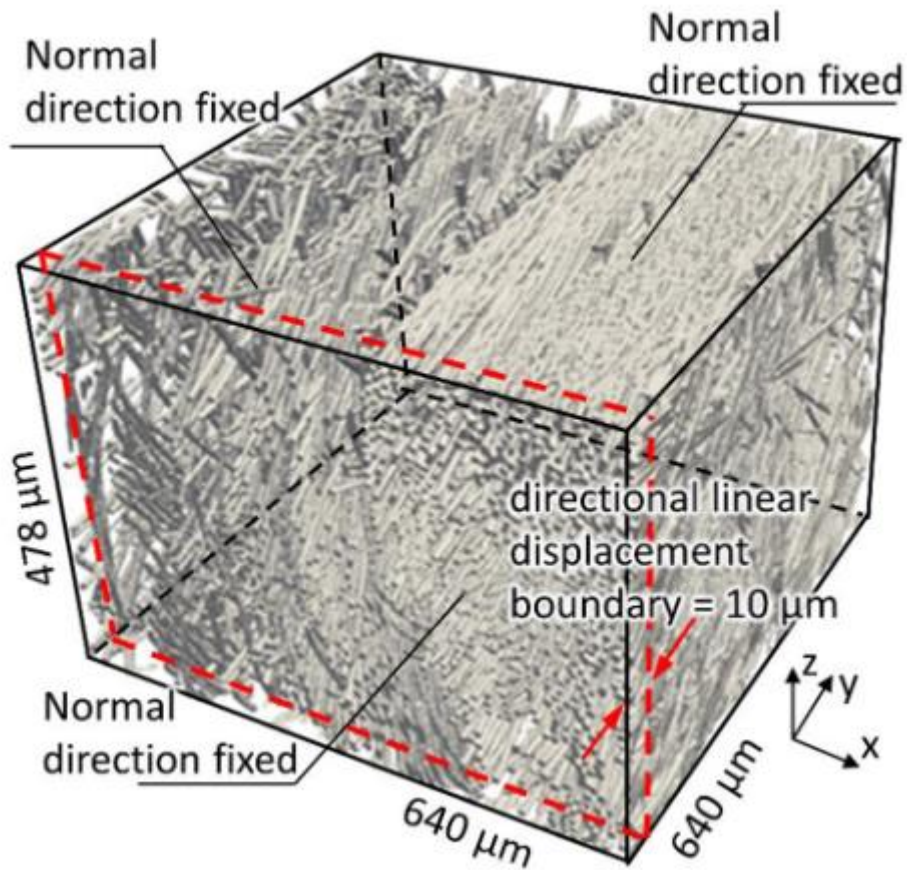


Figure 2.15. Finite element model of discontinuous fiber-reinforced composite [30].

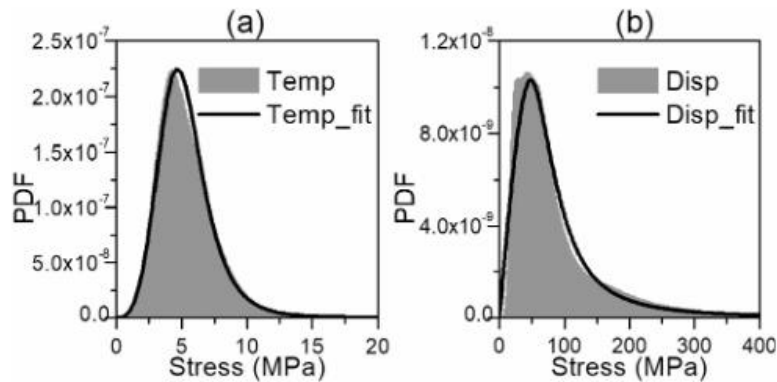


Figure 2.16. PDF of Von Mises stress on mechanical loading. [30]

Barbero et al. [31] presented a formulae based on Weibull statistics to analyze the variability of the composite material's mechanical properties. Based on two-parameter Weibull distribution, a three-parameter Weibull distribution is proposed for composite materials.

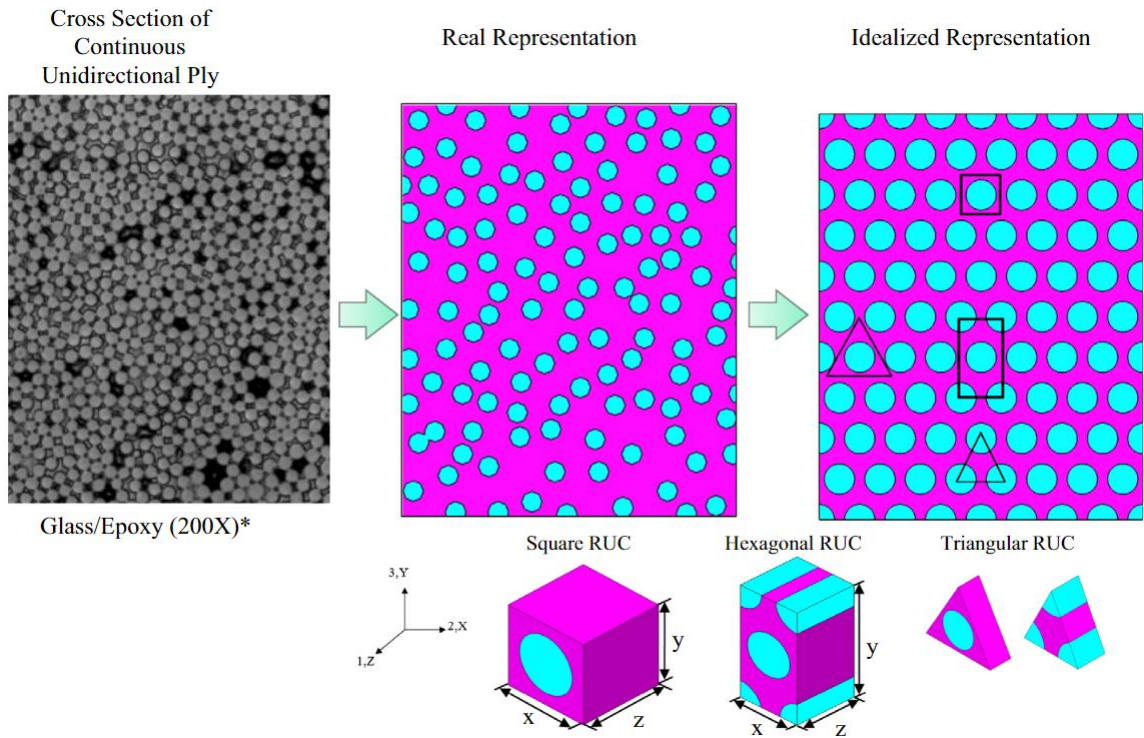


Figure 2.17. Unit Cell models used [32].

Mustafa et al. [32] presented an approach for stiffness properties prediction of composite materials used in wind turbine blades. For the estimation of composite equivalent properties, square and hexagonal unit cells were used (**Figure 2.17**). The results from the numerical analysis are compared with the modified rule of mixture method results and the test data (**Figure 2.18**). With the help of Monte Carlo simulation, a probabilistic analysis was performed. Monte Carlo simulation was coupled with a homogenization-based stiffness calculation procedure. First, random variables for unidirectional properties of fiber and matrix were generated via the Latin Hypercube Sampling method. Secondly, they simulated the UD properties against each set of realizations using the representative unit cell and homogenization method. Last, statistical response sensitivities of the output response parameters were calculated (**Figure 2.19**). The method was then applied to a 5 MW wind turbine blade structural analysis. The study concluded that the sensitivity analysis highlights the most influenced input properties of the composite. Therefore, unimportant variables can be disregarded from the designer's analysis to reduce the time and expensive testing for these parameters. However, an idealized fiber distribution is used in the analysis to reduce the computation time.

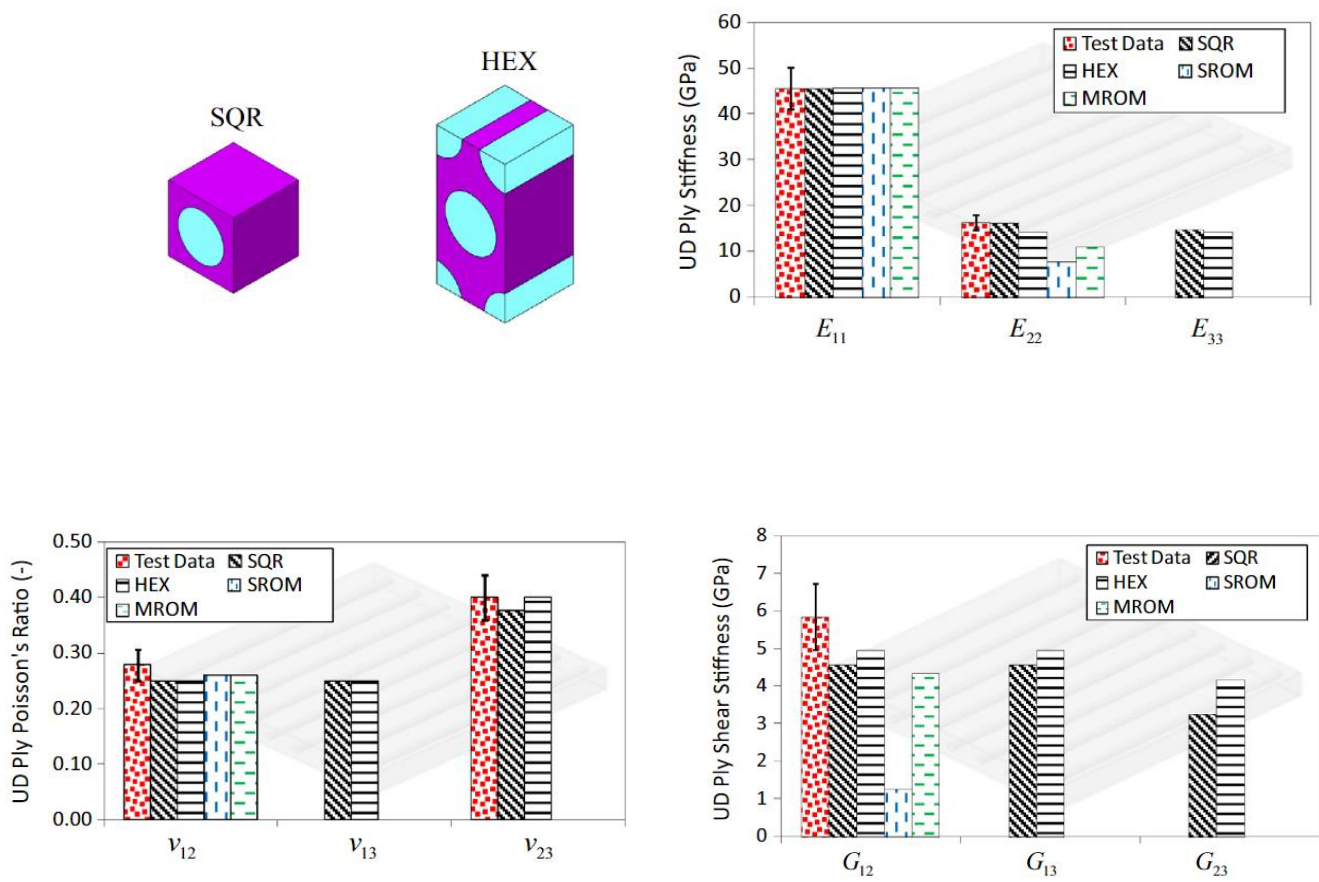


Figure 2.18. Stiffness properties comparison for hexagonal unit cell (HEX), square unit cell (SQR), Simple Rule of Mixture (SRM), Modified Rule of Mixture (MROM) and test data [32].

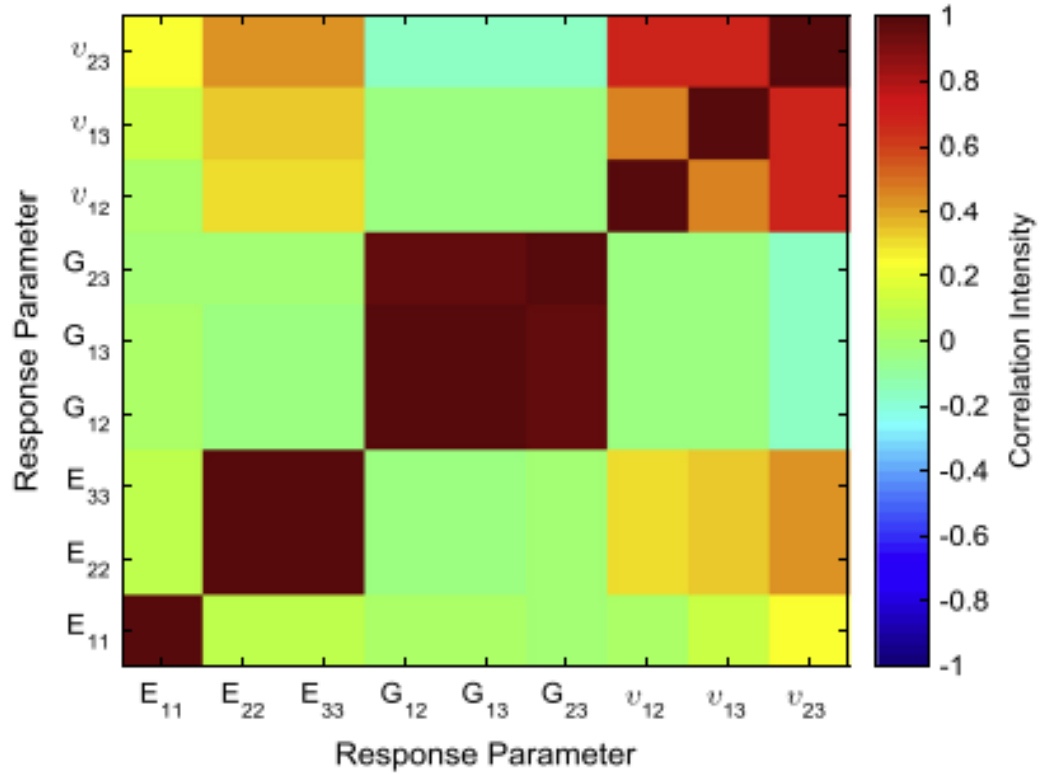


Figure 2.19. Spearman Rank Order correlation coefficient matrix [32].

In this study, the effect of material parameters on the micro-scale stress distribution in fiber reinforced composites in transverse loading is statistically determined via a commonly known statistical analysis method called parametric correlation. This method reveals the relation between the design inputs and stress concentration outputs by calculating correlation values that show their level of effect on each other. In order to reduce the workload, glass fiber was chosen as the fiber material.

3. MONTE-CARLO AND PARAMETRIC CORRELATION METHODS

In this thesis, Monte-Carlo simulations were used for the sensitivity analysis. Monte Carlo simulations use random distributions to find a solution to mathematical problems. An example of Monte Carlo simulation is given below (**Figure 3.1**).

To compute the value of π ;

- In a square domain, define a circle.
- Generate random points lying inside the square domain and count the points that lie in the circle.
- The ratio of the number of points inside the circle to the total number of points generated is the $\pi/4$. [33]

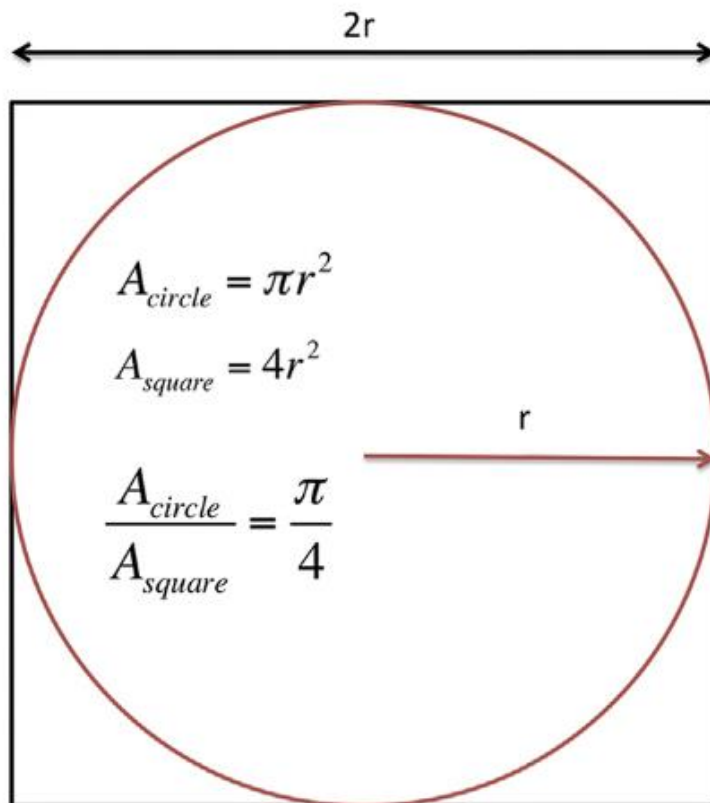


Figure 3.1. Monte Carlo simulation example [33].

Monte Carlo methods are widely used in the simulation of physical, chemical, and biological systems [34]. In engineering, Monte Carlo methods are widely used for

sensitivity analysis. As described, Monte Carlo methods use random numbers. Therefore, a source of random numbers is required [35]. In this thesis, random numbers are generated from fibers Young's modulus values. A more detailed explanation was given in the following chapters.

After performing the Monte Carlo method, results need to be examined. Moreover, the relation between design inputs and the mechanical behavior of the composite is analyzed in this thesis. Therefore, the correlation between these parameters are used in this thesis study. Correlation is an analysis that measures the degree of the relation between two variables. The relationship is measured as a correlation coefficient. The value of the correlation coefficient varies between -1 and $+1$, where the ± 1 value indicates perfect relation between the two variables. $+$ and $-$ signs indicate a positive and negative relationship, respectively (**Figure 3.2**). There are different types of correlation methods, such as Pearson correlation, Kendall rank correlation, and Spearman correlation.

Correlation methods can generally be divided into parametric and non-parametric correlation. Depending on the data, a particular statistical method should be used. Parametric correlation assumes that the used data corresponds to a specific distribution (such as Gaussian distribution, Weibull distribution) (**Figure 3.3**).

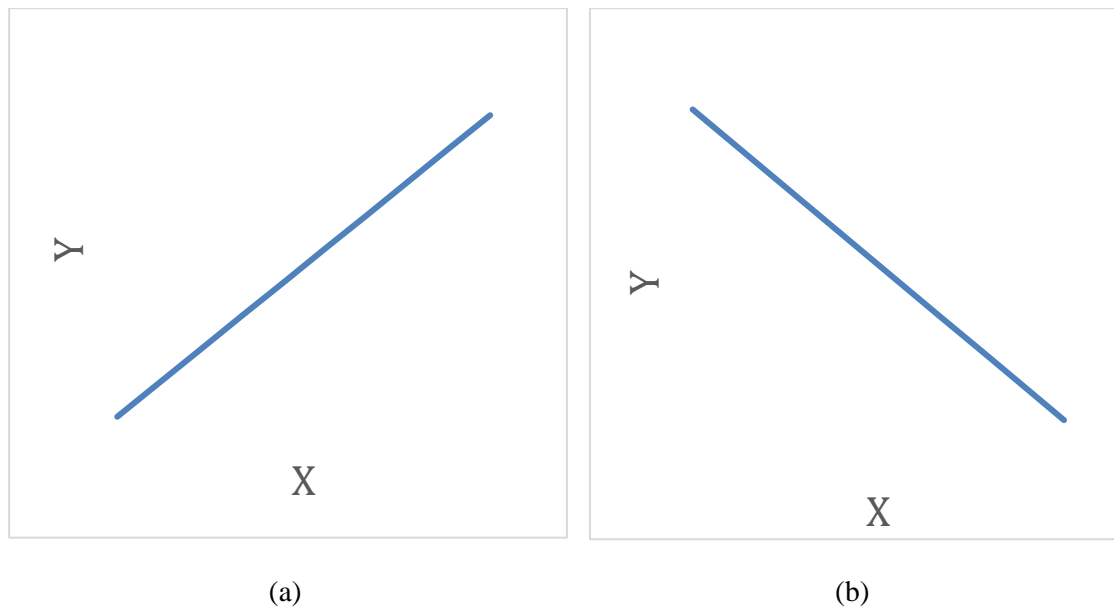


Figure 3.2. (a) $+1$ correlation coefficient example, (b) -1 correlation coefficient example.

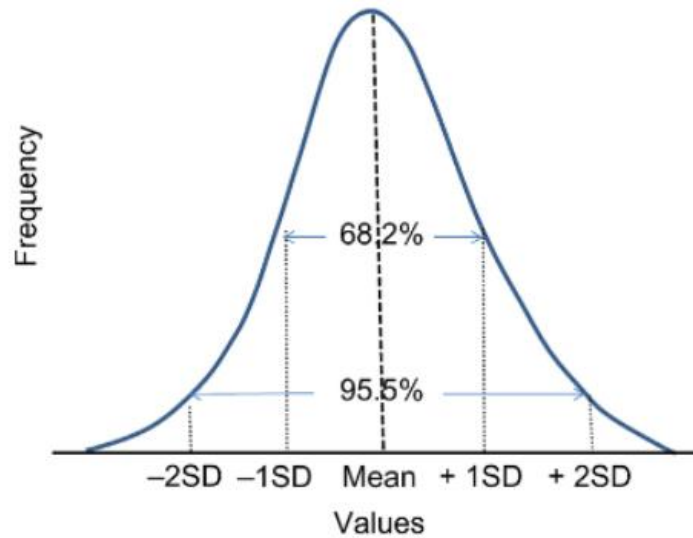


Figure 3.3. Normal (Gaussian) distribution [36].

3.1. Pearson Correlation

The Pearson correlation coefficient (r) is one of the most used methods to measure a linear correlation. It is also known as, the correlation coefficient, Bivariate correlation. It describes the relation and direction of the linear relationship between the two variables. If the r value is between 0 and 1, when one of the corresponding variables changes, the other variable changes in the same direction. If the r value is 0, there is no relation between the related variables. If the r value is between 0 and -1, when one of the corresponding variables changes, the other variable changes in the opposite direction. +1 and -1 indicate a perfect positive and negative association, respectively. A general rule of thumb rules for the r value is given in **Table 3.1**.

Table 3.1. General Rule of Thumb for r values

r value	Relation	Direction
$0.5 < r$	High	Positive
$0.3 < r \leq 0.5$	Moderate	Positive
$0 < r \leq 0.3$	Low	Positive
0	No Relation	No Relation
$0 > r \geq -0.3$	Low	Negative
$-0.3 > r \geq -0.5$	Moderate	Negative
$-0.5 > r$	High	Negative

r can be calculated via the following Eqn. 3.1

$$r = \frac{n \sum xy - (\sum x) - \sum(y)}{\sqrt{[n \sum x^2 - (\sum x)^2][n \sum y^2 - (\sum y)^2]}} \quad (3.1)$$

where n is the sample size, x and y are the variables investigated.

Pearson correlation coefficient gives accurate results if the following are met:

1. The relationship between the variables is linear.
2. All of the data has similar pattern.
3. Variable data are approximately normally distributed.
4. Both variables are quantitative.

3.2. Spearman Correlation

Spearman's rank correlation coefficient (r_s) is the non-linear version of the Pearson correlation. As in Pearson correlation coefficient, +1 and -1 r_s value indicates perfect association, respectively, where 0 indicates no relation between variables.

As stated in the Pearson correlation coefficient, it is better to use Spearman's rank correlation:

1. If the relationship between the variables are non-linear
2. If all of the data does not have the same pattern.
3. Variable data are not normally distributed.
4. If the variables are ordinal.

r_s can be calculated via the following Eqn. 3.2

$$r_s = 1 - \frac{6 \sum d_i^2}{n(n^2 - 1)} \tag{3.2}$$

Where d_i is the difference between two ranks of each observation and n is the number of observations. An input-output graph is plotted after the sensitivity analysis to determine which correlation should be used. Although the input 1 (composite Young’s modulus ratio) - output (maximum stress concentration) graph (Figure 3.4) for only one RVE and matrix Young’s moduli value of 1 GPa shows a linear relation, the input 1 (composite Young’s modulus ratio) - output graph (Figure 3.5) for only one RVE and all matrix Young’s modulus values shows a non-linear relation. Therefore, Spearman’s Rank correlation is more convenient for the analysis since it is a non-linear correlation method. Also, input 2 (overstressed volume percentage) – output graph is given in (Figure 3.6). Therefore, Spearman’s Rank Correlation Coefficient will be used in the sensitivity analysis of the glass fiber reinforced composite due to input and output parameters have non-linear relation with each other.

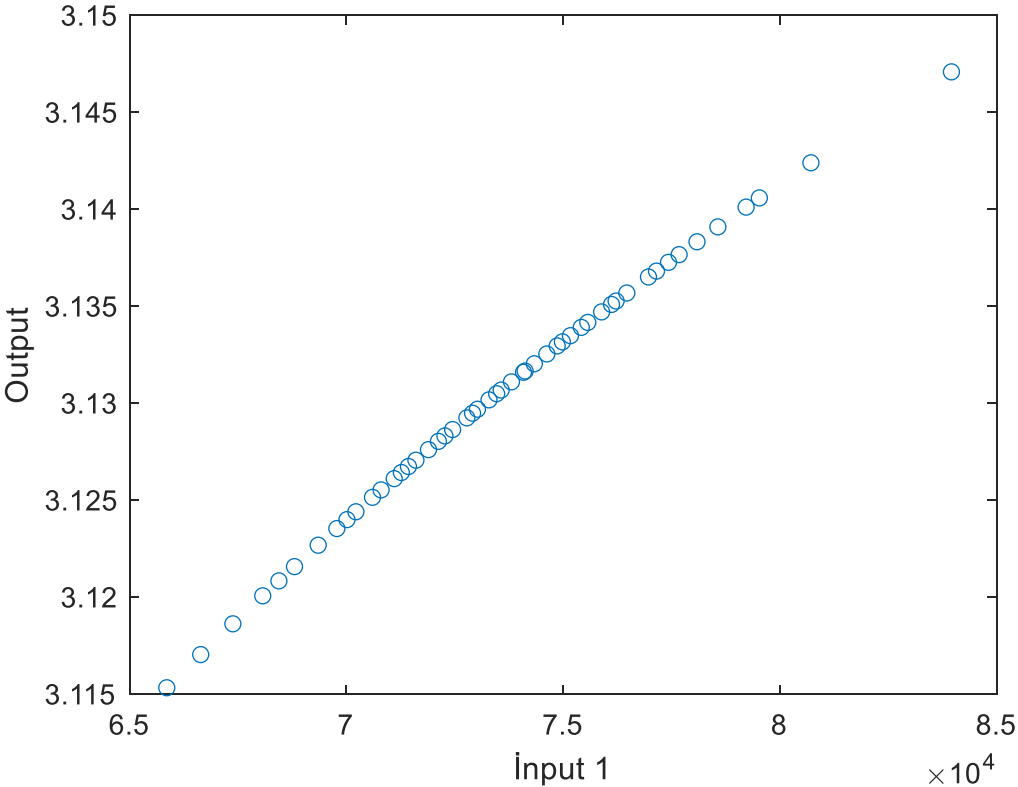


Figure 3.4. Input 1 - Output Graph for only 1 RVE and matrix Young’s moduli of 1 GPa.

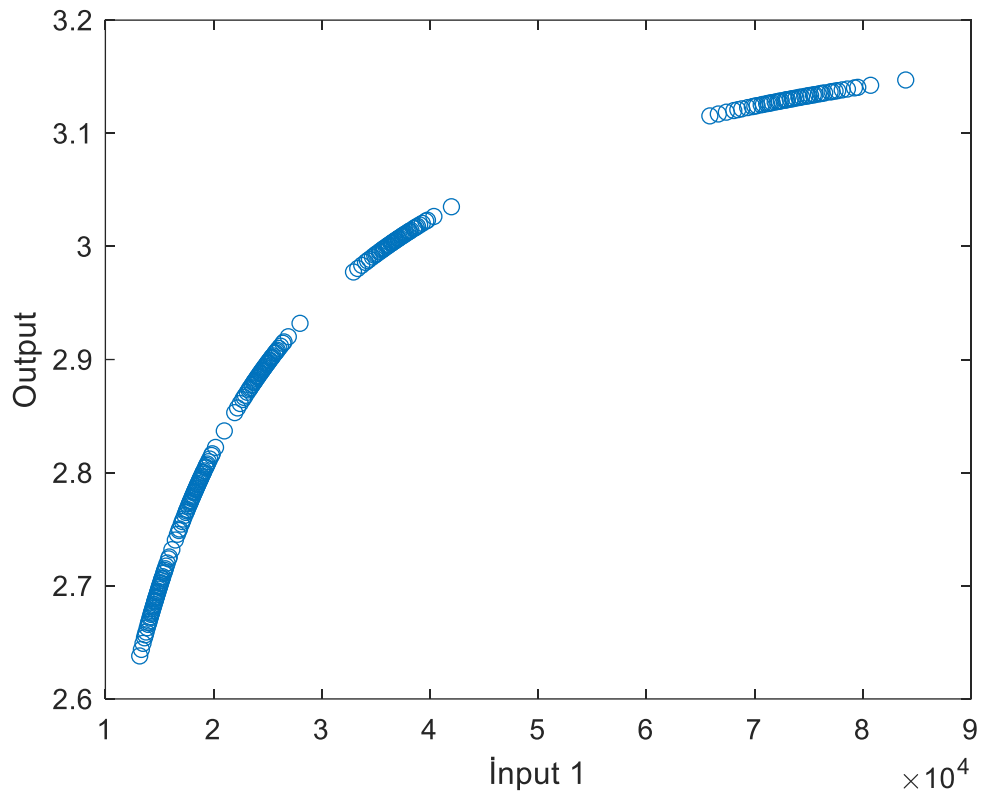


Figure 3.5. Input 1 - Output Graph for one of the RVE and all matrix Young's modulus values.

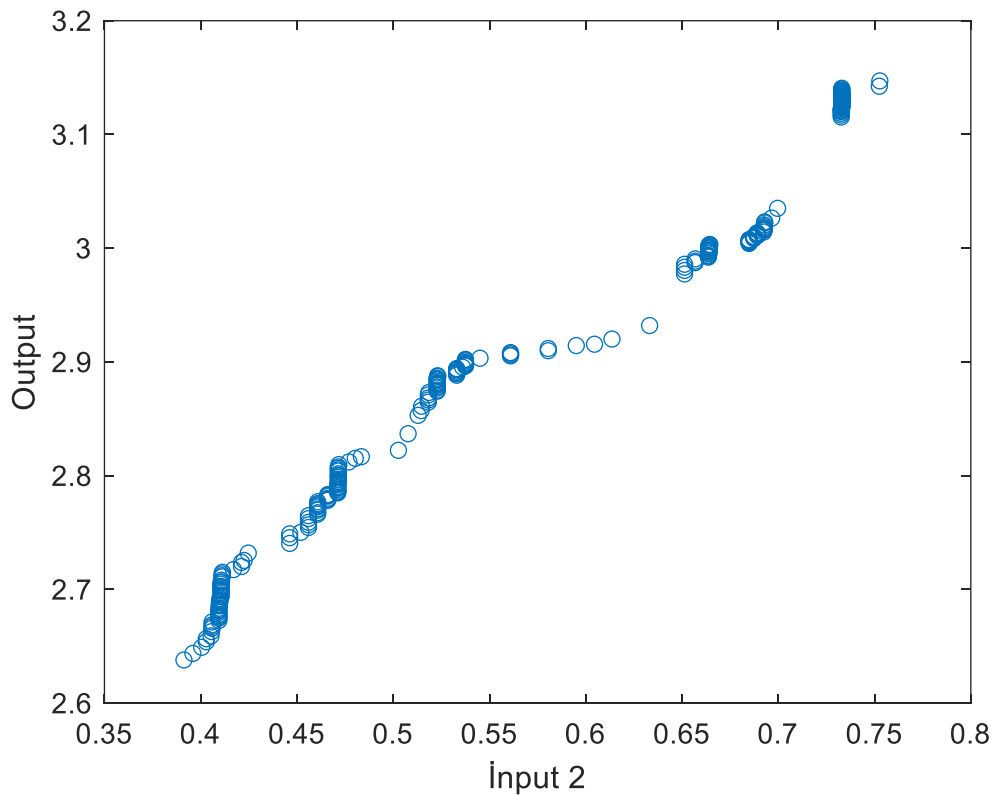


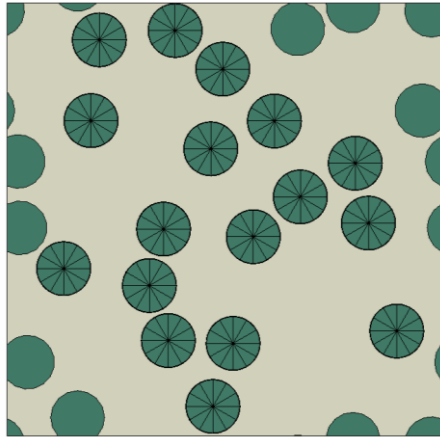
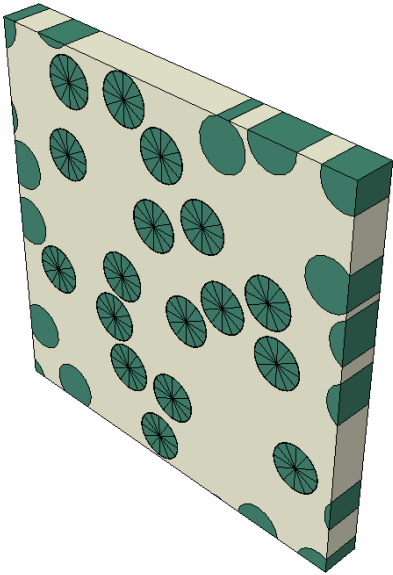
Figure 3.6. Input 2 - Output Graph for one of the RVE and all matrix Young's modulus values.

4. MICROMECHANICAL MODELS USED IN THE STUDY

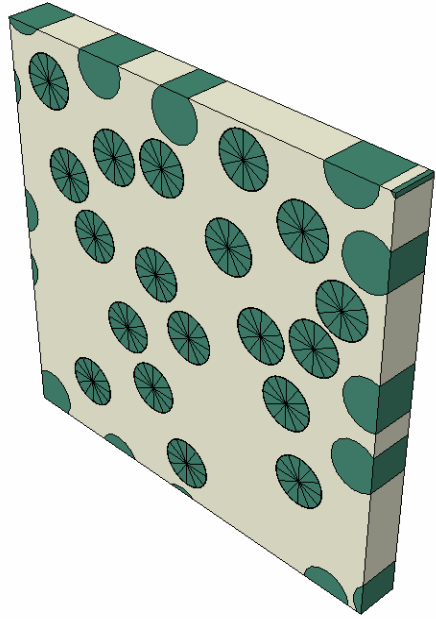
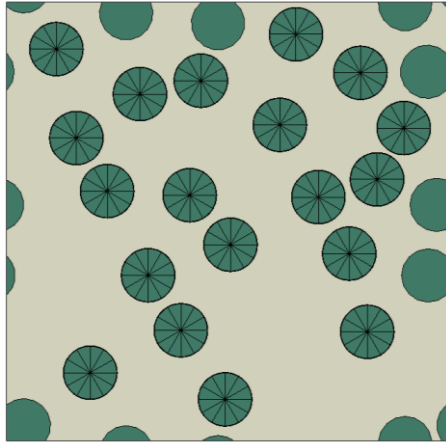
4.1. RVE Used in the Analysis

As mentioned in previous sections, all micromechanical models used in the study were generated with fibers randomly distributed in the matrix. Random microstructure generation (RMG, [22]) method was used to create fiber distributions. First, preliminary analyses were performed to see the effect of fibers Young's moduli (E_f) and matrix Young's moduli (E_m). Various RVE models with different fiber numbers and V_f values were modeled for preliminary analyses. A total of 9 different RVEs (**Table 4.1**) were modeled with corresponding fiber diameters, fiber numbers and V_f given in **Table 4.2**. An example of the RVE model with V_f value of approximate 0.45 can be seen in (**Figure 4.1**). RMG algorithm makes iterations to reach the requested V_f . Thus, the generated models V_f 's are not whole numbers. To represent the realistic behavior of the composites all models used in the sensitivity analysis includes 30 to 35 fibers [37]. The effect of fiber diameter was normalized due to RVE size automatically adjusted according to the fiber diameter and number of fibers. Isotropic material properties were assigned to glass fibers and the surrounding epoxy matrix.

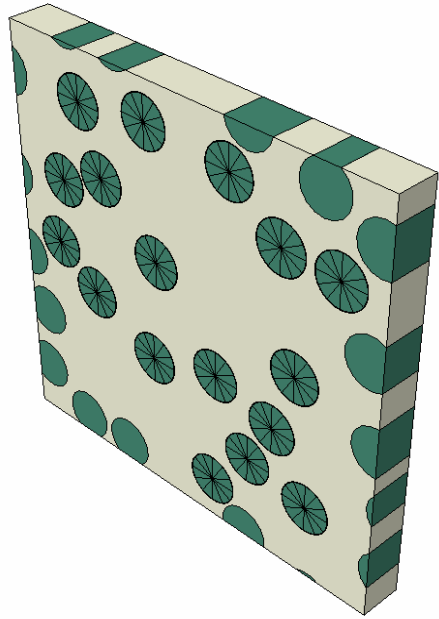
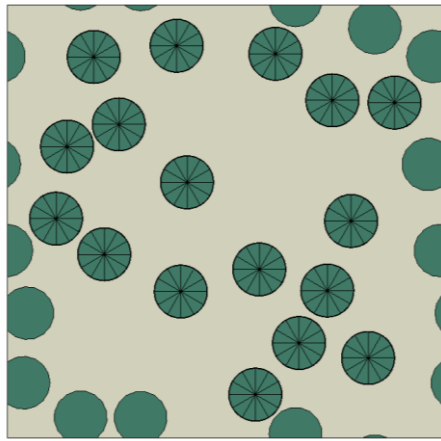
Table 4.1. RVE models used in the sensitivity analysis.

V_f	Front Face	Isometric View
0.30258		

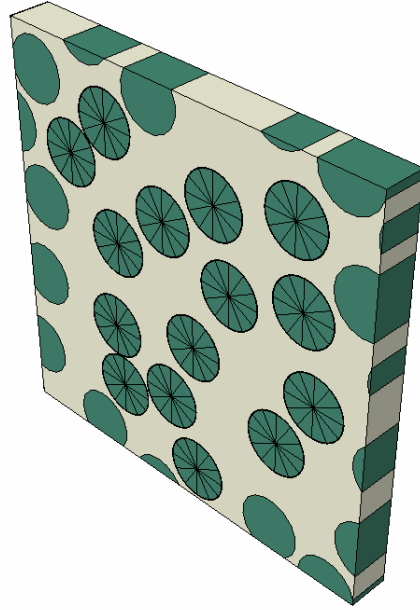
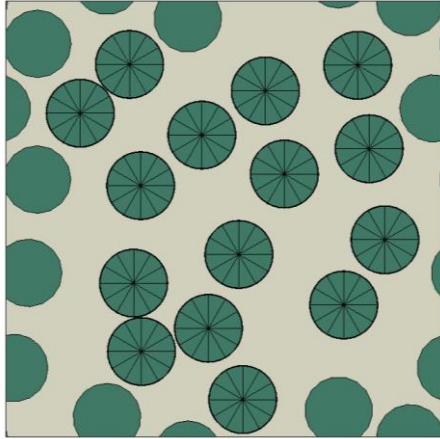
0.30279



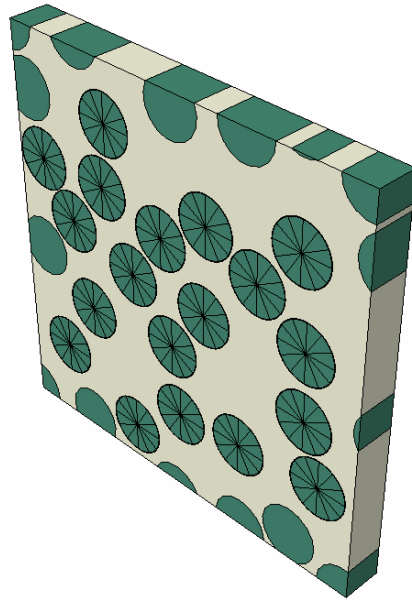
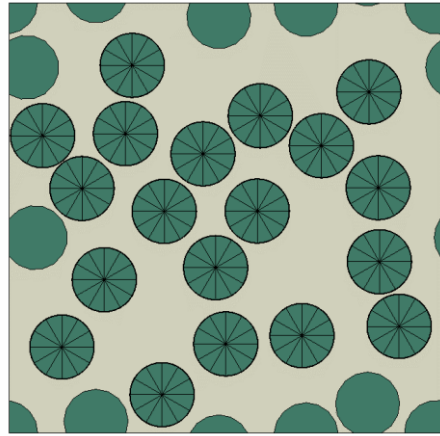
0.30423



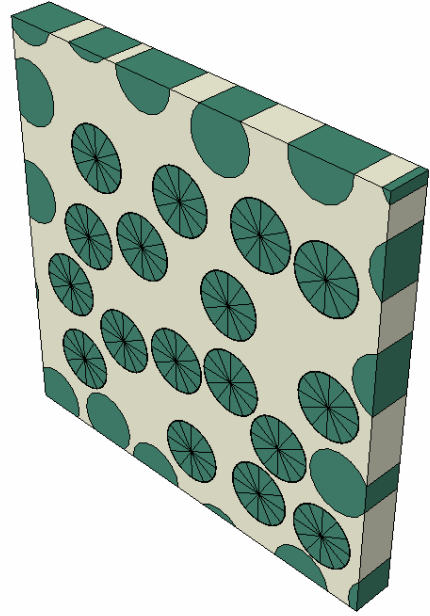
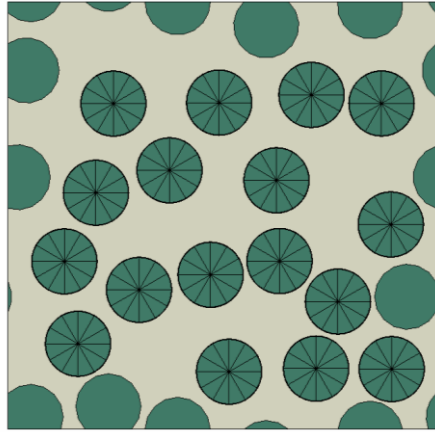
0.45368



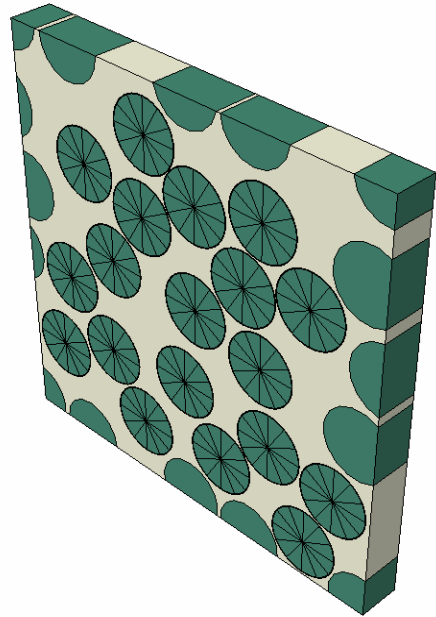
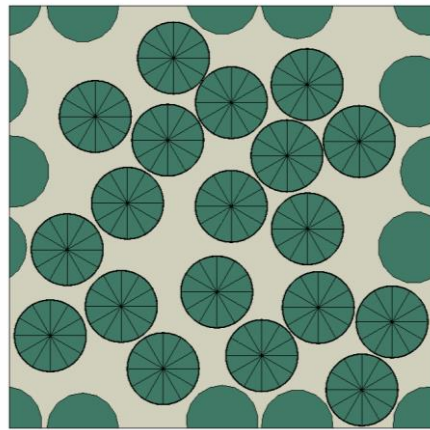
0.45437



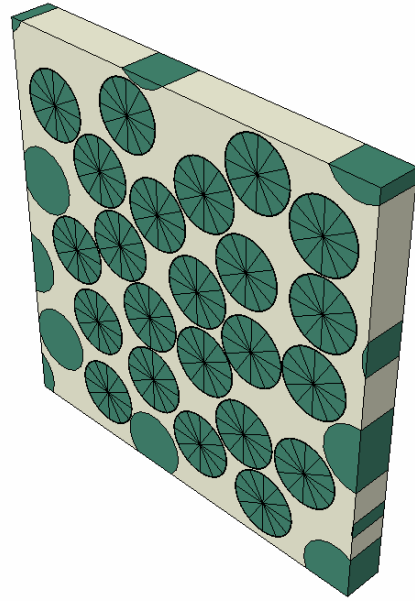
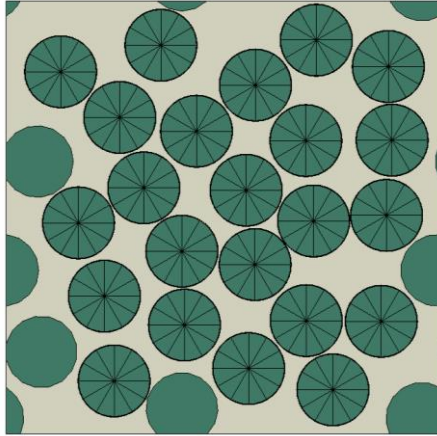
0.45689



0.58884



0.60410



0.61829

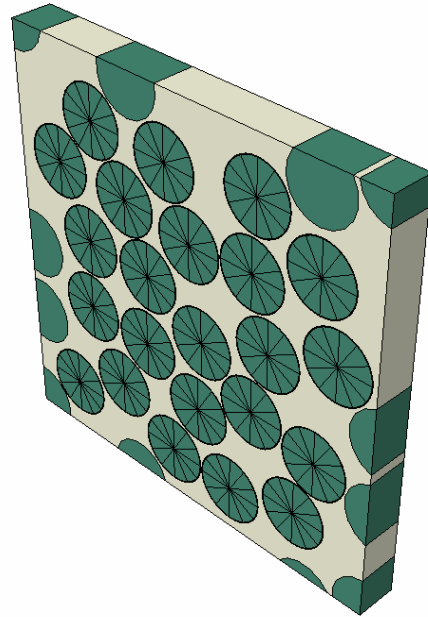
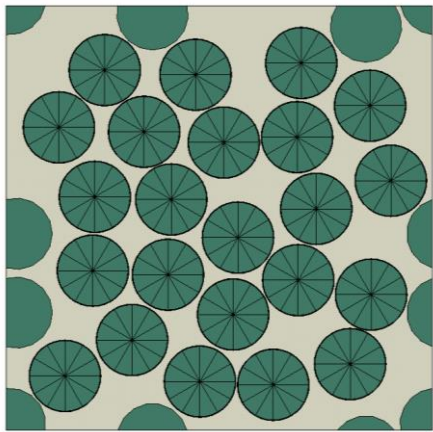


Table 4.2. RVE model properties used in the sensitivity analysis.

V_f	No. of fibers	d_f (μm)
0.30258	35	18.0
0.30279	35	17.9
0.30423	35	16.6
0.45368	35	16.6
0.45437	35	17.9
0.45689	35	18.0
0.58884	35	18.0
0.60410	35	17.9
0.63219	35	16.6

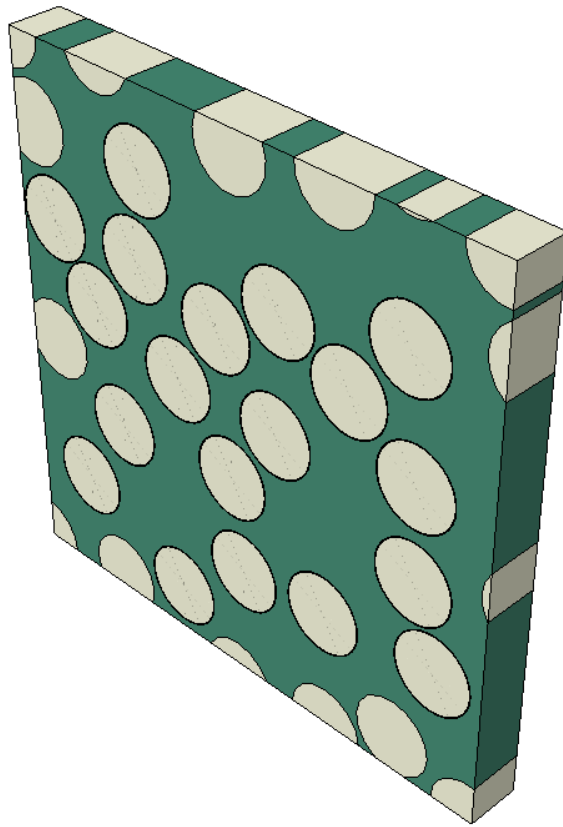


Figure 4.1. Example RVE model with $V_f = 0.45$.

Four-noded elements with a reduced integration scheme were used as these elements have shown accurate results [17]. In order to eliminate sudden stress jumps due to sudden changes in Young's modulus, relatively small elements are used in the fiber/matrix interface (**Figure 4.2**).

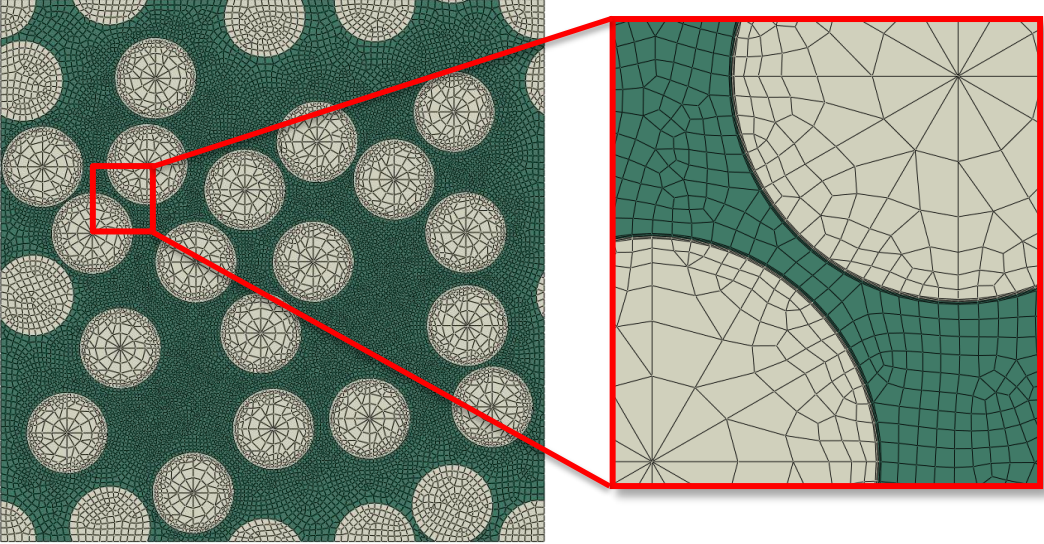


Figure 4.2. Example mesh structure used for the RVE model.

4.2. Application of Periodic Boundary Conditions

The position of the nodes are adjusted to be the same on the opposite sides to apply periodic boundary conditions (PBC, **Figure 4.3**) properly on the vertical and horizontal sides of the RVE.

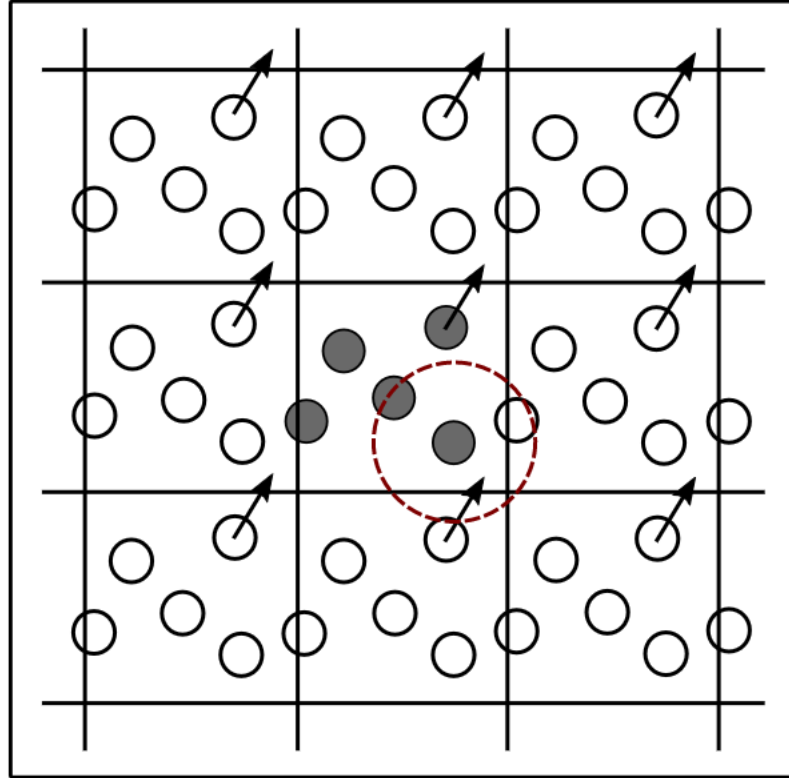


Figure 4.3. Graphical representation of PBC [38].

The mathematical explanation of PBC is as follows. The periodic structure's displacement field can be written as:

$$u_i = (x_1, x_2, x_3) = \varepsilon_{ij}^0 x_j + u_i^*(x_1, x_2, x_3) \quad (4.1)$$

where ε_{ij}^0 is the global strain tensor, $\varepsilon_{ij}^0 x_j$ is the linear distributed displacement field and $u_i^*(x_1, x_2, x_3)$ is the periodic function that runs from one unit cell to the next and represents a modification to the linear displacement field brought on by the composite's heterogeneous nature. Periodic array of the repeated unit cell represents a continuous physical body. Therefore, two continuities must be satisfied at the boundaries of the adjacent unit cells. The displacement must be continuous, and that the traction distributions at a unit cell's opposing parallel boundaries be identical. In equation (4.1) the latter assumption is not satisfied. The opposite boundary surfaces of each unit cell

must be observed in parallel pairs, and the displacement between them can be expressed as follows:

$$u_i^{k+} = \varepsilon_{ij}^0 x_j^{k+} + u_i^* \quad (4.2)$$

$$u_i^{k-} = \varepsilon_{ij}^0 x_j^{k-} + u_i^* \quad (4.3)$$

where k^+ and k^- depict the k^{th} couple of two opposite parallel boundary surfaces of a repeated unit cell. Since $u_i^*(x_1, x_2, x_3)$ is the same at two parallel boundaries, the difference between equation (4.2) and equation (4.3) is

$$u_i^{k+} - u_i^{k-} = \varepsilon_{ij}^0 (x_j^{k+} - x_j^{k-}) = \varepsilon_{ij}^0 \Delta x_j^k \quad (4.4)$$

where Δx_j^k is constant for each pair of parallel boundary surfaces with specified ε_{ij}^0 , the right side of the equation becomes constants. Equation (4.4) does not guarantee traction continuity conditions. Traction continuity condition is

$$\sigma_n^{k+} - \sigma_n^{k-} = 0, \sigma_t^{k+} - \sigma_t^{k-} = 0 \quad (4.5)$$

where σ_n and σ_t are normal and shear stresses at the corresponding parallel boundary surfaces, respectively. For general purposes, equation (4.4) and equation (4.5) are a complete set of boundary conditions [39].

4.3. Loading and Boundary Conditions

A strain ($\varepsilon_0 = 0.5\%$) in the transverse direction on the vertical sides of the RVE were applied to stimulate the transverse load. Since the stress results were normalized with the average applied stress and stress concentrations were calculated, strain value does not have any effect on the results, as long as it is not very high to cause plastic deformation. PBC was applied to all faces of the RVE to represent periodicity in the structure. Standard / Implicit solver was used in ABAQUS/CAE. Boundary conditions can be seen in **Figure 4.4**.

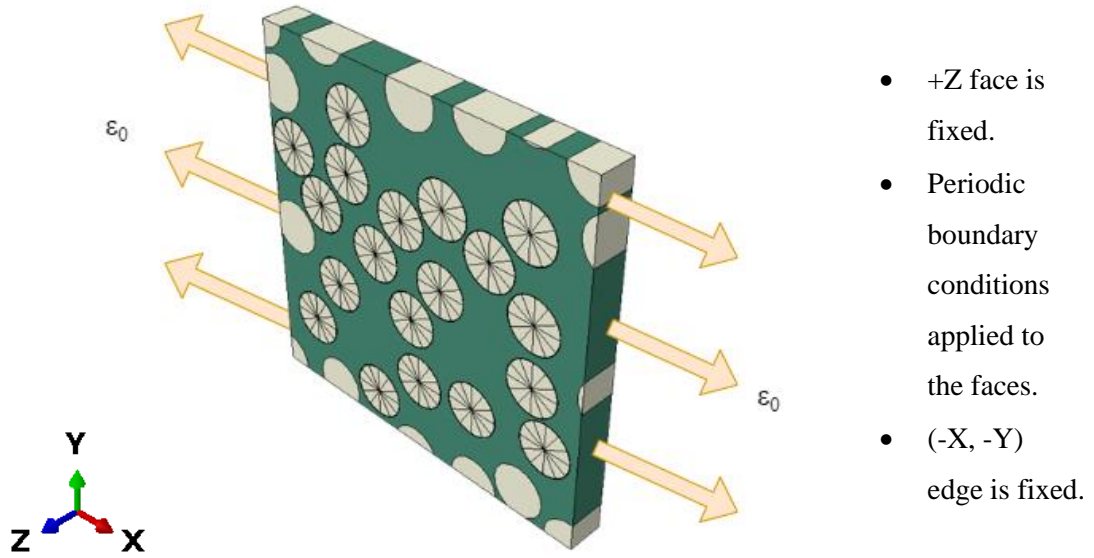


Figure 4.4. Boundary conditions of the RVE model.

4.4. Stress Concentration Calculation

Maximum principle stress ($S1_{max}$) in the matrix was chosen to be the critical stress type because of matrix brittle nature. $S1_{max}$ distribution for one of the models used in the sensitivity analysis can be seen in **Figure 4.5**. As mentioned previously, the principle stress values are normalized as in equation 4.6 to eliminate the effect of the applied load.

$$S_{average} = \frac{\sum_j^N (V_j) \times S1_{max}(j)}{\sum_j^N (V_j)} \quad (4.6)$$

where $S1_{max}(j)$ is the principal stress of the respected element (at node j), V_j is the volume of each element and N is total number of elements in the RVE. This was performed by a Python subroutine in the post-process stage of each analysis.

Average stress concentration from every element defined in FEM was calculated via equation 4.7 to normalize the stresses with the applied load and generate the stress concentration histograms for the matrix.

$$K = \frac{S1_{max}}{S_{average}} \quad (4.7)$$

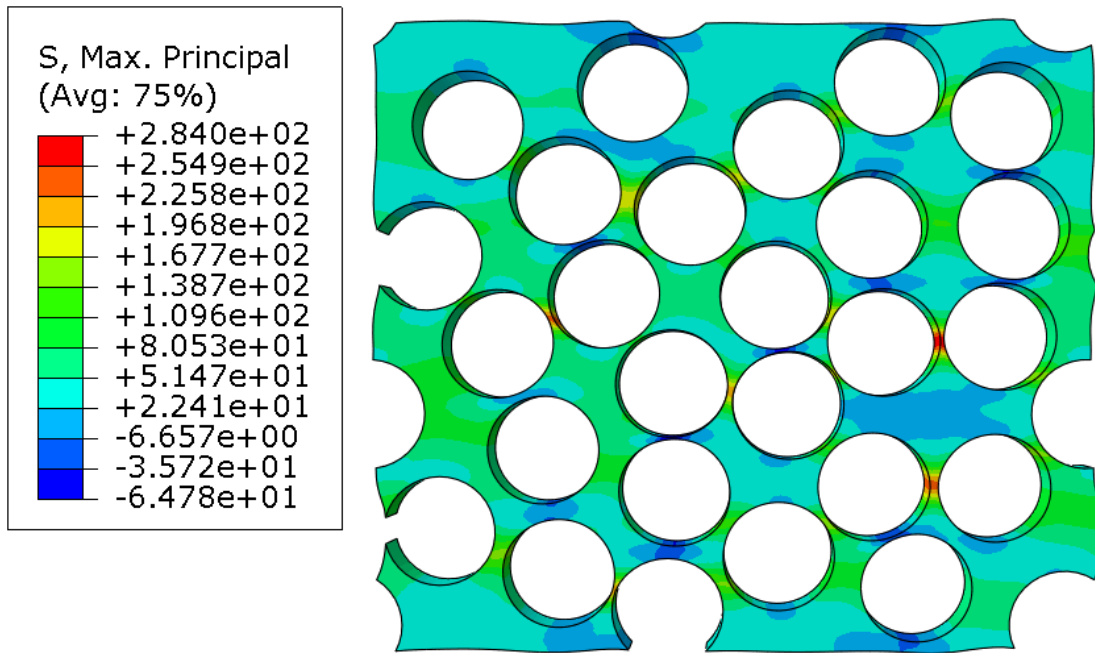


Figure 4.5. Maximum principle stress result for a RVE used in the sensitivity analysis, $V_f \cong 0.60$.

5. SELECTION OF MATERIAL PARAMETERS

The effect of the material parameters was considered in the thesis study. Therefore, the required material parameters need to be determined. First, chosen parameters must be adjustable for the need in the design. Secondly, with preliminary analyses, it should be understood that the parameter affects the stress distribution. Five material parameters were chosen for the preliminary analyses (**Table 5.1**).

Table 5.1. Preliminary Analysis Material Parameters

Material Parameter
Fiber Young's Modulus (E_f)
Matrix Young's Modulus (E_m)
Fiber Poisson's Ratio (ν_f)
Matrix Poisson's Ratio (ν_m)
Fiber Volume Ratio (V_f)

For the preliminary analyses, distributions for E_f and E_m (**Figure 5.1**) were created via MATLAB[®]. Number of occurrence shows the frequency of the Young's modulus values in the distribution. For the E_f distribution, analysis was performed with a constant E_m value of 3 GPa. For the E_m distribution, analysis was done with a constant E_f value of 120 MPa. 6 different RVE models with V_f in the range of 0.30 to 0.60 were created for only this purpose. Similar mesh structure and boundary conditions explained in the previous section were used.

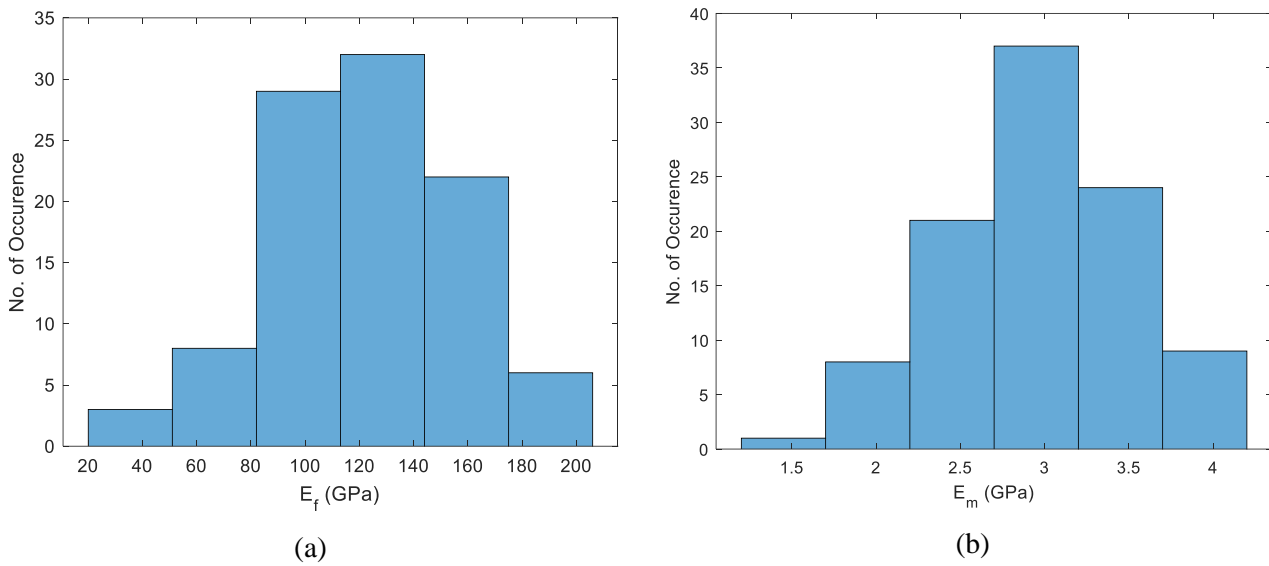


Figure 5.1. (a) E_f distribution, (b) E_m distribution.

As can be seen from the overstressed volume percentage (OVP) histograms for E_f distribution (**Figure 5.2**), std values are large enough to say that E_f parameter affects the OVP in every V_f value. OVP is the percentage of volume of elements with an average K value greater than 2. OVP is explained in more detail in Chapter 6. OVP histograms for E_m distribution (**Figure 5.3**) also indicates the same effect for E_m .

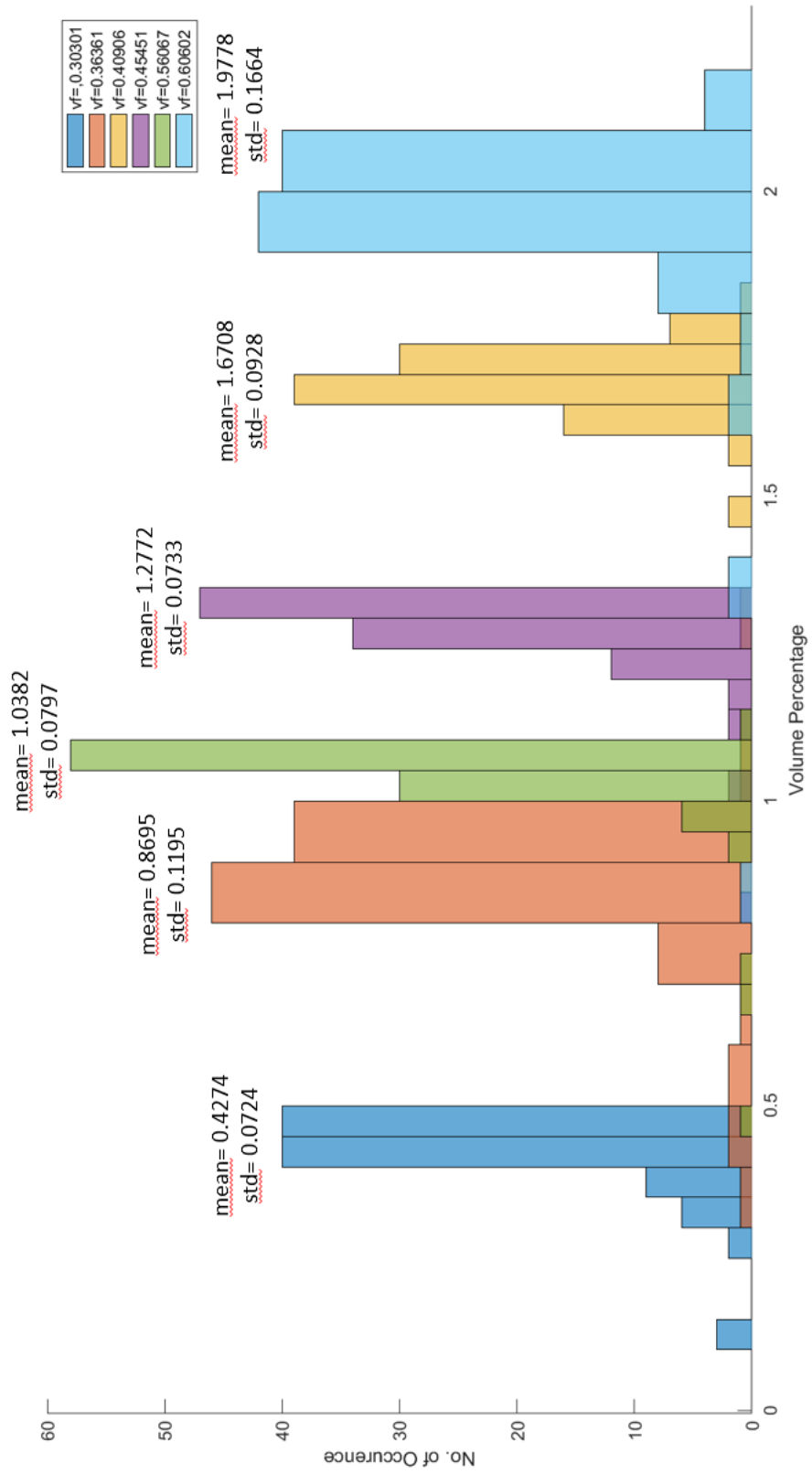


Figure 5.2. E_f distribuion OVP histograms.

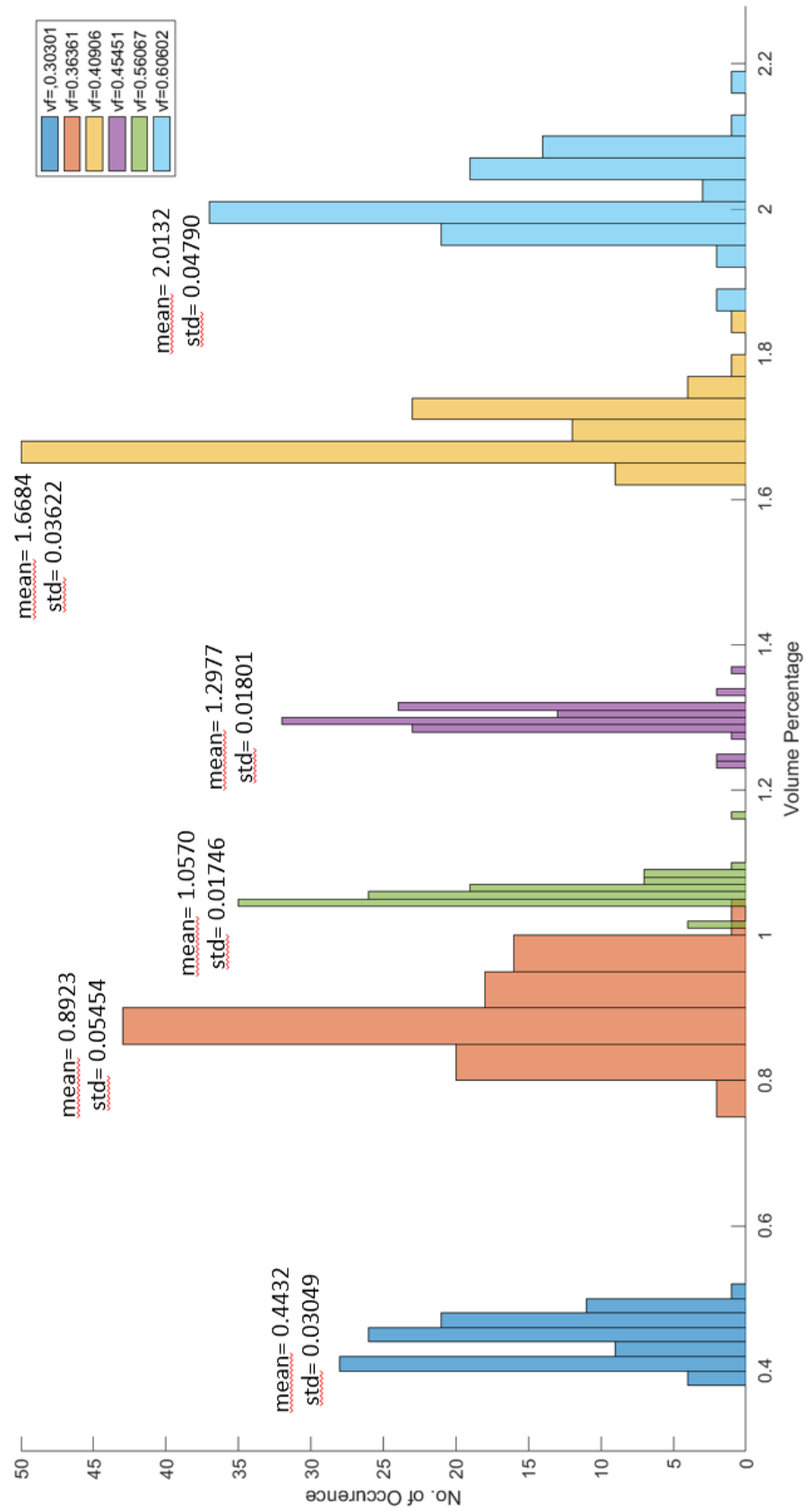


Figure 5.3. E_m distribution OVP histograms.

For the Poisson ratio of fiber (ν_f), a distribution for the range between 0.2 and 0.4 values was created (**Figure 5.4**) and defined in the RVE models. These RVE models were solved, and the histograms of K_{\max} values are plotted in (**Figure 5.5**). It reveals that ν_f does not have much impact on stress concentration and was not included in the sensitivity analysis. Variation in the Poisson's ratio of matrix (ν_m) was not considered as it is expected to have negligible influence similar to ν_f .

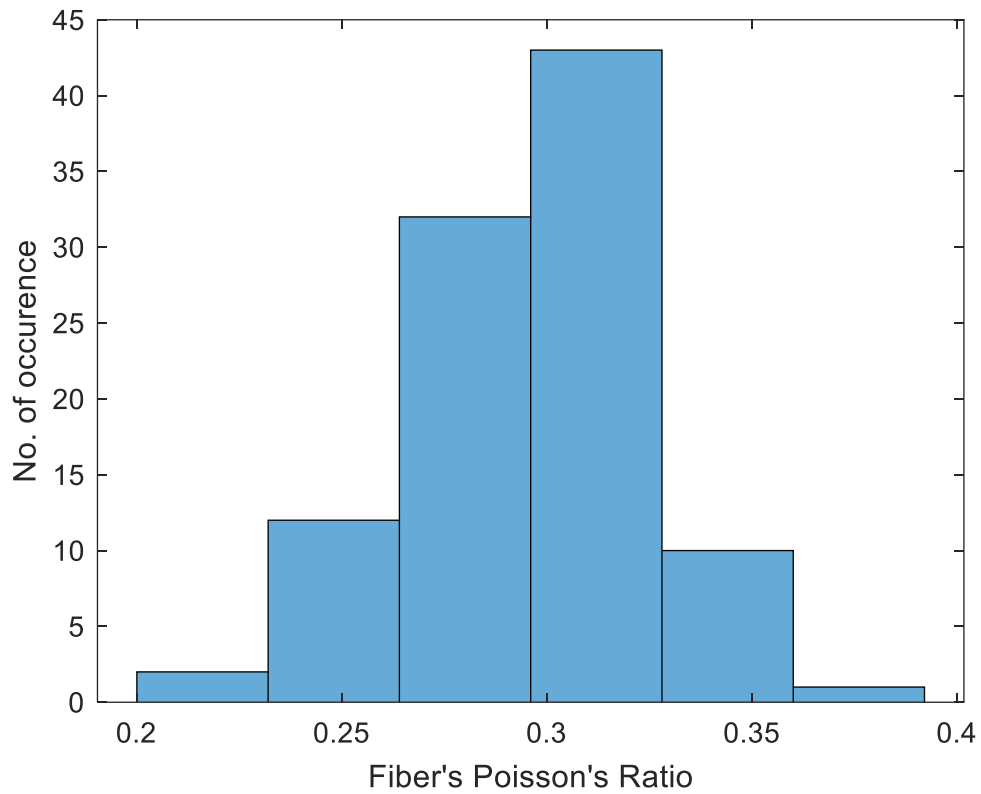


Figure 5.4. ν_f distribution defined to the RVE models.

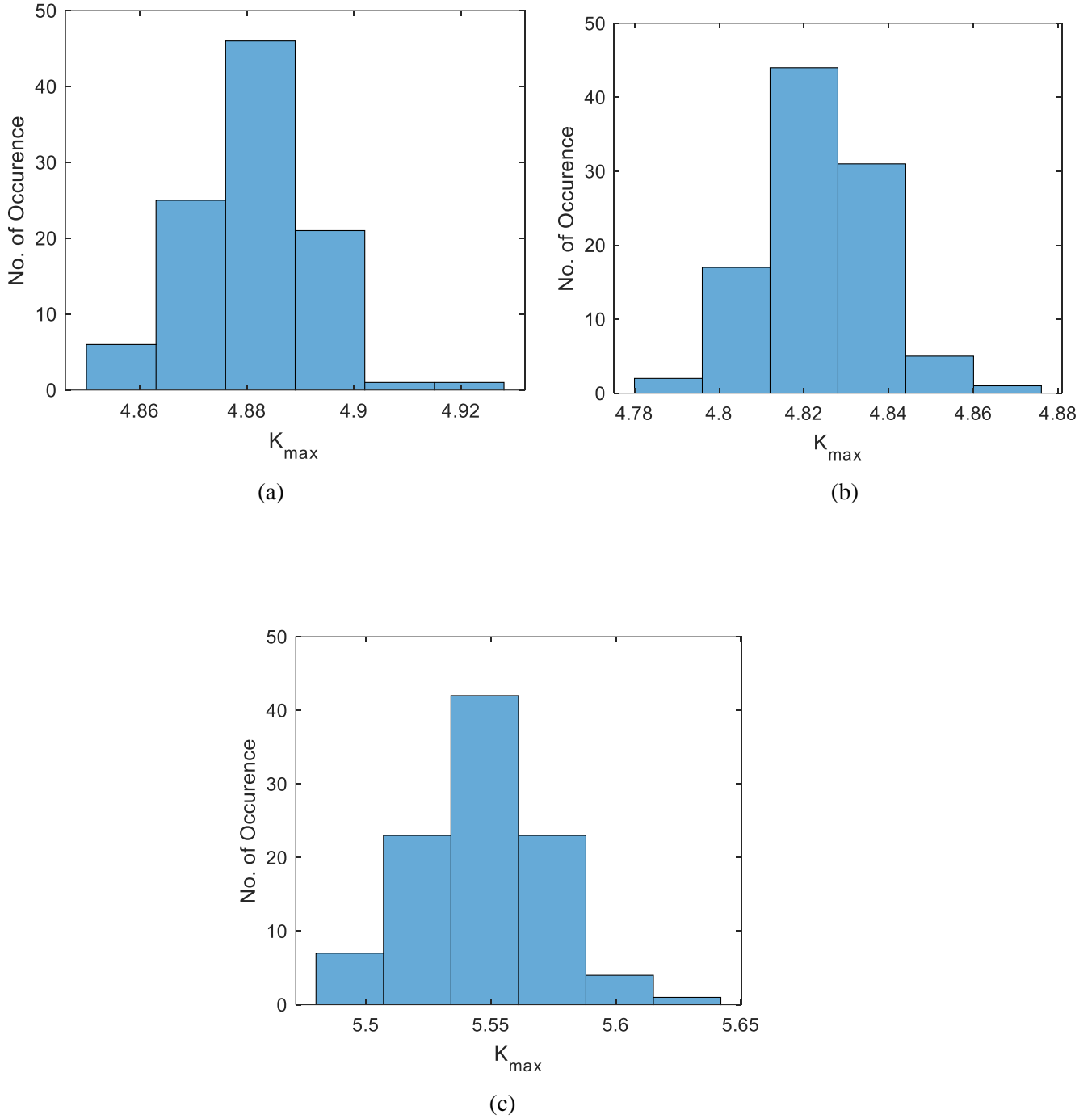


Figure 5.5. K_{\max} distribution of $V_f \approx$ (a) 0.30, (b) 0.45, (c) 0.60 for Poisson's ratio distribution.

With the preliminary analyses in mind, $\frac{E_f}{E_m}$ ratio and V_f was chosen for the sensitivity analysis. For the sake of reducing the computation time to solve the models, V_f was selected to be 0.30, 0.45, and 0.60. Skudra et al. [40] showed that $\frac{E_f}{E_m}$ ratio governs the stress concentration instead of E_f and E_m as two separate parameters. Therefore, in this

thesis, $\frac{E_f}{E_m}$ ratio is used as a material parameter. To this end, the uniformly distributed five discrete E_m values (1-5 GPA) are normalized with randomly generated 50 E_f values with mean and std of 73.6 MPa and 3.73 MPa, respectively (**Figure 5.6**) [41-43].

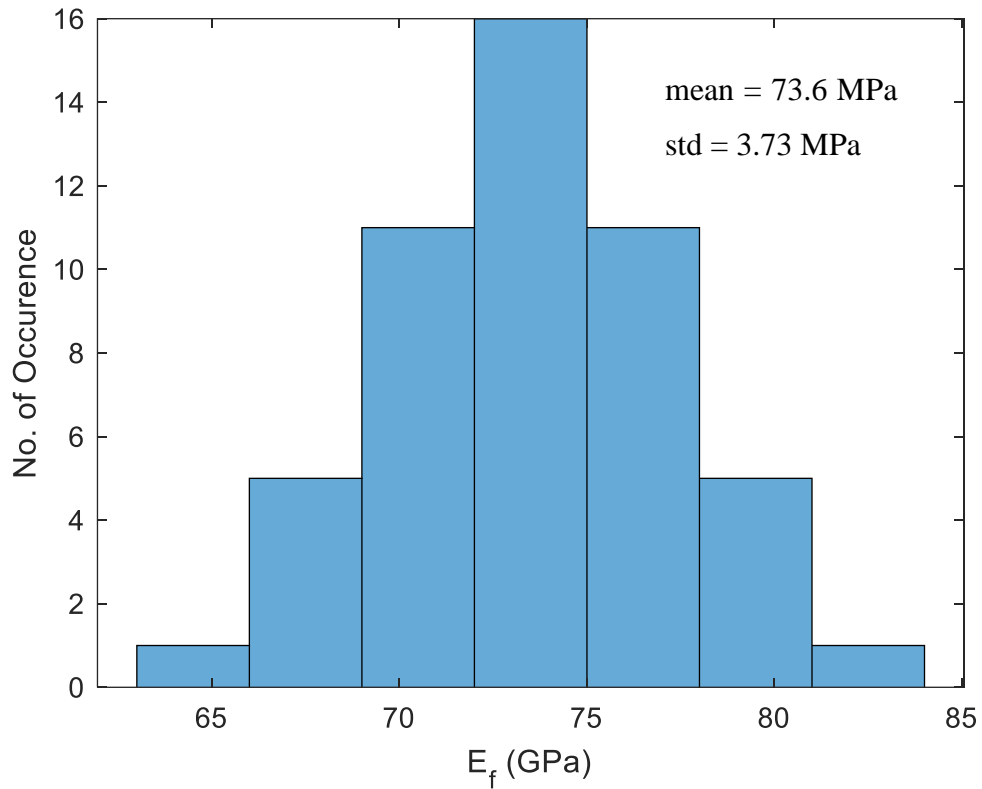


Figure 5.6. E_f distribution used in the sensitivity analysis.

6. SENSITIVITY ANALYSIS METHOD

6.1. Monte-Carlo Method

A Monte-Carlo simulation was used to perform the sensitivity analysis with material parameters on stress distribution and concentration. E_f distribution given in **Figure 5.6** is defined for RVE models shown in **Table 4.2**. The procedure is repeated for five discrete E_m values. Therefore, a total of 2250 simulations were performed. The structure of the analysis can be seen in **Figure 6.1**. Although K_{max} is analysed in this thesis, this parameter cannot represent the stress distribution correctly. Therefore, K depending on the volume of elements, was visualized via Normalized Volume – K histograms (**Figure 6.2**). In order to represent these histograms in parametric correlation, a parameter called overstressed volume percentage (OVP) is introduced. OVP is selected to be the volume of elements with an average K value greater than 2. It was calculated from histogram bins with Eqn. **6.1** and Eqn. **6.2**.

$$Normalized\ Volume = \frac{Volume\ of\ Element}{Total\ Volume} \quad (6.1)$$

$$OVP = \left(\sum_{K \geq 2}^{Max\ K} \frac{Volume\ of\ Element}{Total\ Volume} \right) \times 100 \quad (6.2)$$

To analyze the relation between design inputs and outputs, the correlation between those parameters was calculated in pairwise. As mentioned in the earlier chapters, Spearman's rank correlation coefficient was calculated between parameters.

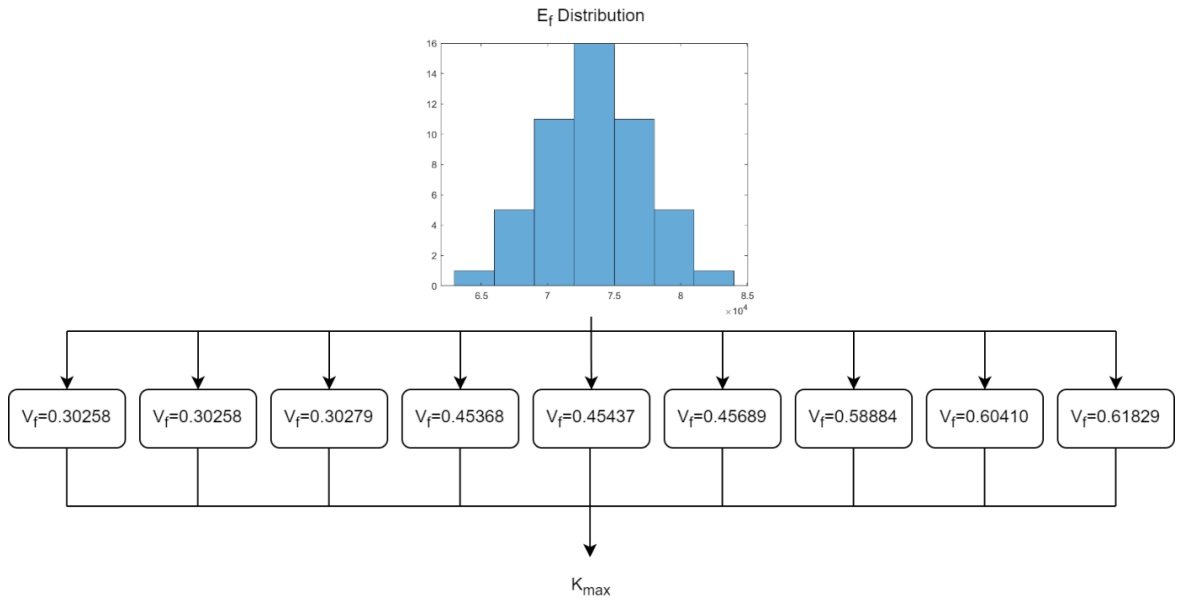


Figure 6.1. Structure of the Sensitivity Analysis for a single E_m

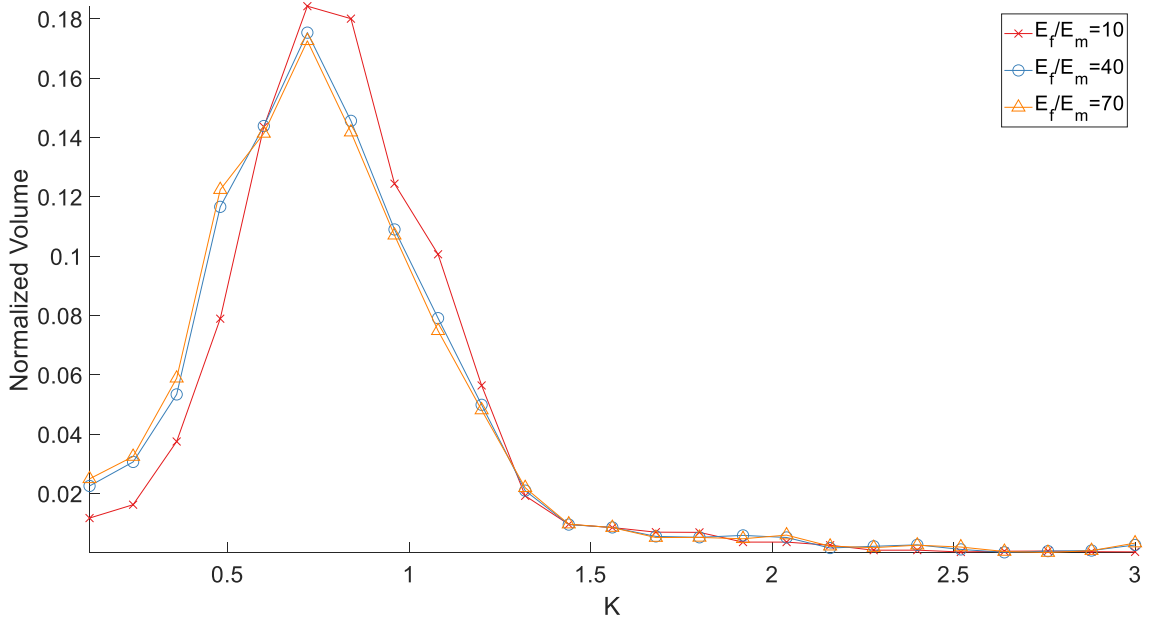


Figure 6.2. Normalized Volume – Stress Concentration histogram of V_f = 0.40675 RVE model. E_f = 70.9 GPa

6.2. Fibers Young's Modulus Variance

With the Monte-Carlo method, many analyses were performed with various Young's moduli for fibers. But in all of them, all the fibers had the same single value of Young's modulus in a RVE, meaning that values did not vary within a single model. It is known that this is not the case for fibers. Therefore, analyses with fibers in the RVE having different Young's modulus value was performed. They are defined so that the value defined to the RVE is equal to the mean value of the E_f distribution in the compared RVE (Figure 6.3).

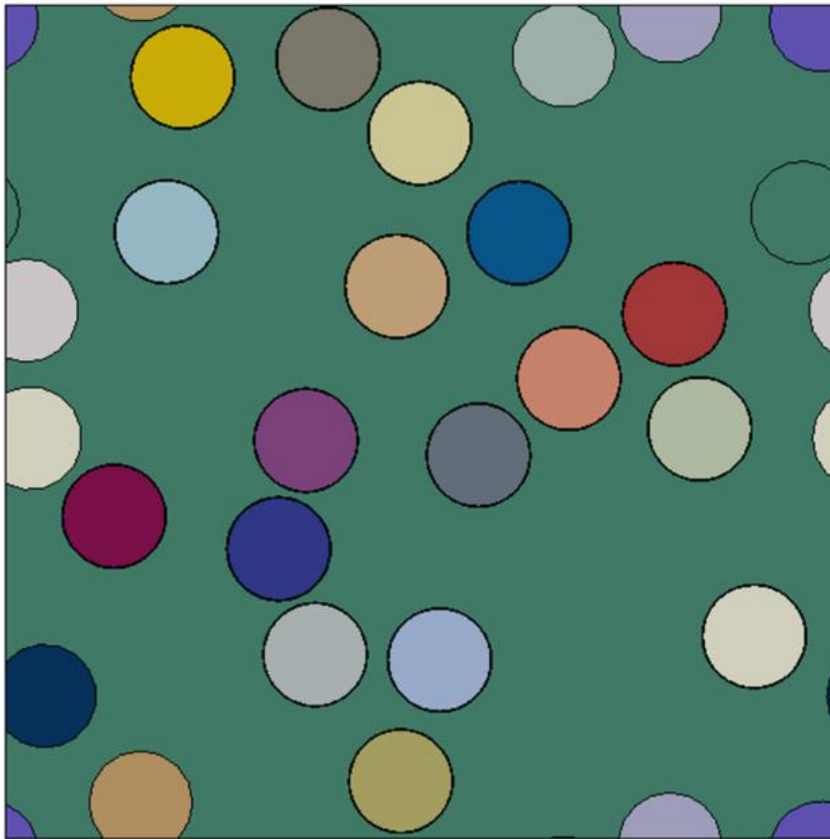
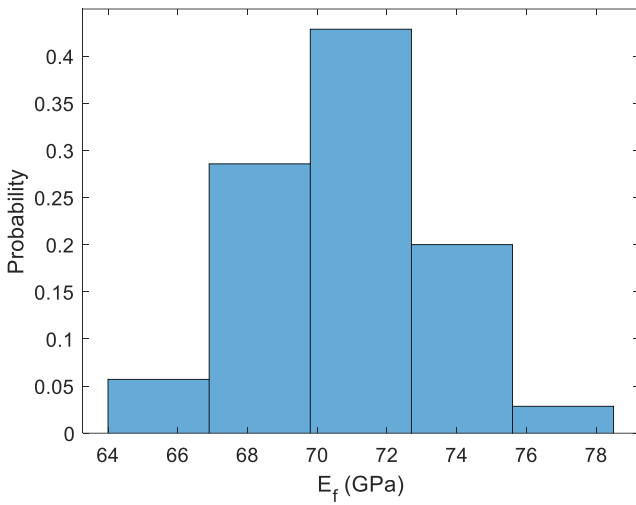


Figure 6.3. E_f distributed RVE model. Each color represents a different Young's Modulus value.

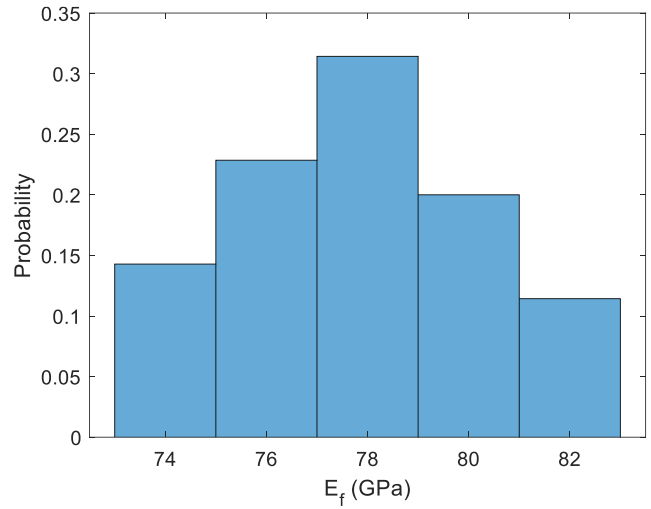
Four different E_f values with given in **Table 6.1** were considered for the analysis. Ranges were taken from Lefeuvre et al. [44]. Distributions were created with to respect to the ranges (**Figure 6.4**). Since no distribution was given in the literature, normal distribution type was used. All models have the same E_m to compare the results with each other. Same boundary conditions were applied for the models.

Table 6.1. Glass fiber properties used in the fiber variance analysis.

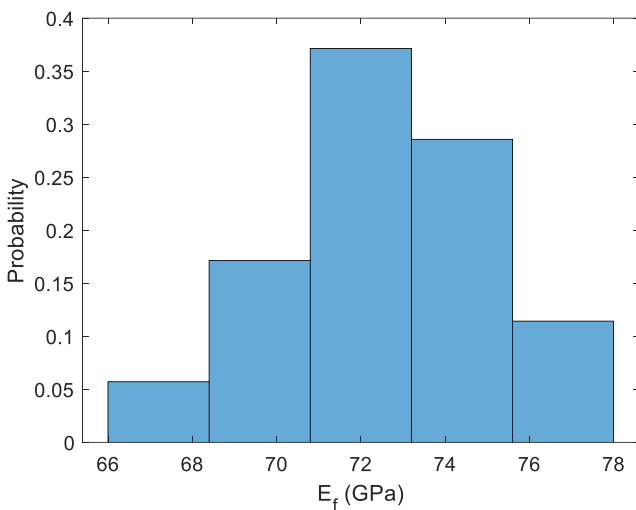
Name	E_f (GPa)
G1	70.9 (± 6.2)
G2	77.8 (± 4.8)
G3	72.6 (± 5.2)
G4	70.3 (± 5.8)



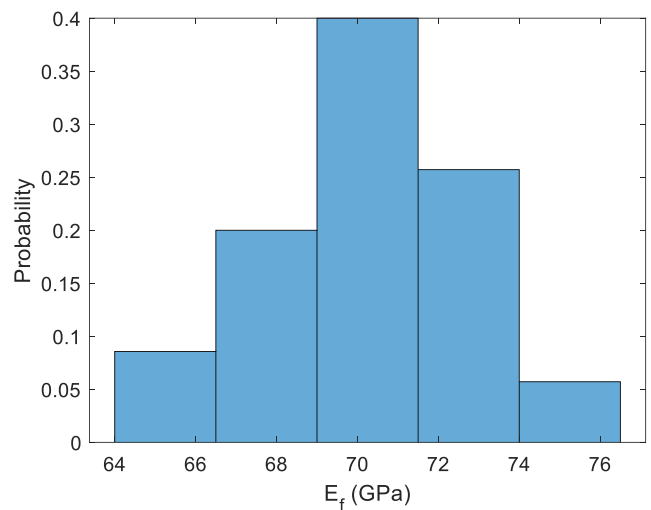
(a)



(b)



(c)



(d)

Figure 6.4. E_f distributions defined to the RVE models. (a) G1, (b) G2, (c) G3 and (d) G4.

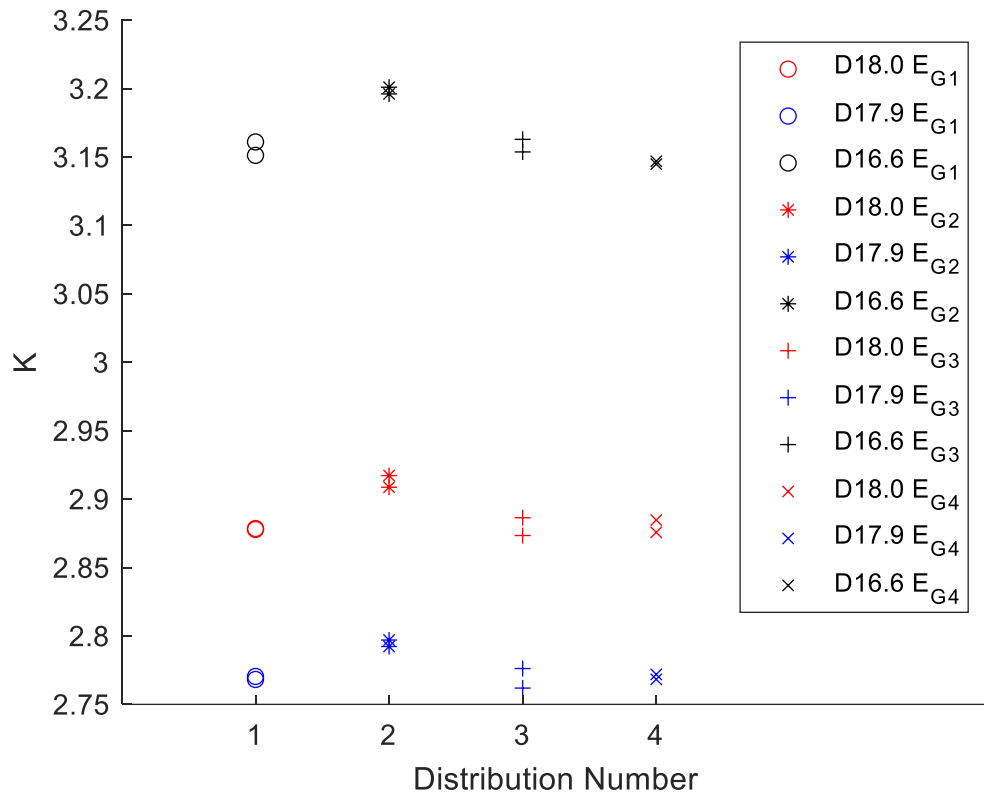
7. RESULTS

7.1. Fibers Young's Modulus Variance Results

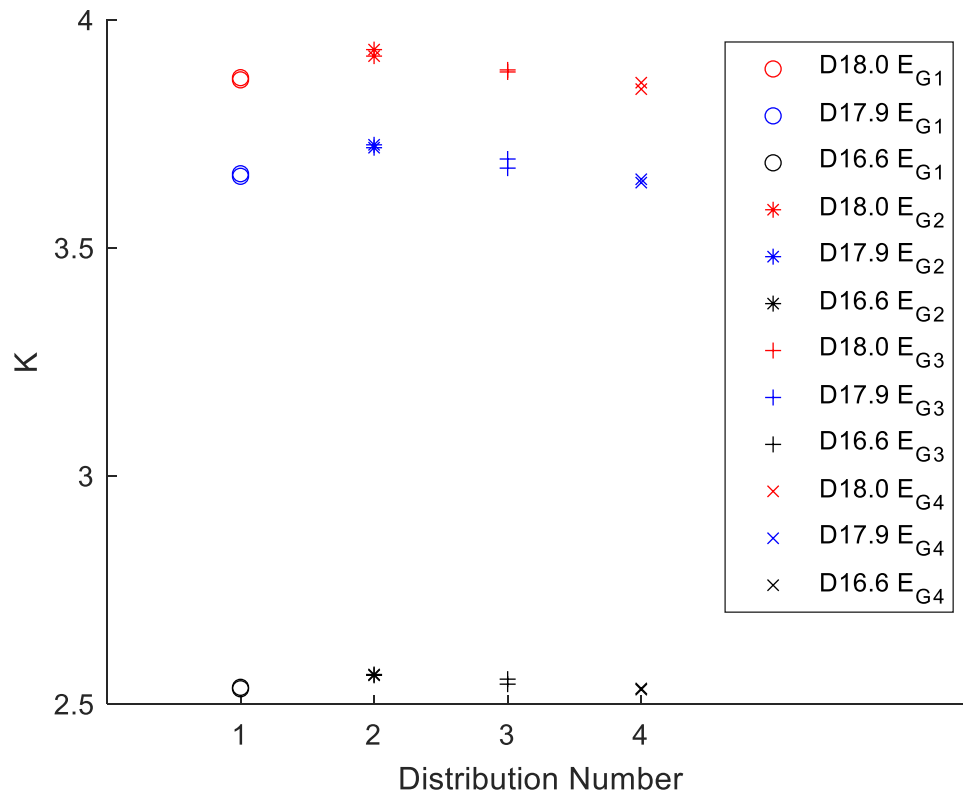
Different Young's modulus values were defined to the RVE in order to see the effect of fiber Young's modulus variance in GFRC. K_{\max} results were gathered from all the analyses and compared with the respected RVE model having only one Young's moduli for the fibers. In **Figure 7.1**, symbols of the same shape and color represents the difference between maximum stress concentrations of distributed E_f and constant E_f . E_f variance has very low impact on stress concentration. K_{\max} values are very close to each other. However, in some cases, in $V_f \cong 0.60$ RVE model, there were more differences than the other cases. The reason was attributed to the fact that Young's modulus values corresponding to the fibers, where the stress concentration is high, are larger than the average value in the distribution. In order to investigate in more detail, simulations were performed with different $\frac{E_f}{E_m}$ ratios while keeping the same E_f distribution that was defined to the RVE. As the $\frac{E_f}{E_m}$ ratio goes lower, K decreases. A comparison was made again with the constant Young's modulus defined to the fibers (**Table 7.1**). Although the % difference between the two cases goes higher as the $\frac{E_f}{E_m}$ ratio goes lower, the difference between the K_{\max} value is still low.

Table 7.1. Maximum stress concentration results for the fiber Young's modulus variance analysis.

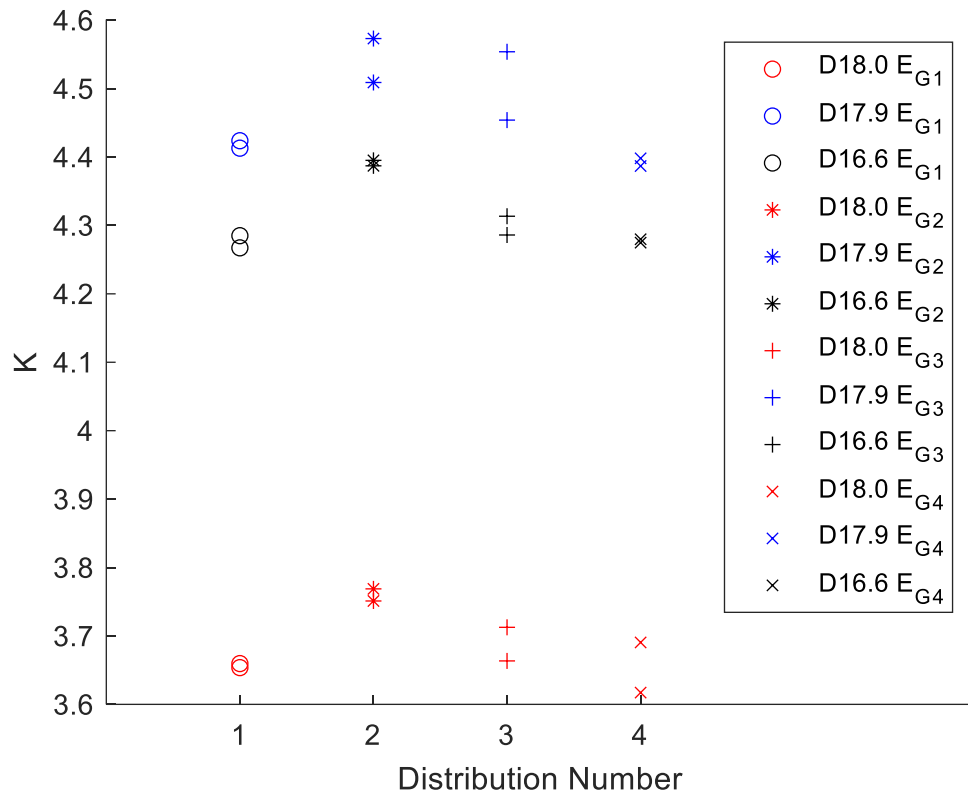
Description	$E_f/E_m = 145.2$	$E_f/E_m = 24.2$	$E_f/E_m = 14.52$	$E_f/E_m = 7.26$
K_{\max} for distributed E_f	6.7465	4.5538	3.6654	2.5810
K_{\max} for constant E_f	6.7081	4.4539	3.5631	2.4948
% Difference	0.57	2.2	2.8	3.35



(a)



(b)



(c)

Figure 7.1. Maximum stress concentration differences in fibers distributed RVE models for (a) $V_f \cong 0.30$, (b) $V_f \cong 0.45$, (c) $V_f \cong 0.6$. (DXX.X represents the fiber diameter used while creating the RVE).

7.2. Monte-Carlo and Sensitivity Analysis Results

For 2250 simulations, solutions were gathered, and stress concentration histograms were created. $S1_{\max}$ results and their *Normalized Volume/K* histograms of RVEs for $E_f \cong 73.6$ (MPa) (mean value of the Young's modulus distribution) can be seen in (Figure 7.2 - Figure 7.16) and (Figure 7.17 - Figure 7.25), respectively.

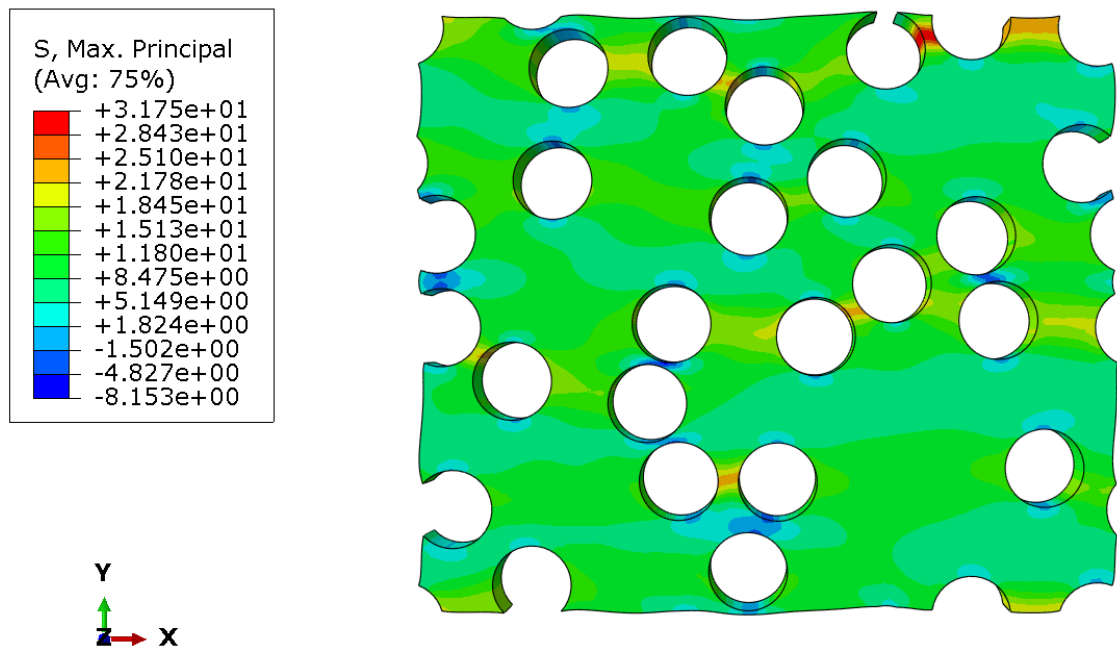


Figure 7.2. $V_f = 0.30258$, $S1_{\max}$ result for $E_m = 1$ GPa

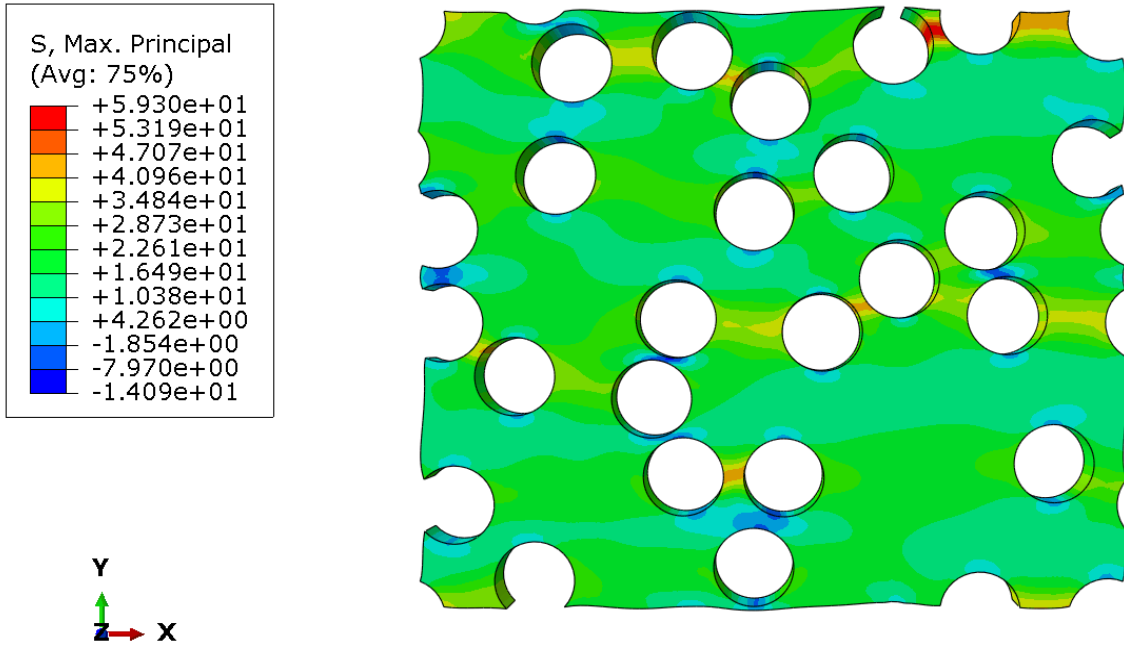


Figure 7.3. $V_f = 0.30258$, $S1_{max}$ result for $E_m = 2$ GPa

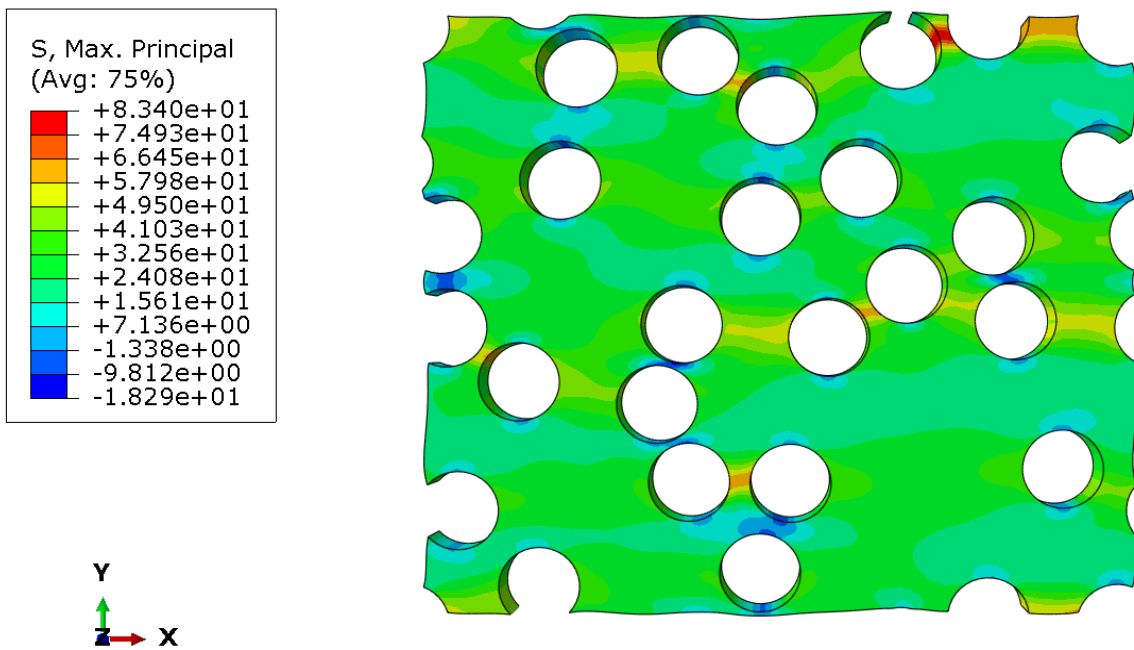


Figure 7.4. $V_f = 0.30258$, $S1_{max}$ result for $E_m = 3$ GPa

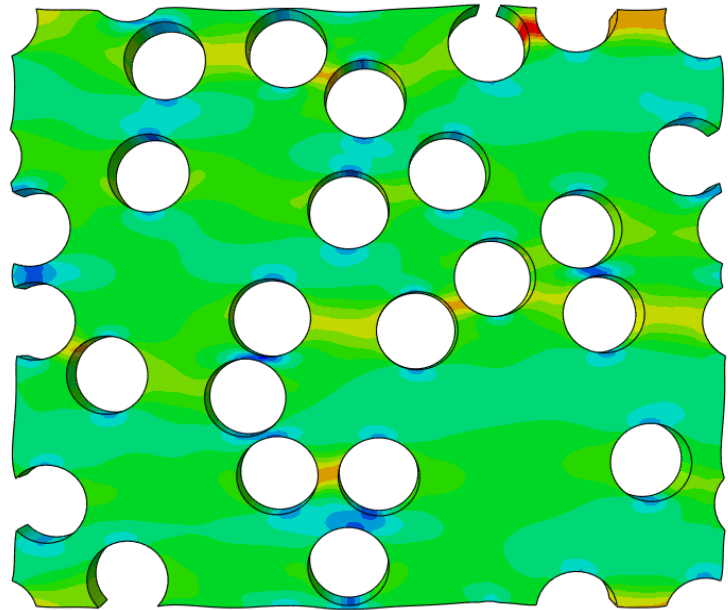
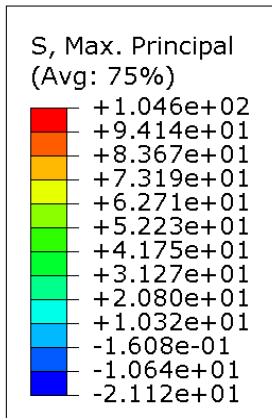


Figure 7.5. $V_f = 0.30258$, $S1_{max}$ result for $E_m = 4$ GPa

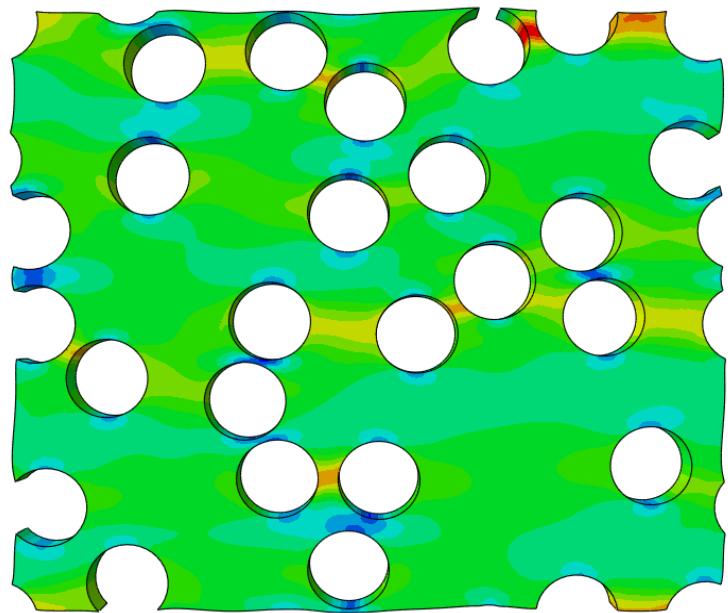
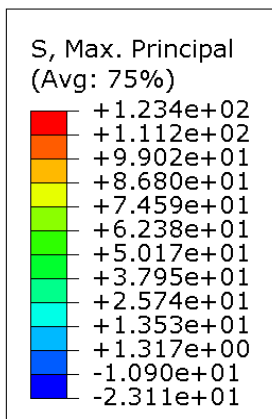


Figure 7.6. $V_f = 0.30258$, $S1_{max}$ result for $E_m = 5$ GPa

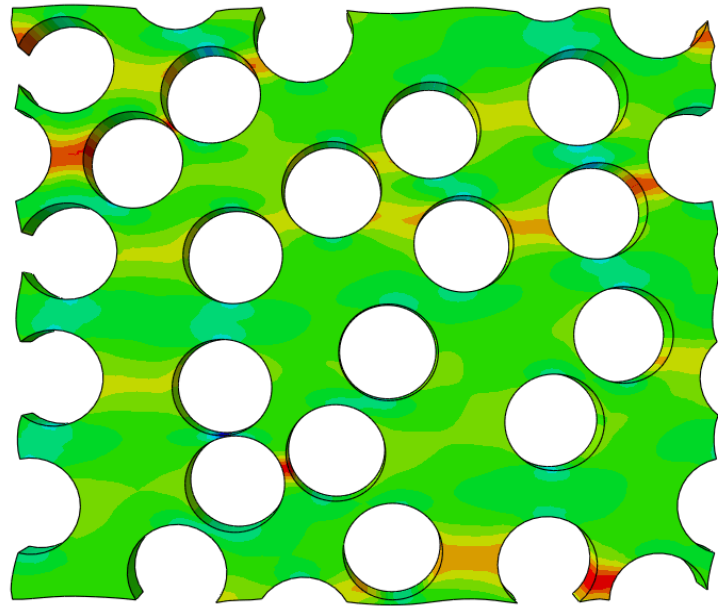
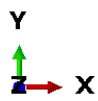
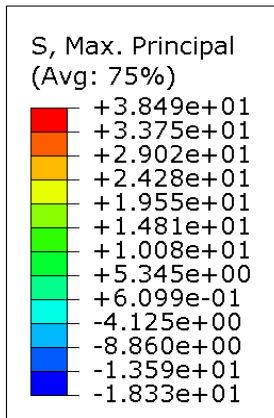


Figure 7.7. $V_f = 0.45368$, $S1_{max}$ result for $E_m = 1$ GPa

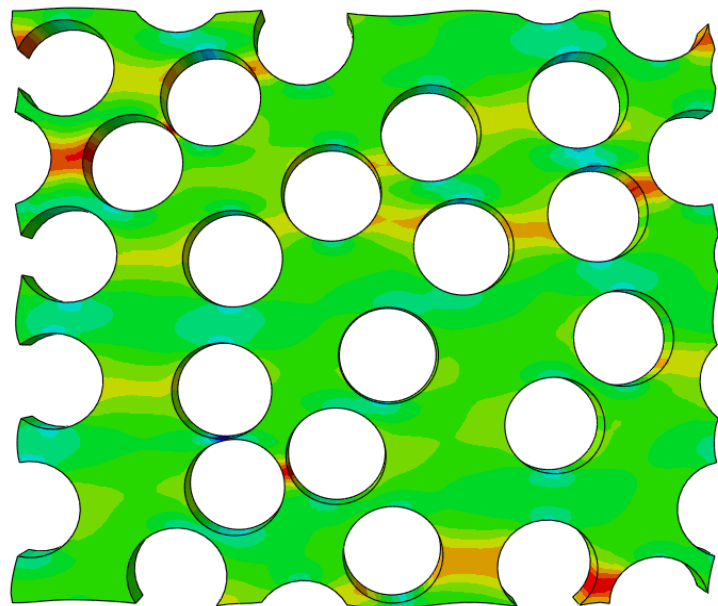
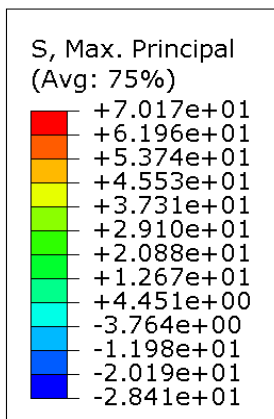


Figure 7.8. $V_f = 0.45368$, $S1_{max}$ result for $E_m = 2$ GPa

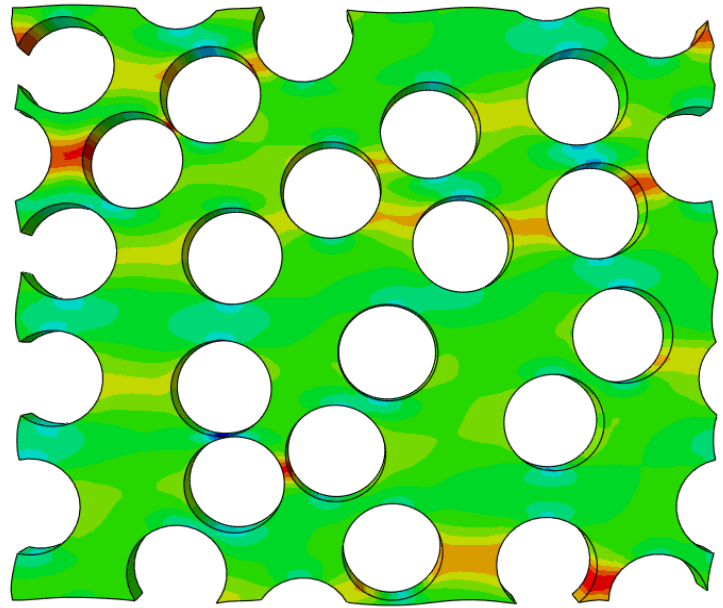
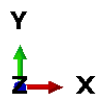
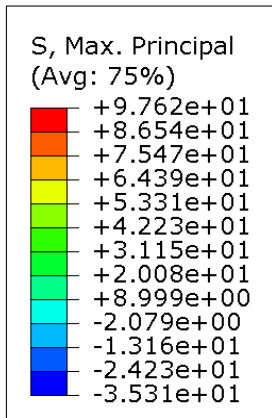


Figure 7.9. $V_f = 0.45368$, $S1_{max}$ result for $E_m = 3$ GPa

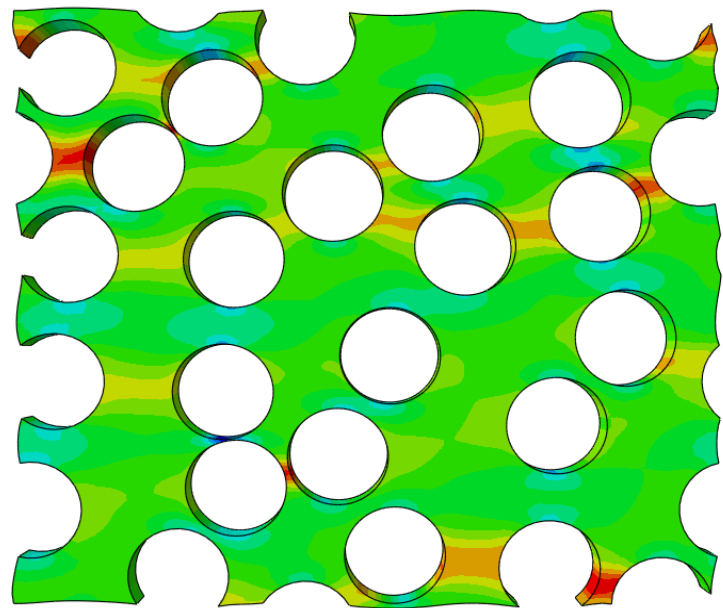
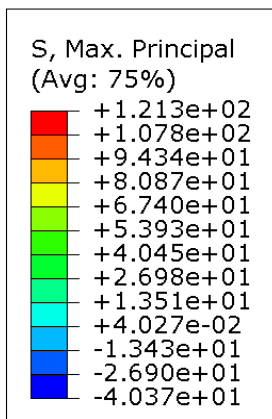


Figure 7.10. $V_f = 0.45368$, $S1_{max}$ result for $E_m = 4$ GPa

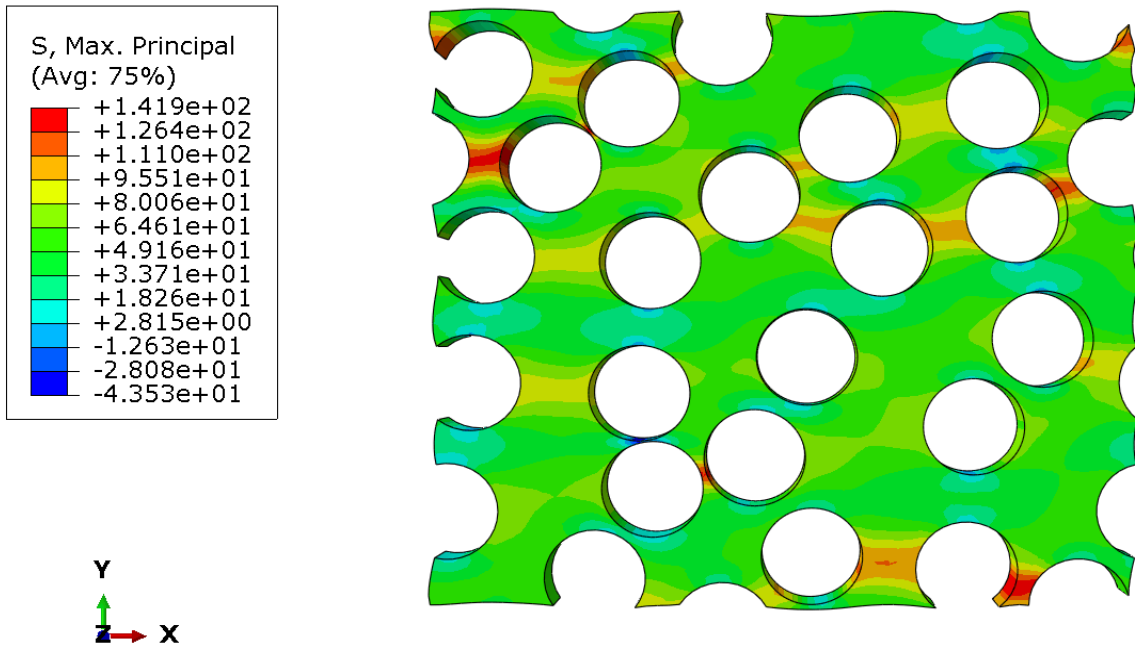


Figure 7.11. $V_f = 0.45368$, $S1_{\max}$ result for $E_m = 5$ GPa

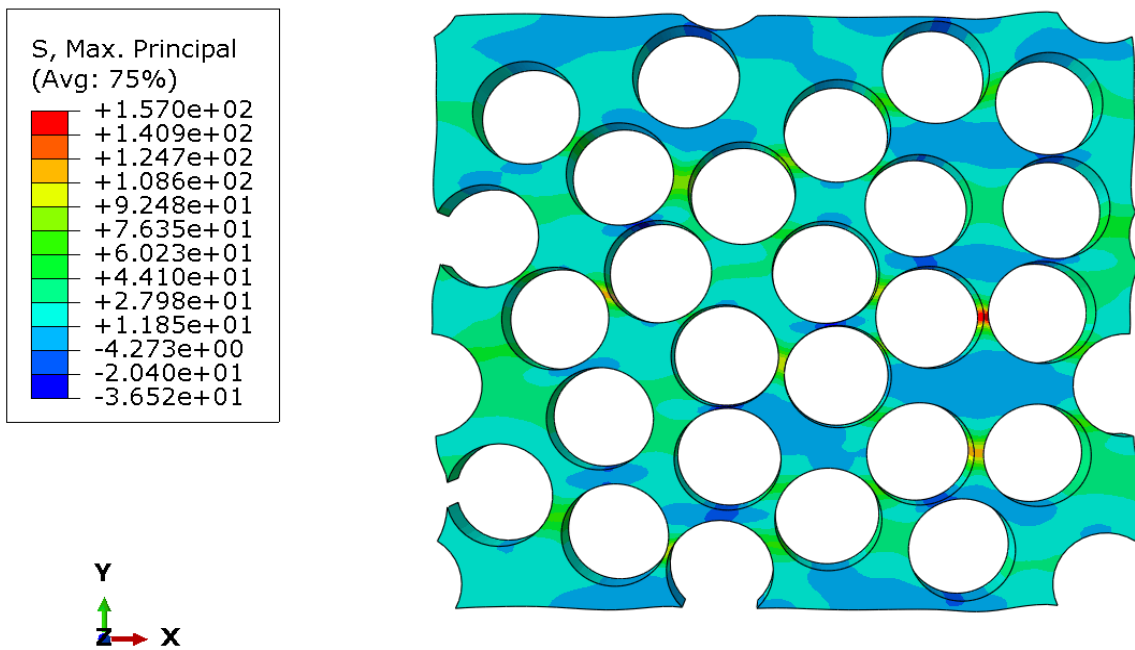


Figure 7.12. $V_f = 0.60410$, $S1_{\max}$ result for $E_m = 1$ GPa

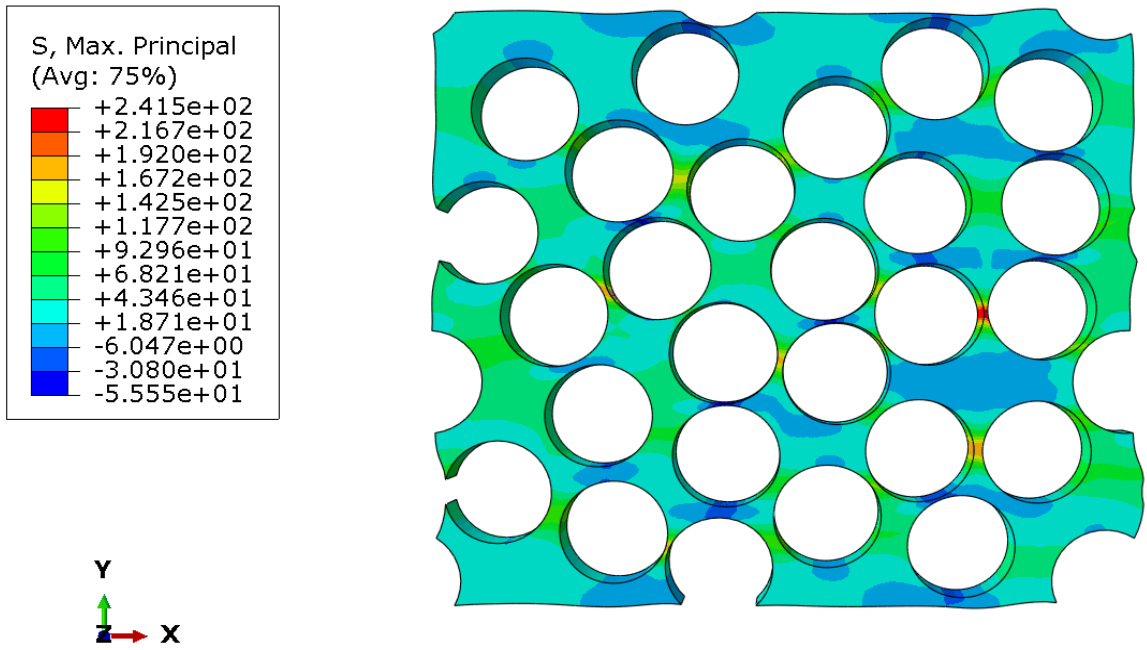


Figure 7.13. $V_f = 0.60410$, $S1_{max}$ result for $E_m = 2$ GPa

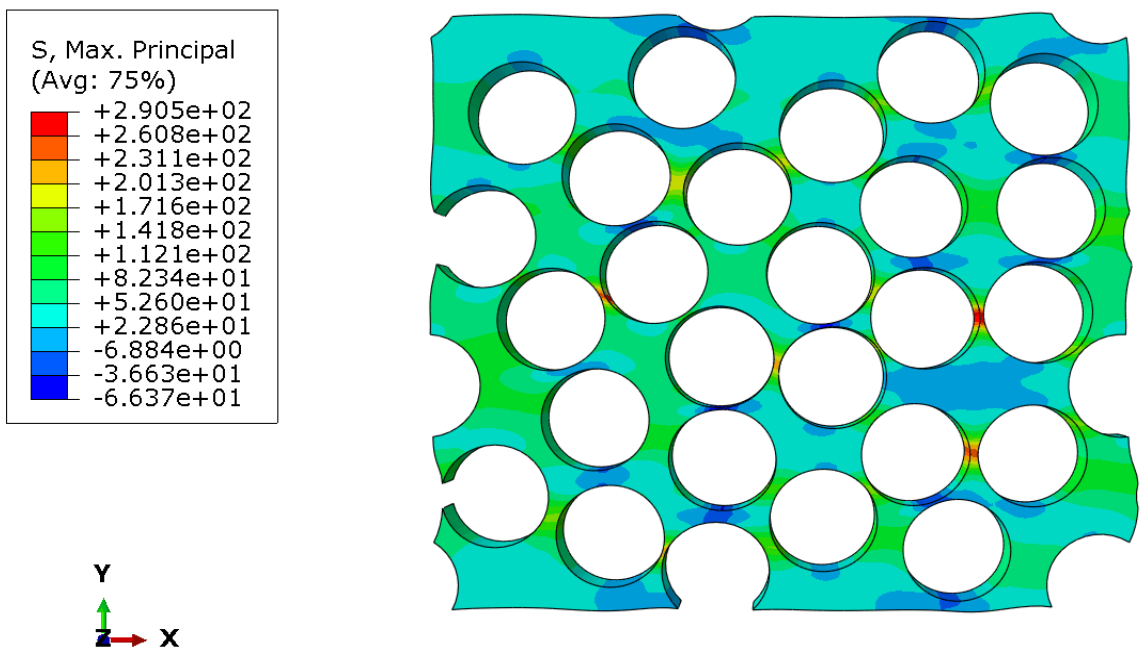


Figure 7.14. $V_f = 0.60410$, $S1_{max}$ result for $E_m = 3$ GPa

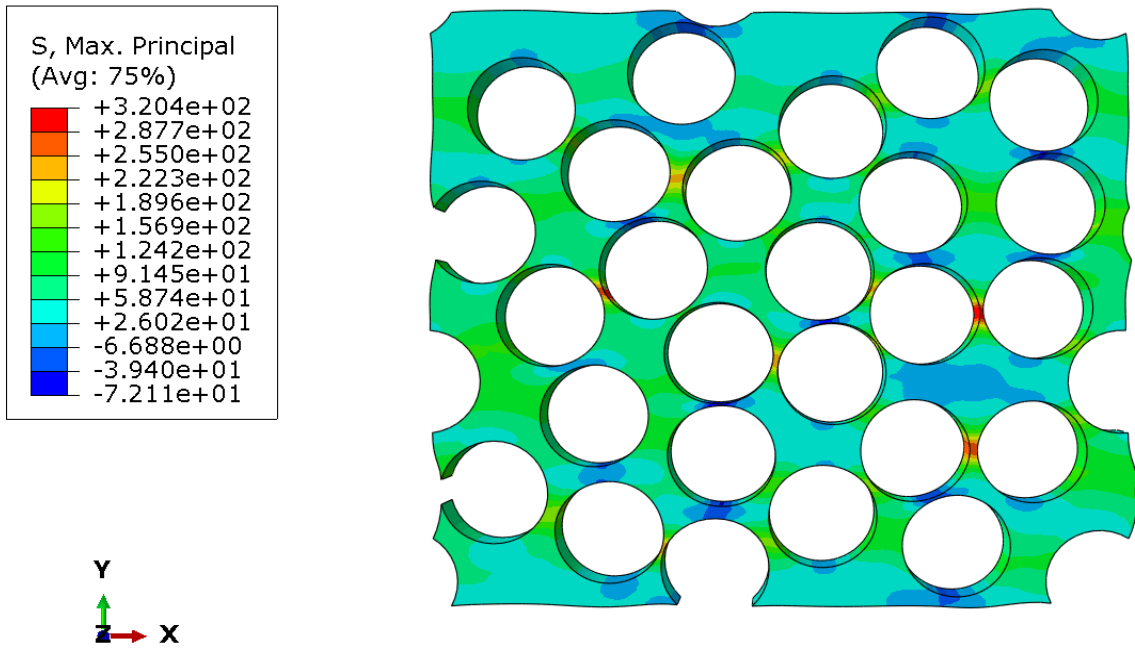


Figure 7.15. $V_f = 0.60410$, $S1_{\max}$ result for $E_m = 4$ GPa

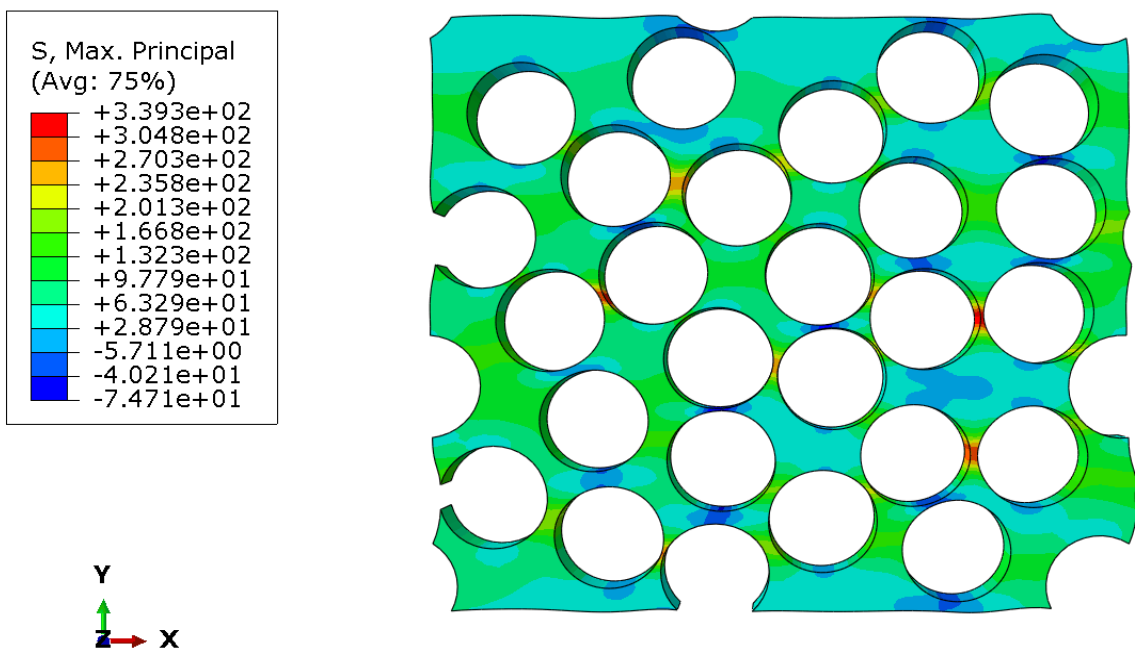


Figure 7.16. $V_f = 0.60410$, $S1_{\max}$ result for $E_m = 5$ GPa

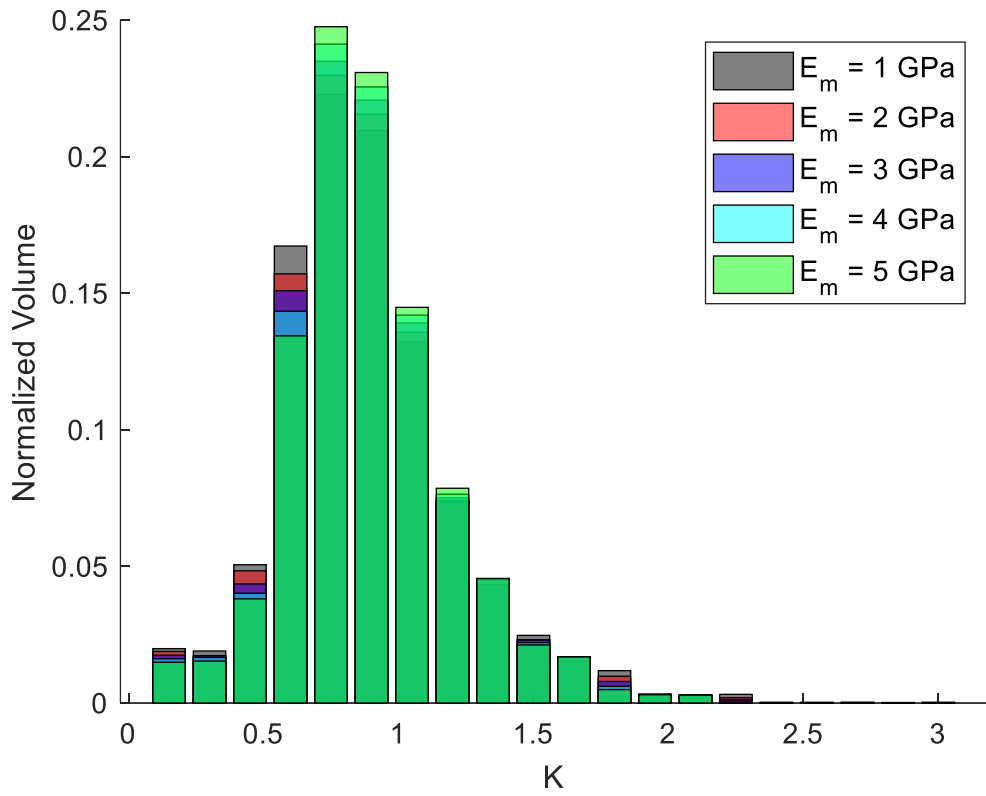


Figure 7.17. Normalized Volume/ K histogram of $V_f = 0.30258$

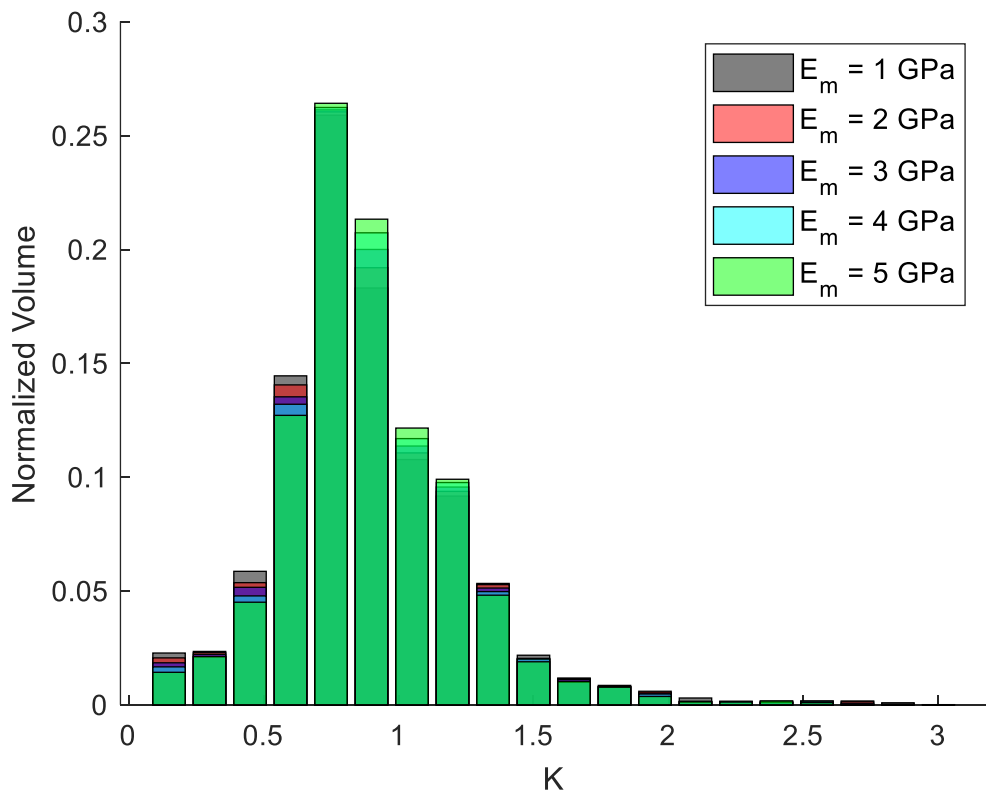


Figure 7.18. Normalized Volume/ K histogram of $V_f = 0.30279$

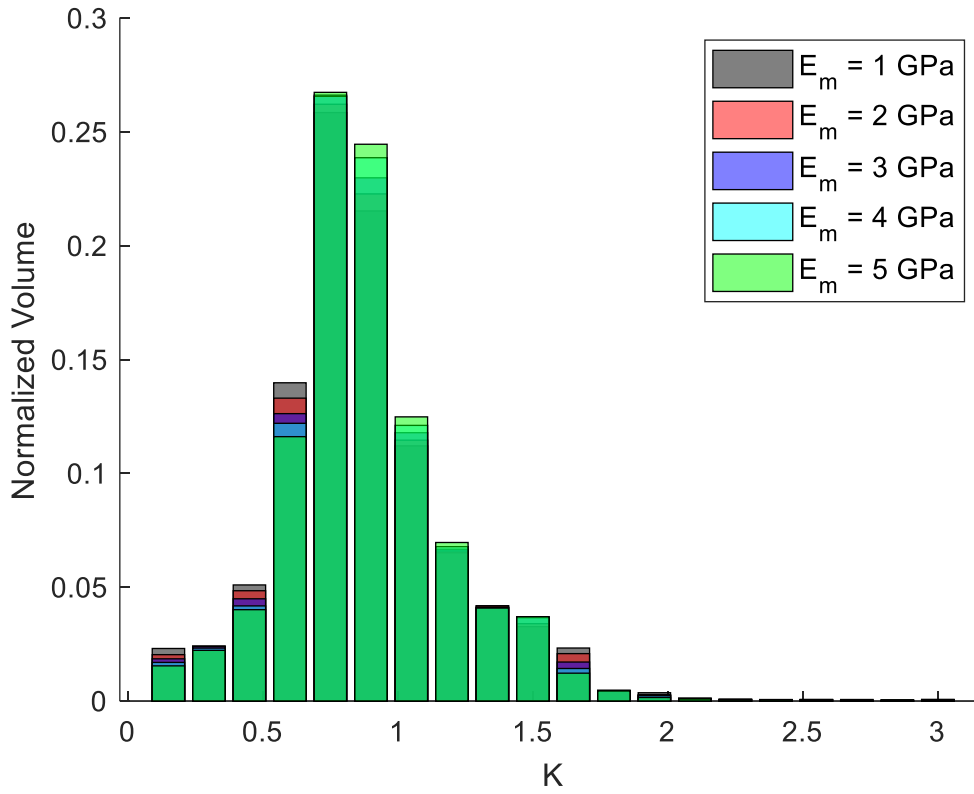


Figure 7.19. Normalized Volume/ K histogram of $V_f = 0.30423$

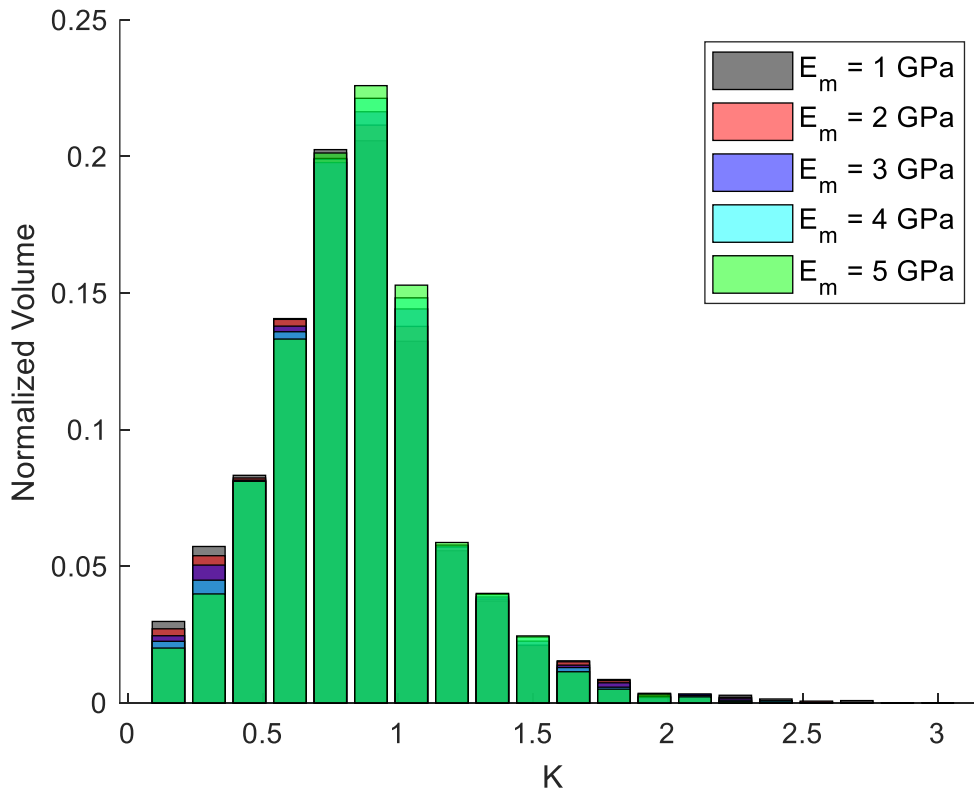


Figure 7.20. Normalized Volume/ K histogram of $V_f = 0.45368$

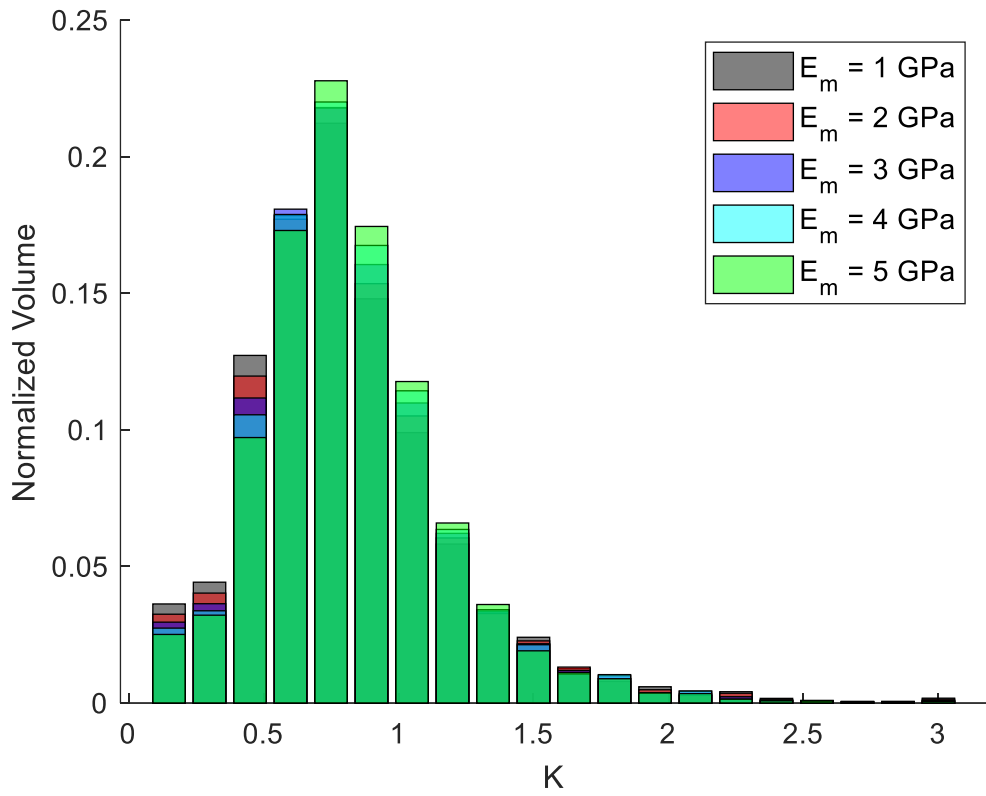


Figure 7.21. Normalized Volume/ K histogram of $V_f = 0.45437$

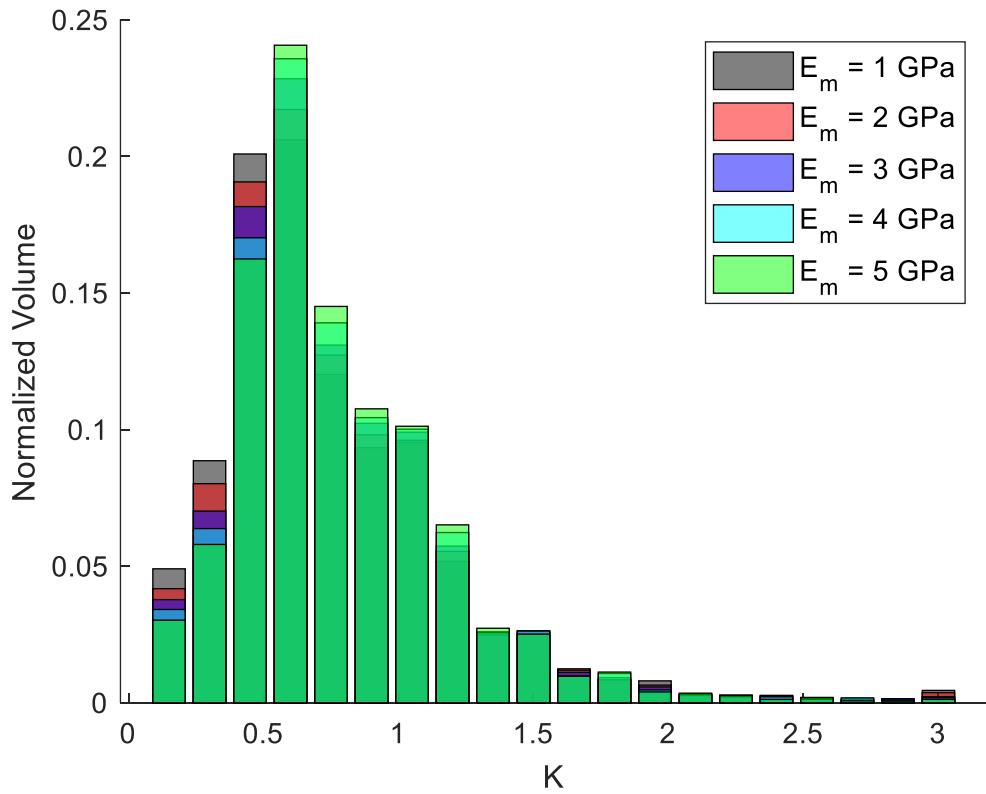


Figure 7.22. Normalized Volume/ K histogram of $V_f = 0.45689$

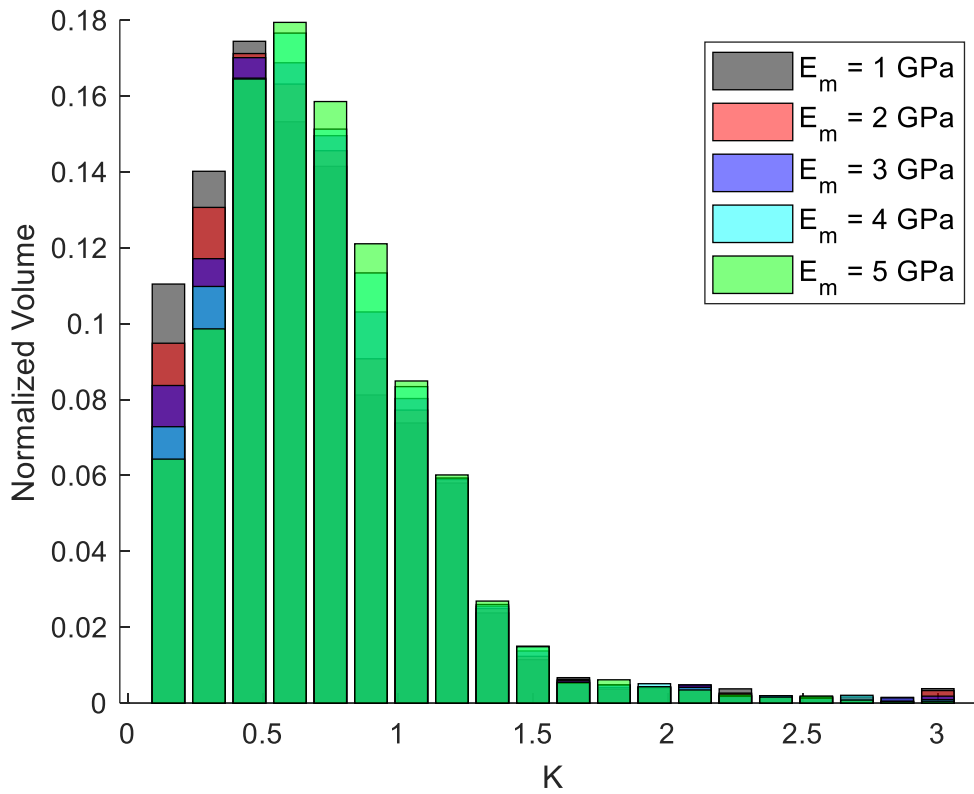


Figure 7.23. Normalized Volume/ K histogram of $V_f = 0.58884$

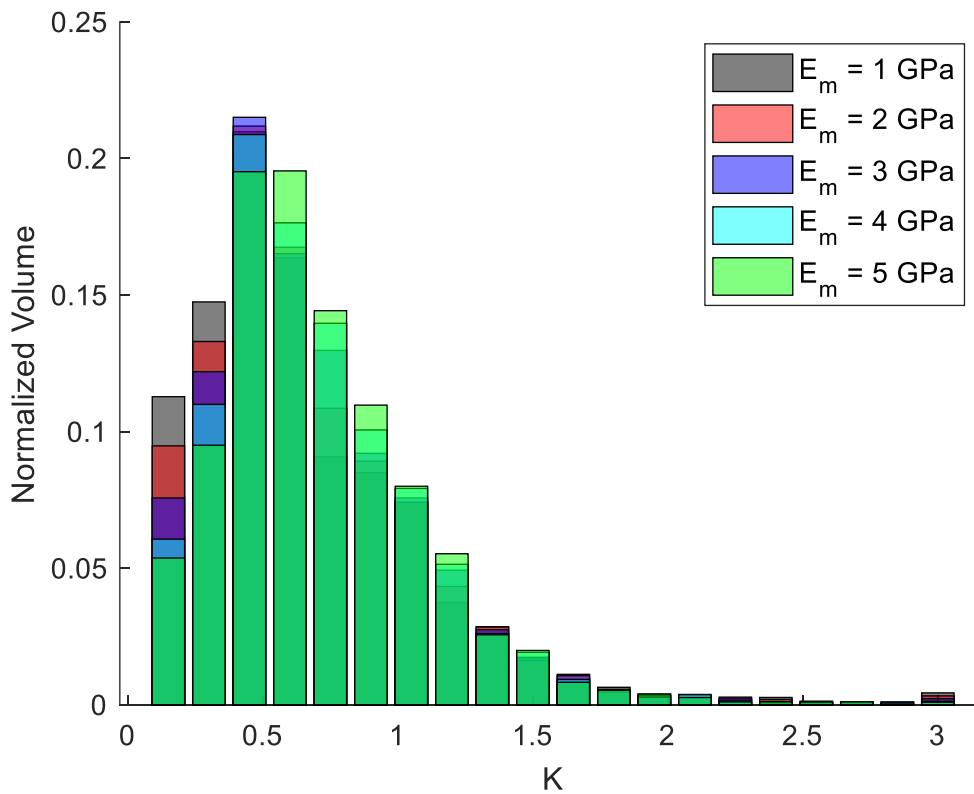


Figure 7.24. Normalized Volume/ K histogram of $V_f = 0.60410$

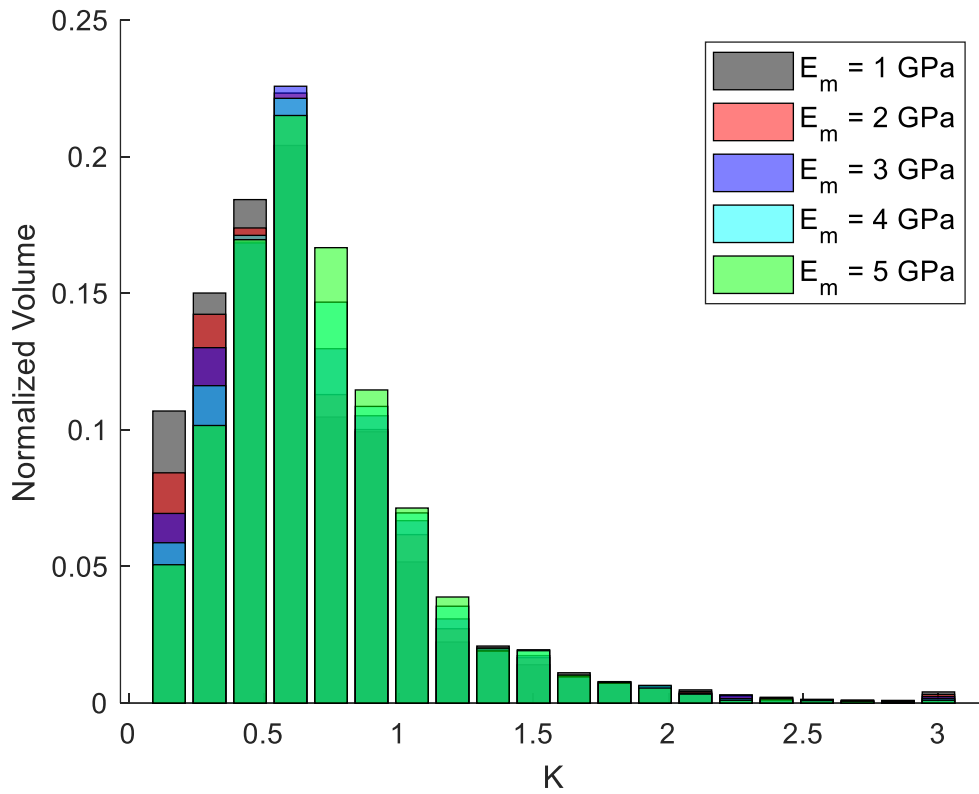


Figure 7.25. Normalized Volume/ K histogram of $V_f = 0.61829$

A probability histogram plot including all K results can be seen in (Figure 7.26). With the K_{max} and OVP results, a parametric correlation was done between the parameters chosen in the earlier chapters. In order to determine the number of simulations required for the parametric correlation, simulation numbers were increased until the difference between the previous results was acceptable. The parametric correlation matrices and their values for 450, 900, 1350, 1800, and 2250 simulations can be seen in Figure 7.28-Figure 7.32.

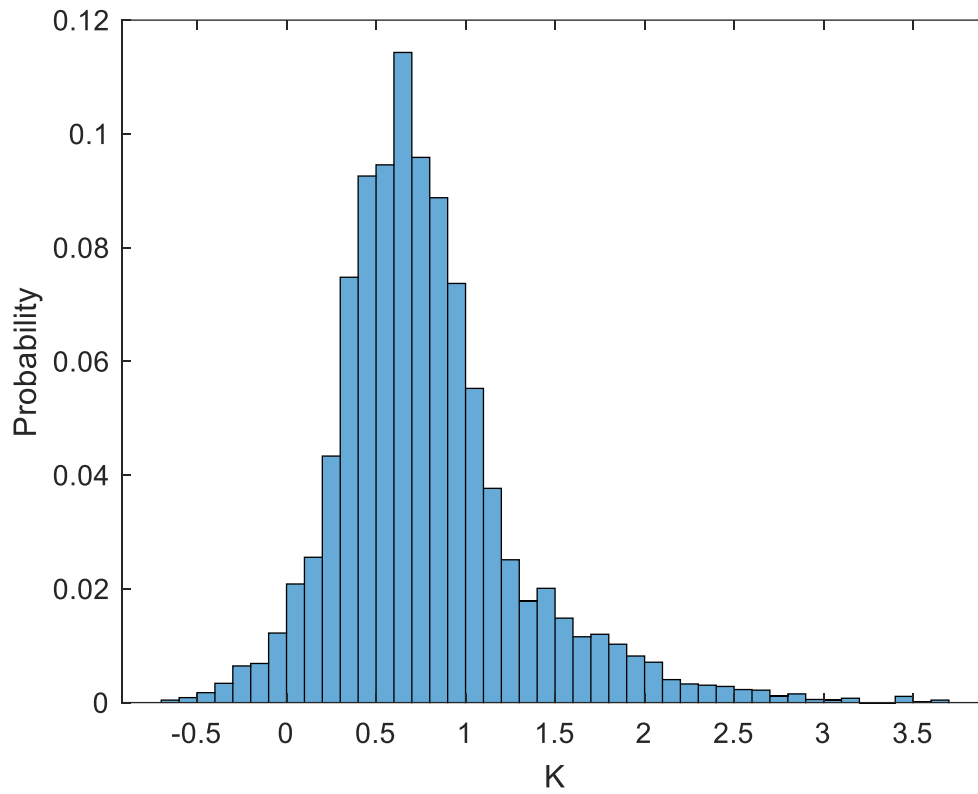


Figure 7.26. Probability Histogram for all K results

OVP output histogram can be seen in **(Figure 7.27)**.

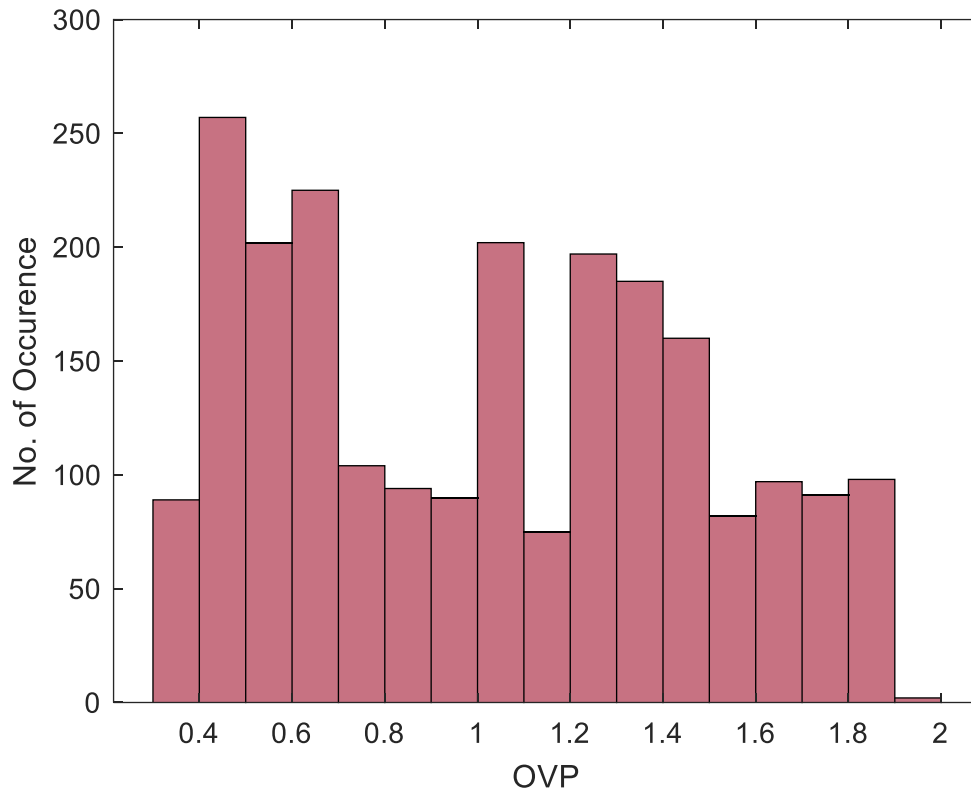


Figure 7.27. OVP histogram of the sensitivity analysis.

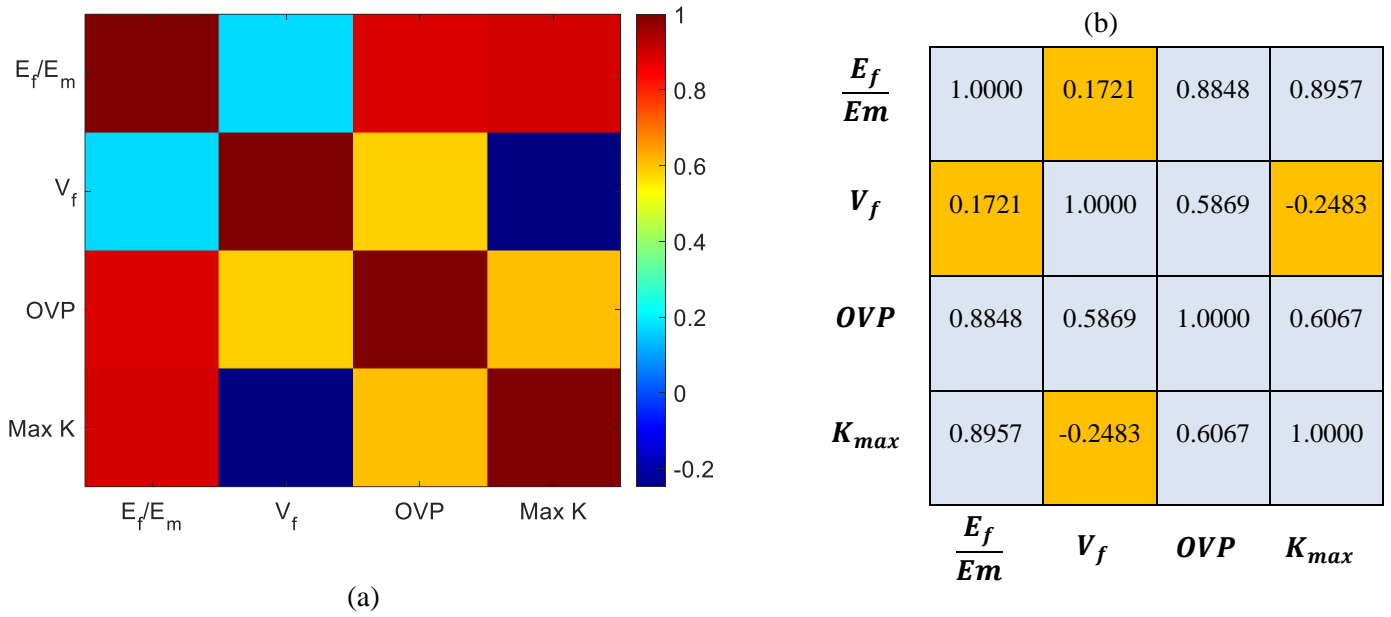


Figure 7.28. Parametric correlation matrix. (a) Graphic representation and (b) Spearman's correlation values for 450 simulations.

In (Figure 7.28), the correlation between E_f/E_m ratio and V_f is 0.1721. Since these parameters are chosen by the designer/user, it is known that they are not related to each other. Therefore, their correlation should be zero. Also V_f and K_{max} having negative correlation is not realistic. With more fiber concentration in the matrix, stress concentration in the matrix should increase.

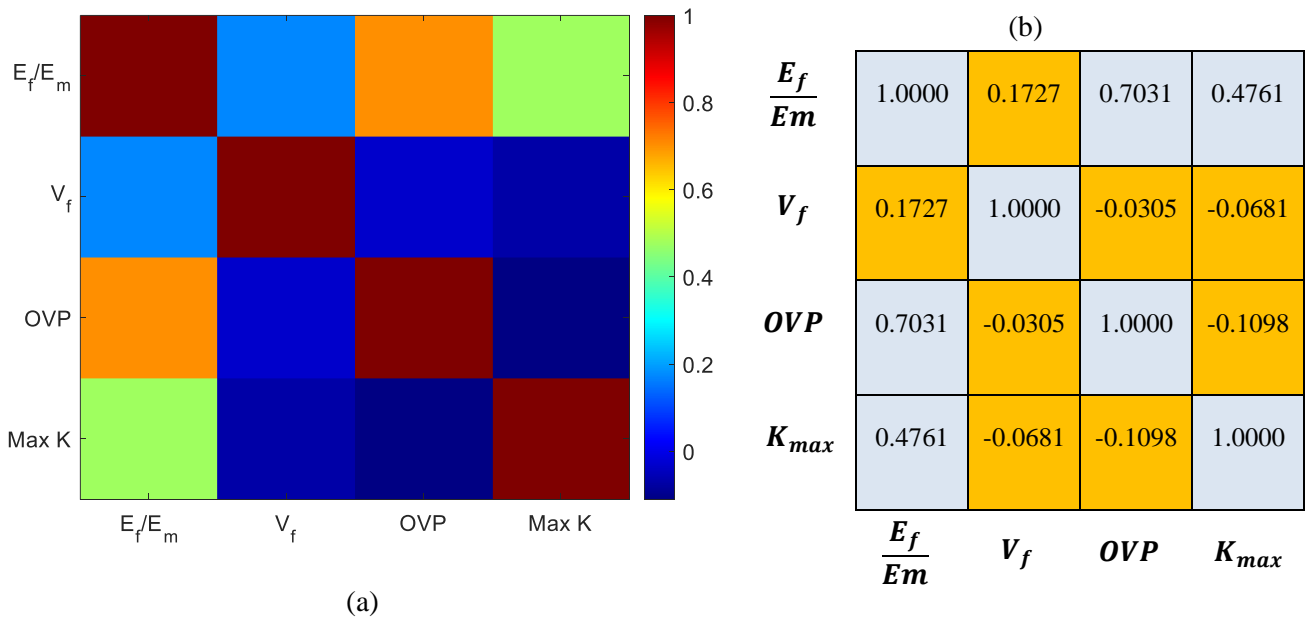


Figure 7.29. Parametric correlation matrix. (a) Graphic representation and (b) Spearman's correlation values for 900 simulations.

In addition to the same problems, OVP and K_{max} , OVP and V_f have negative correlation in (Figure 7.29). OVP and K_{max} are expected to have high positive correlation.

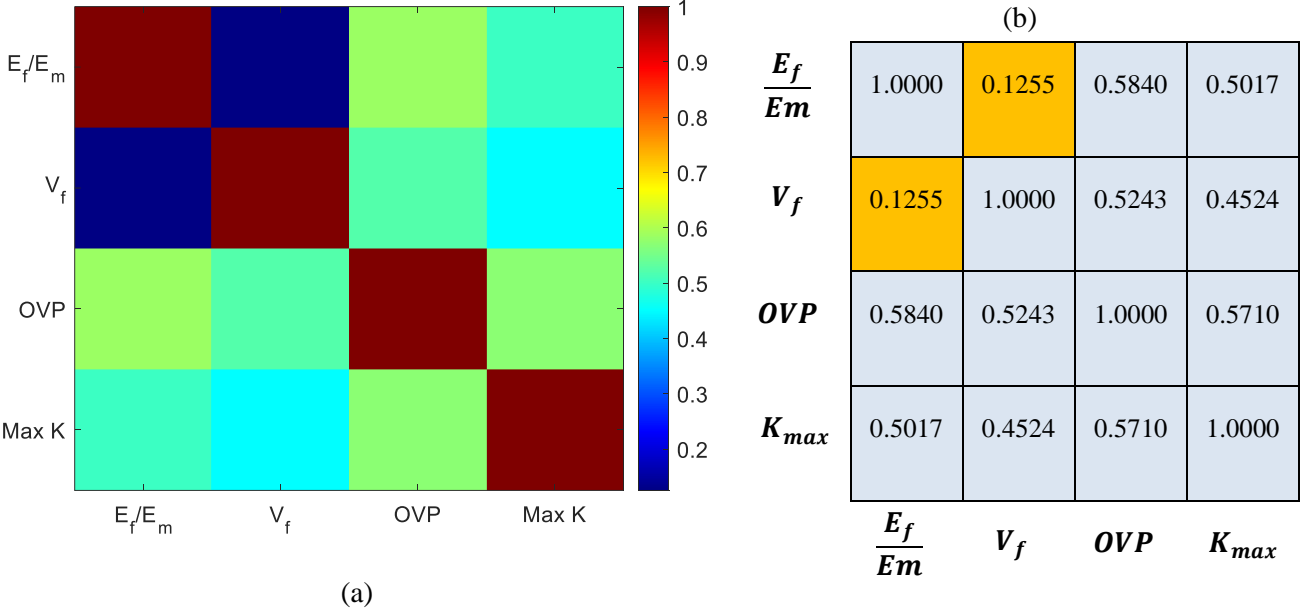


Figure 7.30. Parametric correlation matrix. (a) Graphic representation and (b) Spearman's correlation values for 1350 simulations.

In (Figure 7.30), although the correlation between E_f/E_m ratio and V_f is still not 0; OVP and V_f , OVP and K_{max} have positive correlation. Compared with (Figure 7.29), the correlation between E_f/E_m ratio and K_{max} and correlation between E_f/E_m ratio and OVP got lower.

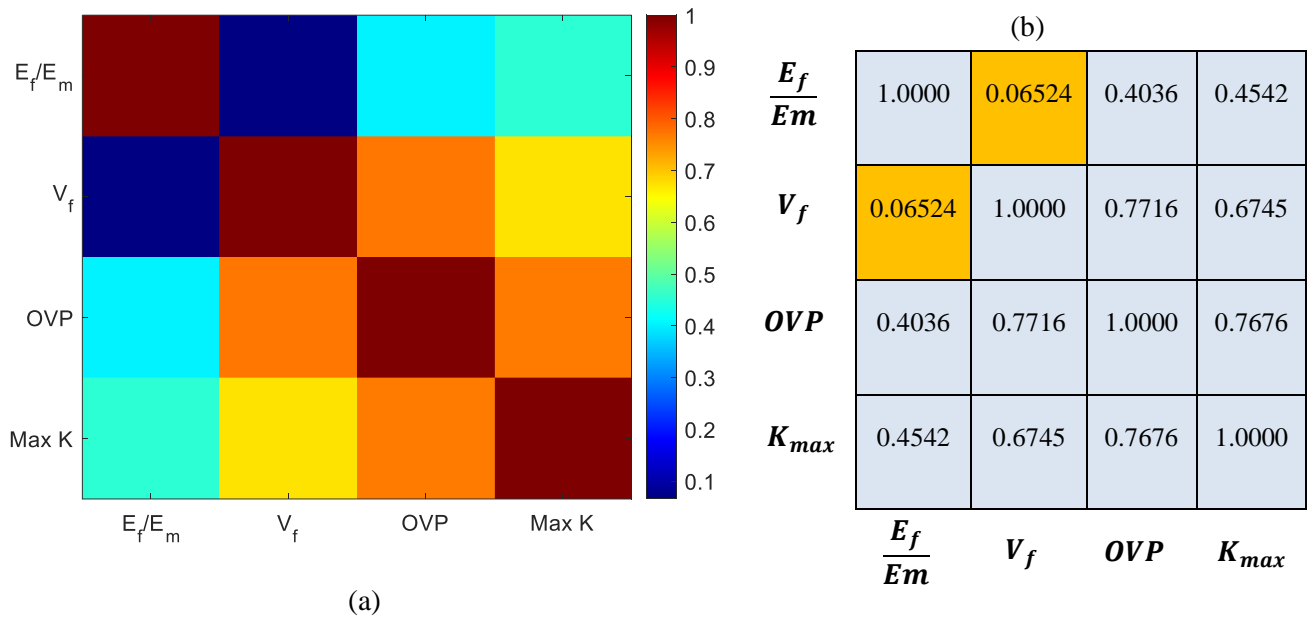


Figure 7.31. Parametric correlation matrix. (a) Graphic representation and (b) Spearman's correlation values for 1800 simulations.

In **(Figure 7.31)**, the correlation between E_f/E_m ratio and V_f is very close to zero. From the previous results, the correlation between OVP and K_{max} got higher and the correlation of E_f/E_m ratio with OVP and K_{max} got lower.

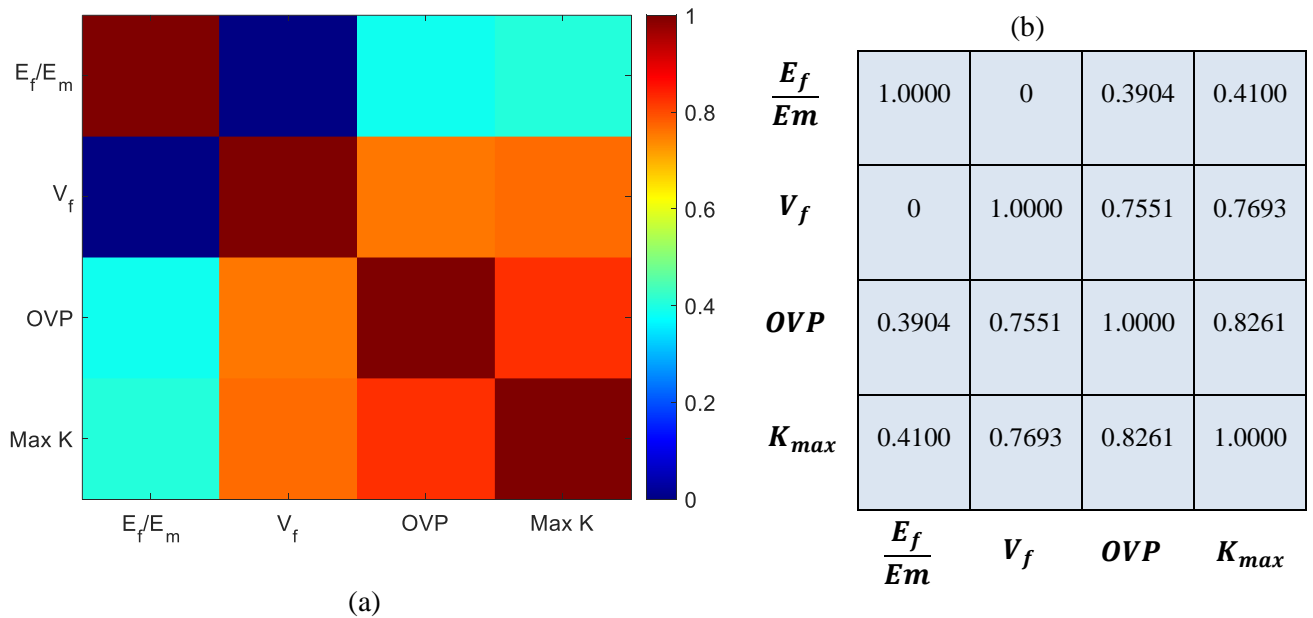


Figure 7.32. Parametric correlation matrix. (a) Color Graph and (b) Spearman's correlation values for 2250 simulations.

Between **(Figure 7.31)** and **(Figure 7.32)**, there are no significant changes in the correlations. As stated before, the correlation between E_f/E_m ratio and V_f is expected to be zero. This is confirmed for the accuracy of the analyses from the correlation matrix values in **(Figure 7.32)**. Also, V_f having more correlation with OVP and K_{\max} than E_f/E_m 's correlation with OVP and K_{\max} contributes to that the analysis is done correctly. Therefore, 1850 simulations were determined to be enough for the analysis.

- E_f/E_m has 0.3904 and 0.4100 correlation with OVP and K_{\max} , respectively. Thus, E_f/E_m seems to have slightly more influence on K_{\max} than OVP.
- V_f has 0.7551 and 0.7693 correlation with OVP and K_{\max} , respectively. Same conclusion for influence on K_{\max} and OVP can be said for the V_f .
- As mentioned before, V_f 's correlation with OVP and K_{\max} is higher than E_f/E_m 's correlation with OVP and K_{\max} . This indicates that changing V_f will have more effect on changing stress distribution and stress concentration than E_f/E_m .
- OVP and K_{\max} has 0.8261 correlation. Although this shows that these two parameters' relation is very high with each other, it also indicates that having a high OVP does not always mean having high K_{\max} .

8. CONCLUSION

8.1. Summary of the Study

Engineers need to understand the mechanical behavior of the composite material. Various micro-scale methods have been used in the literature to understand the mechanical behavior. FEM is the most widely used method for the micro-scale. While creating the RVE for the finite element analysis, to capture the actual conduct of the composite, random distributed fibers are created via algorithms. Therefore, sensitivity analysis is needed to understand the mechanical behavior. In this thesis study, a sensitivity analysis with the help of the Monte-Carlo method was done to analyze the effect of material parameters on the micro-scale stress concentrations. RVE models were created with different V_f values. Glass fiber was chosen as the fiber material. Stress concentrations and over-stressed volumes were calculated with the help of FEM. Results were gathered, and Spearman's correlation coefficients between " $E_f/E_m, V_f$ " and " K_{max}, OVP " were calculated. A further analysis was done with Young's modulus variance of fiber.

8.2. Outcomes of the Study

According to the results, the following conclusions were obtained,

1. Parametric correlation between material parameters and stress concentration was calculated and given.
2. Because of the randomness of the composite, different models and many simulations are needed to calculate the parametric correlation truly.
3. Input and output parameters show non-linearity between each other. Therefore, Spearman's rank correlation coefficient was suitable for calculating the correlation.
4. As seen from the preliminary Poisson's ratio analysis, ν_f does not have any significant effect on stress concentration within realistic ranges.

5. Fiber's Young's modulus and Matrix Young's Modulus can only be taken into account separately on effecting stress concentration if E_f value is much higher than the E_m and vice versa.
6. E_f/E_m ratio has almost the same influence on the OVP and K_{max} . Therefore, E_f/E_m ratio can be changed to reach the desired stress concentration and its distribution.
7. V_f has a higher influence on the OVP and K_{max} than E_f/E_m ratio. This means changing V_f instead of E_f/E_m ratio will have more effect on changing K_{max} and OVP.
8. Young's modulus variance of glass fiber only makes a difference on the maximum stress concentration if Young's modulus of the fiber and matrix Young's modulus values are close. Although the difference is higher; since the stress concentration compared with higher E_f/E_m ratio results are lower, and it is concluded that this will have very little change in the maximum stress concentration value.

8.3. Further Studies

In this study, only glass fiber material was considered in the sensitivity analysis to reduce the computation time. For future work, different fiber materials can be used and compared within. Future studies can be done with varying types of loading.

Fiber diameter was not included in this thesis due to problems while creating the RVE. Therefore, for future work, a sensitivity analysis including the fiber diameter can be done.

9. REFERENCES

- [1] F. C. Campbell, "Chapter 1 - Introduction to Composite Materials and Processes: Unique Materials that Require Unique Processes," in *Manufacturing Processes for Advanced Composites*, F. C. Campbell Ed. Amsterdam: Elsevier Science, 2004, pp. 1-37.
- [2] P. Chowdhury, H. Sehitoglu, and R. Rateick, "Damage tolerance of carbon-carbon composites in aerospace application," *Carbon*, vol. 126, pp. 382-393, 2018/01/01/ 2018, doi: <https://doi.org/10.1016/j.carbon.2017.10.019>.
- [3] V. V. Vasiliev and E. V. Morozov, "Chapter 1 - Introduction," in *Advanced Mechanics of Composite Materials (Third Edition)*, V. V. Vasiliev and E. V. Morozov Eds. Boston: Elsevier, 2013, pp. 1-27.
- [4] X. Li, B. Bhushan, and P. B. McGinnis, "Nanoscale mechanical characterization of glass fibers," *Materials Letters*, vol. 29, no. 4, pp. 215-220, 1996/12/01/ 1996, doi: [https://doi.org/10.1016/S0167-577X\(96\)00154-1](https://doi.org/10.1016/S0167-577X(96)00154-1).
- [5] D. D. Edie, "The effect of processing on the structure and properties of carbon fibers," *Carbon*, vol. 36, no. 4, pp. 345-362, 1998/01/01/ 1998, doi: [https://doi.org/10.1016/S0008-6223\(97\)00185-1](https://doi.org/10.1016/S0008-6223(97)00185-1).
- [6] D. Perremans, K. Hendrickx, I. Verpoest, and A. W. Van Vuure, "Effect of chemical treatments on the mechanical properties of technical flax fibres with emphasis on stiffness improvement," *Composites Science and Technology*, vol. 160, 2018, doi: 10.1016/j.compscitech.2018.03.030.
- [7] M. Knight and D. Curliss, "Composite Materials," in *Encyclopedia of Physical Science and Technology (Third Edition)*, R. A. Meyers Ed. New York: Academic Press, 2003, pp. 455-468.
- [8] G. R. Liu and S. S. Quek, "1 - Computational modelling," in *Finite Element Method*, G. R. Liu and S. S. Quek Eds. Oxford: Butterworth-Heinemann, 2003, pp. 1-11.
- [9] J. C. H. Affdl and J. L. Kardos, "The Halpin-Tsai equations: A review," *Polymer Engineering and Science*, vol. 16, no. 5, pp. 344-352, 1976, doi: 10.1002/pen.760160512.
- [10] G. Sendekyj, S. Wang, W. Steven Johnson, W. Stinchcomb, and C. Chamis, "Mechanics of Composite Materials: Past, Present, and Future," *Journal of Composites Technology and Research*, vol. 11, no. 1, p. 3, 1989, doi: 10.1520/ctr10143j.
- [11] T. Mori and K. Tanaka, "Average stress in matrix and average elastic energy of materials with misfitting inclusions," *Acta Metallurgica*, vol. 21, no. 5, pp. 571-574, 1973/05/01/ 1973, doi: [https://doi.org/10.1016/0001-6160\(73\)90064-3](https://doi.org/10.1016/0001-6160(73)90064-3).
- [12] R. Hill, "Theory of mechanical properties of fibre-strengthened materials—III. self-consistent model," *Journal of the Mechanics and Physics of Solids*, vol. 13, no. 4, pp. 189-198, 1965/08/01/ 1965, doi: [https://doi.org/10.1016/0022-5096\(65\)90008-6](https://doi.org/10.1016/0022-5096(65)90008-6).
- [13] B. Budiansky, "On the elastic moduli of some heterogeneous materials," *Journal of the Mechanics and Physics of Solids*, vol. 13, no. 4, pp. 223-227, 1965/08/01/ 1965, doi: [https://doi.org/10.1016/0022-5096\(65\)90011-6](https://doi.org/10.1016/0022-5096(65)90011-6).

- [14] Y.-C. Chiang, "On fiber debonding and matrix cracking in fiber-reinforced ceramics," *Composites Science and Technology*, vol. 61, no. 12, pp. 1743-1756, 2001/09/01/ 2001, doi: [https://doi.org/10.1016/S0266-3538\(01\)00078-1](https://doi.org/10.1016/S0266-3538(01)00078-1).
- [15] J. N. Goodier, "Concentration of Stress Around Spherical and Cylindrical Inclusions and Flaws," *Journal of Applied Mechanics*, vol. 1, no. 2, pp. 39-44, 2021, doi: 10.1115/1.4012173.
- [16] B. Sabuncuoglu, L. Gorbatikh, and S. V. Lomov, "Analysis of stress concentrations in transversely loaded steel-fiber composites with nano-reinforced interphases," *International Journal of Solids and Structures*, vol. 130-131, pp. 248-257, 2018/01/01/ 2018, doi: <https://doi.org/10.1016/j.ijsolstr.2017.09.031>.
- [17] B. Sabuncuoglu, S. Orlova, L. Gorbatikh, S. V. Lomov, and I. Verpoest, "Micro-scale finite element analysis of stress concentrations in steel fiber composites under transverse loading," *Journal of Composite Materials*, vol. 49, no. 9, pp. 1057-1069, 2015/04/01 2014, doi: 10.1177/0021998314528826.
- [18] T. Tang, Y. Hammi, M. F. Horstemeyer, and P. Wang, "Finite element micromechanical analysis of the deformation and stress state dependent damage evolution in fiber reinforced metal matrix composites," *Computational Materials Science*, vol. 59, pp. 165-173, 2012/06/01/ 2012, doi: <https://doi.org/10.1016/j.commatsci.2012.03.001>.
- [19] M. Romanowicz, "A numerical approach for predicting the failure locus of fiber reinforced composites under combined transverse compression and axial tension," *Computational Materials Science*, vol. 51, pp. 7–12, 01/31 2012, doi: 10.1016/j.commatsci.2011.07.039.
- [20] A. R. Maligno, N. A. Warrior, and A. C. Long, "Effects of interphase material properties in unidirectional fibre reinforced composites," *Composites Science and Technology*, vol. 70, no. 1, pp. 36-44, 2010/01/01/ 2010, doi: <https://doi.org/10.1016/j.compscitech.2009.09.003>.
- [21] T. Hobbiebrunken, B. Fiedler, M. Hojo, O. Shojiro, and S. Karl, "Microscopic yielding of CF/epoxy composites and the effect on the formation of thermal residual stresses," *Composites Science and Technology*, vol. 65, pp. 1626-1635, 08/01 2005, doi: 10.1016/j.compscitech.2005.02.003.
- [22] A. R. Melro, P. Camanho, and S. Pinho, "Generation of random distribution of fibres in long-fibre reinforced composites," *Composites Science and Technology*, vol. 68, 07/01 2008, doi: 10.1016/j.compscitech.2008.03.013.
- [23] A. R. Melro, P. P. Camanho, F. M. Andrade Pires, and S. T. Pinho, "Micromechanical analysis of polymer composites reinforced by unidirectional fibres: Part II – Micromechanical analyses," *International Journal of Solids and Structures*, vol. 50, no. 11, pp. 1906-1915, 2013/06/01/ 2013, doi: <https://doi.org/10.1016/j.ijsolstr.2013.02.007>.
- [24] E. Barbero, *Finite Element Analysis of Composite Materials*. 2008.
- [25] M. Bayat and M. M. Aghdam, "A micromechanics-based analysis of effects of square and hexagonal fiber arrays in fibrous composites using DQEM," *European Journal of Mechanics - A/Solids*, vol. 32, pp. 32-40,

- 2012/03/01/ 2012, doi:
<https://doi.org/10.1016/j.euromechsol.2011.09.008>.
- [26] N. K. Balasubramani, B. Zhang, N. T. Chowdhury, A. Mukkavilli, M. Suter, and G. M. Pearce, "Micro-mechanical analysis on random RVE size and shape in multiscale finite element modelling of unidirectional FRP composites," *Composite Structures*, vol. 282, p. 115081, 2022/02/15/ 2022, doi: <https://doi.org/10.1016/j.compstruct.2021.115081>.
- [27] F. Danzi, D. Fanteria, E. Panettieri, and M. Palermo, "A numerical micro-mechanical study of the influence of fiber-matrix interphase failure on carbon/epoxy material properties," *Composite Structures*, vol. 159, 10/01 2016, doi: 10.1016/j.compstruct.2016.09.095.
- [28] N. De Greef, L. Gorbatikh, A. Godara, L. Mezzo, S. V. Lomov, and I. Verpoest, "The effect of carbon nanotubes on the damage development in carbon fiber/epoxy composites," *Carbon*, vol. 49, no. 14, pp. 4650-4664, 2011/11/01/ 2011, doi:
<https://doi.org/10.1016/j.carbon.2011.06.047>.
- [29] S.-P. Lee, J.-W. Jin, and K.-W. Kang, "Probabilistic analysis for mechanical properties of glass/epoxy composites using homogenization method and Monte Carlo simulation," *Renewable Energy*, vol. 65, pp. 219-226, 2014/05/01/ 2014, doi:
<https://doi.org/10.1016/j.renene.2013.09.012>.
- [30] Q. Wu, C. Chen, N. Yoshikawa, J. Liang, and N. Morita, "Microscopic stresses of discontinuous fiber reinforced composites under thermal and mechanical loadings – Finite element simulations and statistical analyses," *Computational Materials Science*, vol. 200, p. 110777, 2021/12/01/ 2021, doi: <https://doi.org/10.1016/j.commatsci.2021.110777>.
- [31] E. Barbero, J. Fernández-Sáez, and C. Navarro, "Statistical analysis of the mechanical properties of composite materials," *Composites Part B Engineering*, vol. 31, 07/01 2000, doi: 10.1016/S1359-8368(00)00027-5.
- [32] G. Mustafa, A. Suleman, and C. Crawford, "Probabilistic micromechanical analysis of composite material stiffness properties for a wind turbine blade," *Composite Structures*, vol. 131, pp. 905-916, 2015, doi: 10.1016/j.compstruct.2015.06.070.
- [33] T. Sterling, M. Anderson, and M. Brodowicz, "Chapter 9 - Parallel Algorithms," in *High Performance Computing*, T. Sterling, M. Anderson, and M. Brodowicz Eds. Boston: Morgan Kaufmann, 2018, pp. 285-311.
- [34] A. M. Johansen, "Monte Carlo Methods," in *International Encyclopedia of Education (Third Edition)*, P. Peterson, E. Baker, and B. McGaw Eds. Oxford: Elsevier, 2010, pp. 296-303.
- [35] J. E. Gentle, "Computational Statistics," in *International Encyclopedia of Education (Third Edition)*, P. Peterson, E. Baker, and B. McGaw Eds. Oxford: Elsevier, 2010, pp. 93-97.
- [36] A. Dasgupta and A. Wahed, "Chapter 4 - Laboratory Statistics and Quality Control," in *Clinical Chemistry, Immunology and Laboratory Quality Control*, A. Dasgupta and A. Wahed Eds. San Diego: Elsevier, 2014, pp. 47-66.
- [37] C. Heinrich, M. Aldridge, A. S. Wineman, J. Kieffer, A. M. Waas, and K. Shahwan, "The influence of the representative volume element (RVE) size on the homogenized response of cured fiber composites," *Modelling*

- and Simulation in Materials Science and Engineering*, vol. 20, no. 7, p. 075007, 2012/09/14 2012, doi: 10.1088/0965-0393/20/7/075007.
- [38] P. R. Budarapu, X. Zhuang, T. Rabczuk, and S. P. A. Bordas, "Chapter One - Multiscale modeling of material failure: Theory and computational methods," in *Advances in Applied Mechanics*, vol. 52, M. I. Hussein Ed.: Elsevier, 2019, pp. 1-103.
- [39] S. Kurukuri, "Homogenization of Damaged Concrete Mesostructures using Representative Volume Elements - Implementation and Application to SLang," 2005.
- [40] A. M. Skudra and M. R. Gurvich, "Structural theory of the strength of reinforced plastics," *Mechanics of Composite Materials*, p. 61, 1990, doi: 10.1007/bf00612903.
- [41] T. Sun, H. Fan, X. Liu, and Z. Wu, "Sandwich-structured graphene oxide@poly (aminophenol-formaldehyde) sheets for improved mechanical and thermal properties of epoxy resin," *Composites Science and Technology*, vol. 207, p. 108671, 2021/05/03/ 2021, doi: <https://doi.org/10.1016/j.compscitech.2021.108671>.
- [42] N. Shoji *et al.*, "Effect of conversion on epoxy resin properties: Combined molecular dynamics simulation and experimental study," *Polymer*, vol. 254, p. 125041, 2022/07/21/ 2022, doi: <https://doi.org/10.1016/j.polymer.2022.125041>.
- [43] X. Mi *et al.*, "Toughness and its mechanisms in epoxy resins," *Progress in Materials Science*, vol. 130, p. 100977, 2022/10/01/ 2022, doi: <https://doi.org/10.1016/j.pmatsci.2022.100977>.
- [44] A. Lefeuvre, A. Bourmaud, C. Morvan, and C. Baley, "Tensile properties of elementary fibres of flax and glass: Analysis of reproducibility and scattering," *Materials Letters*, vol. 130, pp. 289-291, 2014/09/01/ 2014, doi: <https://doi.org/10.1016/j.matlet.2014.05.115>.

APPENDIX